PATHOPHYSIOLOGY OF A MOUSE MODEL OF X-LINKED MENTAL RETARDATION

by

KALBINDER KAUR GILL

A thesis submitted to

The University of Birmingham

For the degree of

DOCTOR OF PHILOSOPHY

Neuronal Networks Group

Clinical and Experimental Medicine

University of Birmingham

July 2013

Authors Declaration

Kalbinder Gill declares that:

I am the sole author of this thesis. The work presented here is original work, completed by me during the period of registration as a postgraduate candidate. The exception to this statement relates to the analysis of brain morphological studies, namely, measurements of ventricular volume and cortical thickness, which were completed by my supervisor Dr. Andrew Powell.

Acknowledgements

I would like to thank Prof. John Jefferys and Dr. Andy Powell for their support, guidance and endless confidence in my abilities when I was lacking. Thank you both for your patience, motivation and enthusiasm; I could not have asked for better leadership during my Ph.D. John, thank you for your immense knowledge, particularly statistics and more importantly, teaching me how to make salt & vinegar infused chips. Andy, thank you for teaching me to be a great electrophysiologist, but above all, thanks for all the trips to Starbucks for the necessary (and unnecessary) frappacinos. Thanks to Attila for teaching me various immunohistochemical techniques, in addition to liberal use of his labs, microscope and reagents. To the lunch bunch, thanks for the camaraderie, the laughter and the ability find any excuse to bring in a celebratory cake! I would also like to thank all members of the Neuronal Networks Group from past to present: Wei-Chih, Barbara, Atif, Gareth, Sahar, Premek, Martin, Mike, Emil; thank you for your support, advice and generosity you have extended, it is sincerely appreciated. Thank you to my housemate and Ph.D. buddy Lucy for being there since the beginning, you've truly been amazing! Thank you to my friends (you know who you are!): you've been there through the tears and the laughter and thank you so much for your encouragement and never-ending support. Finally, I would especially like to thank my family:

ਬਹੁਤ ਧਨਵਾਦ ਮੇਰੇ ਮਾਤਾ ਜੀ ਨਰਿੰਦਰ ਕੌਰ ਅਤੇ ਪਿਤਾ ਜੀ ਮੋਹਿੰਦਰ ਸਿੰਘ ਅਰੇ ਮੇਰੇ ਪਰਵਾਰ: ਬੀਬੀ ਜੀ, ਸੰਨਦੀਪ, ਸੁਖਦੀਪ, ਜਗਜੀਤ, ਪ੍ਰਵੀਰ, ਜੋਧੀ ਅਤੇ ਰਾਜਨ | ਤੁਸੀਂ ਬਹੁਤ ਮਦਦ ਮੇਰੀ ਕੀਤੀ ਤੈ ਸਫਲਤਾ ਮੇਨੂ ਮਿਲੀ | ਤੁਸੀਂ ਮੇਰਾ ਸਹਾਰਾ ਬਣਿਆ ਔਖੀ ਸਮਾਂ ਵਿਚ | ਮੇਰੇ ਕੁਲ ਊਹ ਸ਼ਬਦ ਹੇਨੀ ਜਿਨਾ ਨਾਲ ਮੈ ਤੁਹਾਡਾ ਧਨਵਾਦ ਕਰਾ | ਬਹੁਤ ਬਹੁਤ ਧਨਵਾਦ |

Abstract

Mental retardation (MR) affects 2-3% of the population; those due to X-linked mutations commonly result in moderate to severe MR. The *OPHN1* gene (*Ophn1* in mice) has been implicated in X-linked mental retardation (XLMR) and encodes the RhoGAP protein, oligophrenin-1. Loss of function mutations alter Rho GTPase-dependent signalling pathways and result in altered actin cytoskeleton dynamics which are important in dendritic spine structure, the site of neurotransmission. Here, using electrophysiological recordings combined with intracellular staining techniques and dendritic morphological analysis, I characterise synaptic (dys)function in neocortical and hippocampal neurons from the *Ophn1* mouse model of MR. This study demonstrates an excitatory synaptic deficit in neocortical neurons combined with region specific changes in dendritic spine morphology. Inhibitory transmission was normal in both neocortical and hippocampal neurons. Kainate-induced gamma oscillations were unaltered whereas spontaneous oscillations were reduced which lead to changes in synaptic function in CA3. Morphometric analysis showed ventriculomegaly in *Ophn1* deficient mice that was associated with reduced cortical thickness.

This study shows the loss of several previously reported phenotypes, including, altered inhibitory transmission, gamma oscillations and vesicle dynamics. Their loss, but preservation of morphological deficits, suggests that the model may be susceptible to genetic drift.

Table of Contents

List of Figures

List of Abbreviations

ABC	avidin/biotinylated enzyme complex
aCSF	artificial cerebral spinal fluid
Au1	primary auditory cortex
AHP	afterhyperpolarisation
AMPA	α-amino-3-hydroxy-5-methyl-4-isoxasole-propionic acid
BAR	Bin, amphiphysin, Rvs
DAB-Ni	3'-3'-diaminobenzidine nickel
D-APV	D-(-)-2-amino-5-phosphonopentanoic acid
DHPG	(S)-3,5-dihydroxyphenylglycine
DIC	differential interference contrast
EEG	electroencephalography
EPSC	excitatory postsynaptic current
EPSP	excitatory postsynaptic potential
GAD65	glutamic acid decarboxylase 65
GAP	GTPase activating protein
GDI	guanine nucleotide dissociation inhibitor
GDP	guanine diphosphate
GEF	GTPase exchange factor
GFP	green fluorescent protein
GST	glutathione-S-transferase
GTP	guanine triphosphate
IPSC	inhibitory postsynaptic current
IPSP	inhibitory postsynaptic potential
IQ	intelligence quotient
KAR	kainate receptor
LIMK	LIM-kinase
LTD	long term depression
LTP	long term potentiation
M1	primary motor cortex
mAChR	muscarinic acetylcholine receptor
mGluR	metabotropic glutamate receptor
MLC	myosin light chain
MLCK	myosin light chain kinase
MLCP	myosin light chain phosphatase
MR	mental retardation
NBQX	2,3-dioxo-6-nitro-1,2,3,4-tetrahydrobenzo[f]quinoxaline-7-sulphonamide
NMDA	N-methyl-D-aspartate
OC	optic chiasm

PB	phosphate buffer
PCR	polymerase chain reaction
PFA	paraformaldehyde
PH	pleckstrin homology
P_i	inorganic phosphate
PPF	paired pulse facilitation
PPR	paired pulse ratio
PSP	postsynaptic potential
RMP	resting membrane potential
ROCK	rho kinase
RRP	readily releasable pool
S1	primary somatosensory cortex
SH3	Src homology 3
TBE	tris-borate-EDTA
TBS	tris buffered saline
TEA	tetraethylammonium
TTX	tetrodotoxin
VGLUT1	vesicular glutamate transporter 1
VGLUT2	vesicular glutamate transporter 2
XLMR	X-linked mental retardation
YFP	yellow fluorescent protein

Chapter 1: Introduction

1.1 Mental retardation

Mental retardation (MR) is an overall deficit in cognitive function and two or more adaptive behaviours (e.g. inability to cope with daily tasks, social, interpersonal and communication skills) which onset before the age of 18 years (Chelly *et al*., 2006). MR is defined by an intelligence quotient (IQ) of less than 70 and the degree of cognitive impairment is assessed by the IQ and classified into mild (50-70), moderate (35-50), severe (20-35) and profound MR (<20). Approximately 2-3% of the population are affected by MR, where moderate to severe cases account for ~16% and genetic causes account for 25-50% of severe MR (Chelly *et al*., 2006).

In the majority of patients diagnosed with MR, the aetiology is unknown. Where they are known, origins of MR are diverse and include environmental and genetic factors that affect development and functioning pre-, peri- or post-natally (Chiurazzi *et al*., 2008). Environmental factors encompass: problems during pregnancy such as foetal alcohol syndrome, premature birth and malnutrition; ischaemia or infection. Genetic factors include chromosomal abnormalities such as trisomy 21 (Down syndrome) and monogenic disorders such as Fragile X syndrome (Ramakers, 2002). The exact cause of MR is only known in approximately 50% of moderate to severe MR cases and even lower proportions in mild MR (Chelly *et al*., 2006).

1.2 X-linked mental retardation

X-linked mental retardation (XLMR) are a group of disorders caused by a single gene mutation located on the X chromosome and are major cause of moderate to severe MR. The prevalence of MR in males outnumbers females, an approximate excess of 30-50%, indicating the importance of genes on the X-chromosome in terms of cognitive abilities (Chelly *et al*., 2006; Humeau *et al*., 2009). Approximately 1.8/1000 males have XLMR, Fragile X accounting for approximately 11% of all XLMR cases (Chiurazzi *et al*., 2008).

Classification of X-linked mental retardation

The inherited MR group of disorders can be categorised into syndromic MR which is associated with clinical, biological, radiological or metabolic features and non-syndromic MR, characterised solely by the cognitive impairment (Chelly *et al*., 2006). However with recent improvements in molecular studies alongside detailed clinical and behavioural assessments, the distinction between these two categories are vanishing as some genes responsible for MR give rise to both syndromic and non-syndromic forms (Ropers and Hamel, 2005). For example, Fragile X syndrome was initially classified as non-syndromic MR, however it is now described as the most common form of syndromic MR (Frints *et al*., 2002) with symptoms such as facial anomalies, connective tissue dysplasia and macroorchidism (Jin and Warren, 2003).

Cellular functions of MR related genes

To date, approximately 282 genes related to MR have been identified that encode a diverse range of proteins, many of which are involved in neurogenesis in the developing brain and neuronal migration (Chiurazzi *et al*., 2008). These include transcription factors (e.g. FMR1 encoding Fragile X mental retardation protein involved in Fragile X syndrome)(O'Donnell and Warren, 2002), transmembrane proteins (e.g. NLGN4 encoding neuroligin 4 implicated in Asperger syndrome)(Laumonnier *et al*., 2004), cytoskeleton associated proteins, proteins involved in signalling cascades (e.g. RSK2, a downstream effector of Ras signalling, responsible for Coffin-Lowry syndrome)(Delaunoy *et al*., 2001) amongst others. To date, 82 XLMR genes have been discovered (Chiurazzi *et al*., 2008), approximately 8.8% of X chromosome genes (Skuse, 2005). Many MR-related genes encode proteins that are enriched in synaptic terminals, which play a key role in regulating dendritic spine formation and synaptic activity (Humeau *et al*., 2009).

Microstructural features in X-linked mental retardation

Characteristic alterations in dendrites and dendritic spine morphology are common features of MR and these are thought to underlie the impairments in cognitive function. Dendrites are crucial for neuronal function; they play a key role in plasticity and synaptic integration which is directly related to dendritic arborisation (Hausser *et al*., 2000). The majority of excitatory transmission occurs at dendritic spines. Physiological processes such as synaptic plasticity and learning have been associated with changes in spine structure, whilst dysregulation of spinogenesis is linked to MR (Hotulainen and Hoogenraad, 2010). There are three types of dendritic spines: mature mushroom shaped, immature stubby and thin (or

filopodia) (Hotulainen and Hoogenraad, 2010). Early studies using Golgi impregnations from post-mortem brains of children with MR demonstrated a decrease in spine density with changes in spine morphology (Huttenlocher, 1970; 1974; Purpura, 1974; Kaufmann and Moser, 2000). Golgi studies also reveal a reduction in dendritic length and branching in MR (Huttenlocher, 1974). Spine dysgenesis and alterations in dendritic arborisation are also consistently observed in patients with defined cases of MR, including Down's syndrome, Rett syndrome and Fragile X syndrome (Kaufmann and Moser, 2000). Studies also demonstrated the degree of spine loss is related to the severity of MR (Purpura, 1974). Observations of altered spine morphology have formed a central part of the theories for MR. More recent studies have questioned whether spine anomalies are the cause of the cognitive impairments or are due to a compensatory response as a result of reduced excitatory transmission (Fiala *et al*., 2002).

The actin cytoskeleton modulates neuronal function

Within neurons, the actin cytoskeleton plays an essential role in many cellular functions including formation of synapses, synaptic plasticity, dendritic morphogenesis, morphology and neuronal network formation (Negishi and Katoh, 2002). These processes are crucial for the correct formation of neuronal networks. Therefore mutations in MR-related genes involved in neuronal network activity and synaptogenesis could cause impairments in neuronal connectivity and synaptic plasticity, impairing information processing, resulting in MR (Linseman and Loucks, 2008). Rho GTPases are major signalling proteins that regulate cytoskeletal dynamics in the pre- and postsynaptic compartment and are important for exo- and endocytosis (Humeau *et al*., 2009).

1.3 Rho GTPase signalling pathways

The Rho GTPase family, part of the Ras-small GTPases superfamily which includes RhoA, Rac1, and Cdc42, are proteins that bind guanine nucleotides and function as molecular switches to up- (GTP bound) or down-regulate (GDP bound) signalling cascades. Various molecules regulate GTPase activity; guanine nucleotide exchange factors (GEFs) initiate GTPase activity by catalysing the exchange of GDP for GTP, GTPase activating proteins (GAPs) negatively regulate GTPase activity by stimulating the hydrolysis of GTP to GDP and guanine nucleotide dissociation inhibitors (GDIs) prevent the intrinsic GTPase activity and inhibit exchange of GDP for GTP (see fig 1.1; reviewed in Govek *et al*., 2005).

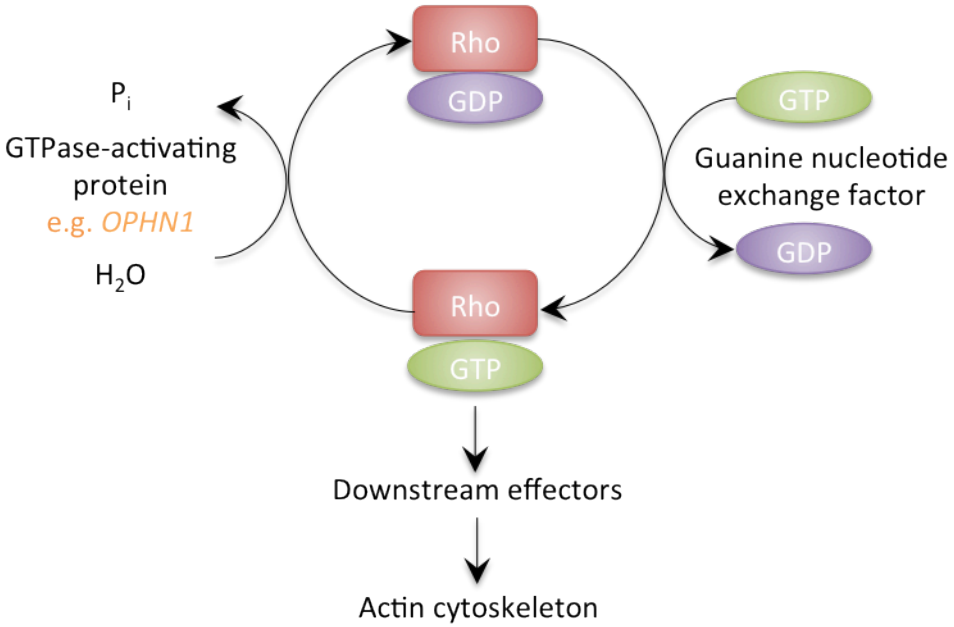

Figure 1.1 – Cyclic activity of Rho GTPases.

Upstream signals induce Rho GTPases to cycle between inactive Rho-GDP to active Rho-GTP. Activation via guanine nucleotide exchange factors (GEFs) exchanges GDP for GTP. Oligophrenin-1 (a GTPase-activating protein, GAP) negatively regulates Rho GTPase activity by stimulating the hydrolysis of Rho-GTP. Active GTP-bound Rho GTPases interact with downstream effectors to mediate their cellular actions on the actin cytoskeleton.

Upstream signals of Rho cascade

Regulation of actin cytoskeletal dynamics is initiated in response to upstream signals by the activation of various membrane bound ligands. Extracellular signals such as ephrins, neurotrophins, semaphorins and NMDA receptors, among others, mediate downstream signalling pathways (Luo *et al.*, 2000). Ephrins are transmembrane molecules that are growth cone collapse factors, neurotrophins are secreted growth factors and semaphorins are

secreted and membrane associated proteins that are also growth cone collapse factors involved in axonal guidance (Negishi and Katoh, 2002). Activation of ephrin receptors by ligand binding is involved in stimulating and increasing RhoA activity and decreasing Rac1 activity via ephrin-A5 receptors, whereas activation of ephrin-B receptors induces Rac1 activity (Govek *et al.*, 2005). Ephrin-B receptor signalling is one of the major pathways implicated in regulating actin cytoskeletal dynamics in dendritic spines. Dendritic growth and morphological changes in dendritic spines could also be activated through synaptic activity through NMDA receptors however little is known how it influences the Rho GTPases (Vaillend *et al.*, 2008).

Downstream effectors of Rho signalling

Activation of Rho, one of many pathways of Rho signalling, via GEFs stimulates Rho kinase (ROCK) activity, one of the many effector molecules of Rho, which stimulates downstream targets involved in a range of cellular processes such as regulating actin cytoskeleton dynamics, microtubule dynamics, transcriptional activation and membrane trafficking (Govek *et al*., 2005; fig. 1.2). LIM-kinase, one of the substrates of ROCK, phosphorylates and consequently inactivates cofilin, which regulates reorganisation of the actin cytoskeleton by inhibiting actin depolymerisation and in neurons, promotes neurite retraction (Maekawa *et al*., 1999). ROCK also regulates the actin cytoskeleton through myosin light chain (MLC) and myosin light chain phosphatase (MLCP); the phosphorylation state controls the assembly of myosin filaments (Mackay and Hall, 1998).

The Rho/ROCK pathway is most studied and described here, but there are other pathways of Rho signalling (e.g. Rac1 and Cdc42). Generally, activation of the RhoA pathway inhibit whereas Rac1 and Cdc42 pathways promote dendritic spine formation and/or maintenance (Tashiro *et al*., 2000). Figure 1.2 summaries the major substrates and effector molecules of Rho signalling involved in neuronal cytoskeleton regulation. Some of the MR-related genes identified code for proteins that are regulators and/or effectors of the Rho GTPase signalling pathways. Mutations in genes that encode Rho proteins such as *OPHN1* (Billuart *et al*., 1998) *ARHGEF6* (Kutsche *et al*., 2000) and *PAK3* (Allen *et al*., 1998) have been implicated in various types of MR. The products of these genes directly interact with Rho GTPase mediated signalling.

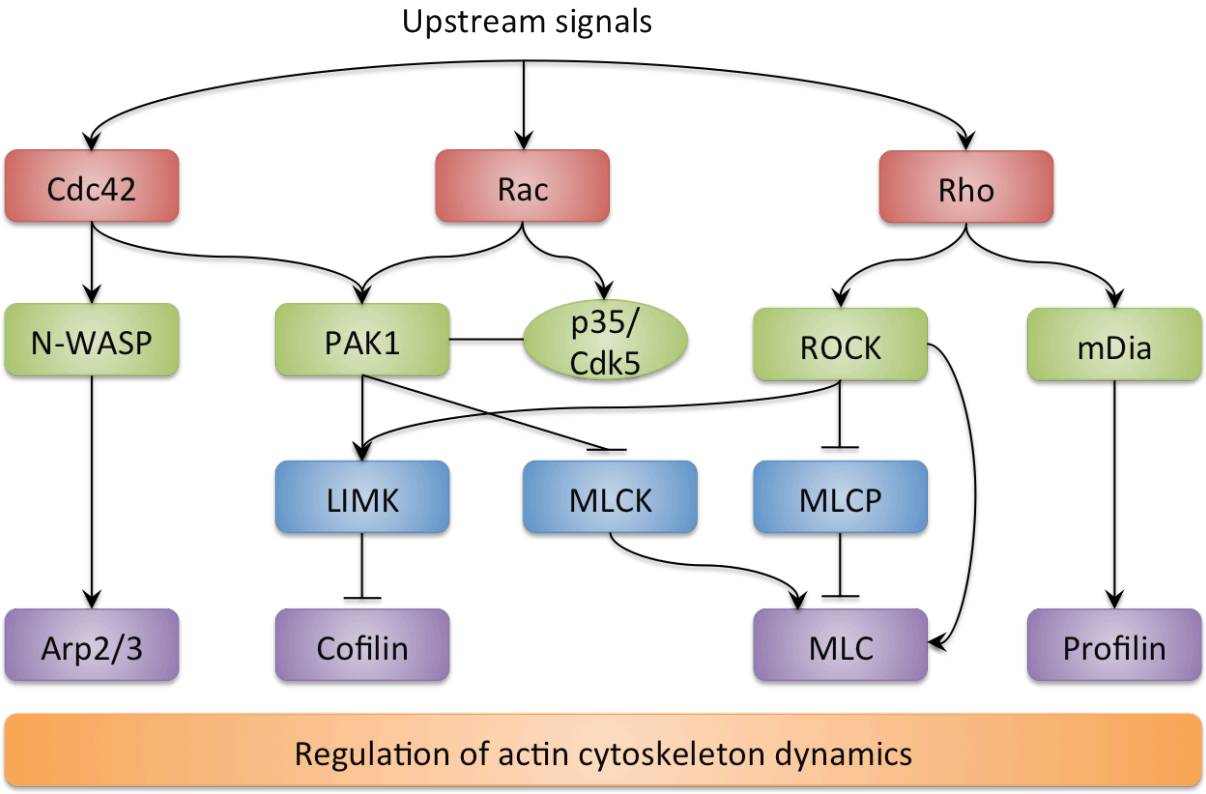

Figure 1.2 – Schematic diagram of Rho signalling cascade.

Upstream signals activate Rho GTPase signalling pathways involved in the regulation of the neuronal actin cytoskeleton. Arrow heads represent activation and flat ends represent inhibition. Arp2/3, actin-related proteins 2 and 3; Cdc42, cell division cycle 42; Cdk5, cyclin-dependent protein kinase 5; LIMK, LIM-kinase; mDia, mammalian diaphanous; MLC, myosin light chain; MLCK, myosin light chain kinase; MLCP, myosin light chain phosphatase; N-WASP, neuronal Wiscott-Aldrich syndrome protein; p35, activator of Cdk5; PAK1, p21-activated protein kinase; ROCK, Rho-associated kinase.

1.4 *OPHN1*: a mental retardation linked gene

One of the first Rho-linked genes implicated in non-syndromic XLMR was *OPHN1* (Billuart *et al*., 1998), which was identified in a female patient with mild MR with a balanced translocation (X;12)(Bienvenu *et al*., 1997). Cloning of the breakpoint revealed a single base pair deletion which resulted in a frameshift and a dramatic reduction or loss of mRNA product (Billuart *et al*., 1998). Since the initial identification of alterations in *OPHN1* expression causing MR, numerous reports have identified mutations in the gene, which include six large deletions, three frameshift, two translocations, three nonsense mutations and one splice mutation all leading to loss of function of the oligophrenin-1 protein (Pirozzi *et al*. 2011 and references therein). Duplication of *OPHN1* has also been associated with MR, suggesting gene dosage of *OPHN1* is important for cognition (Bedeschi *et al*., 2008).

OPHN1: clinical features

The *OPHN1* gene was originally classed as a non-syndromic XLMR gene, however subsequent reports have documented families with other manifestations in addition to cognitive impairments (Tentler *et al*., 1999; Bergmann *et al*., 2003). Clinical studies have reported many pathophysiologies of *OPHN1* MR. All patients show some degree of learning disabilities between mild to severe MR. Most patients present some degree of cerebellar hypoplasia (Pirozzi *et al*., 2011), a number of individuals have ventricular enlargement (Tentler *et al*., 1999; Bergmann *et al*., 2003) and some patients develop epileptic seizures (Tentler *et al*., 1999; Bergmann *et al*., 2003; Philip *et al*., 2003; des Portes *et al*., 2004). Other phenotypes include strabismus, cortico-subcortical atrophy, hyperactivity, anxiety, hypogenitalism,

macrocephaly, hydrocephalus and ataxia, although not all individuals display gross anatomical changes (Bergmann *et al*., 2003; Pirozzi *et al*., 2011). In the case of *OPHN1* duplication, the patient had severe MR and showed different phenotypes to *OPHN1* mutation, such as abnormalities in white matter (e.g. corpus callosum), without alterations in the cerebellum and cerebral ventricles (Bedeschi *et al*., 2008). Some patients with MR have grossly normal brains and in those cases microscopic pathologies or pathophysiologies probably are responsible for deficits in cognitive function, synaptic dysfunction being a likely candidate.

OPHN1: structure

OPHN1 is located on the X chromosome, position Xq12, consisting of 25 exons and encodes the oligophrenin-1 protein, an 802 amino acids RhoGAP protein with a molecular weight of 91 kDa (Billuart *et al*., 1998). Sequence analysis of *OPHN1* demonstrate several domains, these include a highly conserved N-terminus with a BAR (Bin, amphiphysin, Rvs) domain which enables binding to curved membranes (Peter *et al*., 2004), a pleckstrin homology (PH) domain which interacts with phosphoinositides enabling membrane binding, a central RhoGAP domain and C-terminus with three proline rich domains which are Src homology 3 (SH3) binding sites that enables oligophrenin-1 to interact with proteins such as endophilin and amphiphysin (Billuart *et al*., 1998; Khelfaoui *et al*., 2009).

OPHN1: function/regulation

Oligophrenin-1 inactivates Rho signalling which is evident from its RhoGAP domain. It preferentially acts on RhoA, Rac1 and Cdc42 and negatively regulates their activity through

the RhoGAP domain by stimulating hydrolysis of GTP to GDP (Billuart *et al*., 1998). Inactivation of RhoA, Rac1 and Cdc42 by oligophrenin-1 inhibits their effector molecules (e.g. ROCK, PAK1 and N-WASP), leading to neurite extension or spine formation. Loss of oligophrenin-1 expression results in overactivity of Rho signalling thus leading to dendritic spine dysfunction or neurite retraction (see fig 1.1 & 1.2, Govek *et al*., 2004).

Oligophrenin-1: expression

Oligophrenin-1 is expressed in numerous species including human (Billuart *et al*., 1998), mouse (Fauchereau *et al*., 2003), rat (Govek *et al*., 2004) and guinea pigs (Xiao *et al*., 2003). Positive expression of oligophrenin-1 has been reported in many tissues including heart, kidney, liver, pancreas, human placenta, testis, lung, skeletal muscle and blood vessels (Billuart *et al*., 1998; Govek *et al*., 2004; Kohn *et al*., 2004). Up-regulation of the expression of oligophrenin-1 has also been reported in colorectal cancer tissue and glioblastomas, although the functional role of oligophrenin-1 in these tissues is unclear (Ljubimova *et al*., 2001; Pinheiro *et al*., 2001). Oligophrenin-1 is also present in the peripheral nervous system such as the enteric nervous system, sciatic nerve and vagus nerve (Xiao *et al*., 2003; Xiao *et al*., 2004). High levels of the protein are present in the developing brain and spinal cord. In adult tissue, oligophrenin-1 is expressed in all brain regions, particularly those associated with high plasticity (e.g. hippocampus and cortex) (Yuste and Bonhoeffer, 2001; Fauchereau *et al*., 2003). Oligophrenin-1 is expressed virtually in all neuronal cell populations including hippocampal dentate gyrus granule neurons and CA1, CA2 and CA3 pyramidal cells, cerebellar purkinje cells and neocortical pyramidal cells (Fauchereau *et al*., 2003; Govek *et al*., 2004).

Both neurons and glial cells express oligophrenin-1. In glial cells, oligophrenin-1 co-localises with stress fibres and cortical F-actin. In neurons, oligophrenin-1 is enriched in cell bodies, dendrites, dendritic spines and puncta in axons (Govek *et al*., 2004). Subcellular localisation studies reveal the presence of oligophrenin-1 in both the pre- and postsynaptic membrane where it co-localises with the F-actin network, which accumulates in dendritic spines (Fauchereau *et al*., 2003). Oligophrenin-1 is also present in synapses where its immunolabelling overlaps with synaptophysin (Govek *et al.*, 2004).

Ophn1 mouse model of mental retardation

To study the physiological role of oligophrenin-1, various models of *OPHN1* inactivation have been developed (Govek *et al*., 2004; Khelfaoui *et al*., 2007). To study the *in vivo* function of *OPHN1*, Khelfaoui *et al* (2007) generated a mouse model with an *Ophn1* gene loss of function by inserting junk DNA into the coding sequence of the oligophrenin-1 protein. This model recapitulates some of the phenotypes observed in human patients such as ventricular dilatation, without cerebellar abnormalities.

Behavioural phenotype of Ophn-1$^{-/y}$ mice

Khelfaoui and colleagues (2007) performed a series of behavioural tests to assess exploratory, locomotor and emotional behaviours in *Ophn1* knockout mice. Anxiety-related behaviours were evaluated using the elevated O-maze, the dark-light box and the open field test, however no difference was observed. Exploratory and locomotor behaviours were assessed using the Y-maze and the actimeter which demonstrated novelty-driven hyperactivity in *Ophn*-1$^{-/y}$ mice. Furthermore, social interactions were evaluated using the

social memory test and the resident intruder test; the latter demonstrated *Ophn*-$1^{-/y}$ mice show unusually friendly behaviour towards intruders and are less aggressive. The paw preference test showed *Ophn*-$1^{-/y}$ mice have deficits in lateralization. The key finding from the behavioural tests in this study was the impaired spatial learning in *Ophn*-$1^{-/y}$ mice assessed using the Morris water maze (Khelfaoui *et al*., 2007).

Synaptic morphological phenotype of Ophn1

Oligophrenin-1 is enriched in synaptic terminals and plays a key role in regulating dendritic spine formation and maintenance (Govek *et al*., 2004). *In vitro* studies using *Ophn*-$1^{-/y}$ mouse neurons in acute hippocampal slices and knockdown of *Ophn1* in rat hippocampal slice cultures have shown a reduction in spine length and/or density in CA1 pyramidal neurons (Govek *et al*., 2004; Khelfaoui *et al*., 2007; Nadif Kasri *et al*., 2009) and dentate gyrus granule neurons (Powell *et al*., 2012). Spine phenotypes were observed by co-expressing *Ophn1* siRNA with green fluorescent protein (GFP) expression vector and imaged with two-photon microscopy (Govek *et al.*, 2004) or for acute slices, spines were visualised by filling neurons with Alexa 488 tracer and imaged with confocal microscopy (Powell *et al.*, 2012). Prolonged treatment (>48 hr) of slices with the ROCK inhibitor, Y-27632, rescues the dendritic spine phenotype (Govek *et al*., 2004), whereas short term treatment (20 minutes) has no effect (Powell *et al*., 2012). This mechanism of action of prolonged treatment is presumably through the RhoA/ROCK pathway. Loss of *Ophn1* removes the inhibition of RhoA and as a result increases ROCK activity, which causes the reduction in dendritic spine length and density. This effect is presumably due to myosin light chain phosphorylation promoting

actin-myosin contraction (Govek *et al*., 2004) or due to phosphorylation of LIMK and inactivation of cofilin (Maekawa *et al.*, 1999).

Physiological phenotype of Ophn1 deficiency

In addition to regulating actin dynamics through Rho GTPases, oligophrenin-1 has other important physiological roles in the regulation of synaptic activity. This protein regulates the availability of synaptic vesicles in the pre- and postsynaptic terminal (Khelfaoui *et al*., 2009; Powell *et al*., 2012). Presynaptic deficits in vesicle dynamics have been observed in numerous *Ophn*-$1^{-/y}$ hippocampal neurons. Synaptic transmission is reduced in dentate gyrus granule neurons and CA3 pyramidal neurons as a result of a smaller readily releasable pool (RRP) of synaptic vesicles and altered vesicle dynamics (Saintot, 2010; Powell *et al*., 2012). Oligophrenin-1 also regulates kinetic efficiency of synaptic vesicles by interacting with several molecules involved in clathrin-mediated endocytosis (Khelfaoui *et al*., 2009; Nakano-Kobayashi *et al*., 2009). Endophilin A1, amphiphysin II and CIN85 are proteins involved in various phases of synaptic vesicle endocytosis that interact and form complexes with oligophrenin-1 through the BAR/PH domain (Khelfaoui *et al*., 2009; Nakano-Kobayashi *et al*., 2009). Overactivation of the RhoA/ROCK pathway due to knockout of *Ophn1* results in reduced endocytosis of synaptic vesicles and vesicle recycling in the pre- and postsynaptic terminal (Khelfaoui *et al*., 2009).

Oligophrenin-1 also regulates the endocytosis of α-amino-3-hydroxy-5-methyl-4-isoxasole-propionic acid (AMPA) receptor subunit GluR1 at the postsynaptic terminal. Loss of function of oligophrenin-1 results in reduced AMPA receptor endocytosis (Khelfaoui *et al*., 2009).

Postsynaptic oligophrenin-1 has been shown to be important in plasticity of excitatory synapses through regulation of functional and structural stability by controlling AMPA receptor stabilisation. Lack of *Ophn1* inhibits maturation of glutamatergic synapses and thus impairing synaptic structure and function (Nadif Kasri *et al*., 2009). Oligophrenin-1 has also been shown to interact with Homer, a postsynaptic adaptor protein, which is involved in glutamate receptor complexes and influences dendritic spine formation and synaptic transmission (Govek *et al*., 2004). Interaction between the RhoGAP of oligophrenin-1 and Homer are important for regulating low frequency synaptic function but not mGluR-LTD. These interactions are thought to regulate AMPA receptor stabilisation at the synapse (Nadif Kasri *et al*., 2011).

In presynaptic knockdown of *Ophn1*, an increase of synaptic depression is observed under short-term high frequency stimulation at the Schaffer collateral/CA1 glutamatergic synapses (Nakano-Kobayashi *et al*., 2009). In *Ophn*-$1^{-/y}$ slices, paired pulse facilitation is reduced, suggesting impaired presynaptic neurotransmitter release (Khelfaoui *et al*., 2007). mGluR-dependent long term depression (LTD) induced by (S)-3,5-dihydroxyphenylglycine (DHPG) and long term potentiation (LTP) are unaffected whereas N-methyl-D-aspartate (NMDA)-dependent LTD, induced by low frequency stimulation is impaired in *Ophn*-$1^{-/y}$ slices (Khelfaoui *et al*., 2007; Khelfaoui *et al*., 2009). However, knockdown of *Ophn1* in CA1 pyramidal neurons reduced mGluR-dependent LTD (Nadif Kasri *et al*., 2011). The difference in mGluR-dependent LTD could be due to different methods of induction.

Loss of *Ophn1 in vitro* led to a reduction in spontaneous and evoked excitatory and inhibitory neurotransmission in dentate gyrus granule neurons (Powell *et al*., 2012) and CA3 pyramidal neurons (Saintot, 2010). The reduction in inhibitory transmission was associated with impaired synaptic vesicle dynamics and smaller RRP. Spontaneous and kainate-induced gamma oscillations are also reduced in *Ophn*-$1^{-/y}$ slices in the CA3 region. The deficit is presumably due a reduction in synaptic strength which arises from the smaller RRP size and slower vesicle recycling in CA3 neurons. The smaller RRP also means that inhibitory postsynaptic potentials (IPSPs) run down with repetition in the beta-gamma range (Saintot, 2010).

Oligophrenin-1 and GABAergic synapses

Localisation studies of oligophrenin-1 at synapses do not specify whether it is present in excitatory or inhibitory synapses (Govek *et al.*, 2004). Markers for excitatory synapses such as vesicular glutamate transporter 1 and 2 (VGLUT1 and VGLUT2) or for inhibitory synapses such as glutamic acid decarboxylase 65 (GAD65) have not been used to identify whether oligophrenin-1 is present in both types of synapses. Co-localisation studies of oligophrenin-1 and synaptophysin were at dendritic spines, which would suggest oligophrenin-1 is present in excitatory synapses (Govek *et al.*, 2004). This is supported by the many excitatory deficits outlined above. However given that deficits in inhibitory transmission have also been identified in hippocampal studies examining CA3 pyramidal cells and dentate gyrus granule neurons (Powell *et al.*, 2012; Saintot, 2010), this would suggest oligophrenin-1 is also present in inhibitory synapses. The reduced inhibitory postsynaptic current (IPSC) frequency

was associated with a presynaptic deficit due to a smaller RRP and altered vesicle dynamics, suggesting oligophrenin-1 is at least expressed in inhibitory presynaptic terminals.

Treatments of MR

In dentate gyrus granule neurons, application of Y-27632 to *Ophn*-$1^{-/y}$ slices rapidly reverses the inhibitory synaptic deficits and restores the RRP size and vesicle replenishment rate (Powell *et al*., 2012). Application of Y-27632 also rescues the reduction in spontaneous gamma oscillations (Andrew Powell, personal communication). The reversal of several synaptic dysfunctional and dendritic spine phenotypes with the ROCK inhibitor may provide potential therapeutic intervention for MR. At present, no pharmacological intervention is available for most forms of MR and the current treatment is primarily through educational therapy to improve cognitive performance, enabling patients to achieve maximum potential (Inlow and Restifo, 2004). This may be due to the limited understanding of the pathophysiology of cellular and molecular basis of MR. Better understanding of these processes could enable better pharmacotherapy. Recent studies suggest that several phenotypes associated with learning disabilities in mouse models of Fragile X syndrome and Rett Syndrome can be reversed through pharmacotherapy and gene therapy (Dolen *et al*., 2007; Guy *et al*., 2007). Dolen and colleagues (2007) demonstrated that behavioural deficits (e.g. susceptibility to audiogenic seizures) and synaptic phenotypes (e.g. exaggerated hippocampal mGluR-LTD, increased spine density and exaggerated plasticity) could be corrected by reducing levels of mGluR5, which reduces mGluR induced excessive FMRP protein synthesis, characteristic of Fragile X syndrome. Whether these are feasible for ameliorating learning disabilities in humans remains unknown.

1.5 Hippocampal network physiology

Previous studies of examining *Ophn1* physiology have focussed primarily on hippocampal function (Govek *et al.*, 2004; Powell *et al.*, 2012). The hippocampus is critical to many functions, including learning and memory. It is defined by its unidirectional laminar structure; comprised of multiple layers, with the pyramidal cell bodies localised to the stratum pyramidale, basal dendrites in the stratum oriens and the apical dendrites projecting into the stratum radiatum. The major input into the hippocampus arises from the entorhinal cortex via the perforant pathway. The axons project to dentate gyrus granule cells and CA3 pyramidal cells, although they also input to CA1 and the subiculum. Granular cells of the dentate gyrus project onto CA3 pyramidal cells. These axons form the mossy fibre pathway that terminates on CA3 apical dendrites. CA3 pyramidal cells project axons to CA1 pyramidal cell apical dendrites via the Schaffer collaterals and to CA1 pyramidal cells of the contralateral hippocampus via the associational commissural pathway. The primary output from the hippocampus is from CA1 projecting to the subiculum and onto the entorhinal cortex (Shepherd, 2004).

1.6 Neuronal oscillations

Various electroencephalography (EEG) studies from MR patients show abnormal cortical brain activity (Huttenlocher, 1974; Wittwer *et al.*, 1996; Cantagrel *et al.*, 2004; Babiloni *et al.*, 2010). Patients display weaker/abnormal alpha, beta and theta rhythms. Altered oscillatory activity in the neocortex, namely gamma oscillations, has been demonstrated in patients with MR related pathologies such as autism and William syndrome; Grice and colleagues (2001) observed that affected individuals do not show gamma burst activity during visual processing tasks. At present, EEG studies examining abnormal neuronal oscillations have not been studied in *OPHN1* patients. However it has been identified *in vitro* that inhibitory synaptic transmission in *Ophn*-$1^{-/y}$ synapses fails at high frequencies fundamental to oscillations associated with cognitive functions (Saintot, 2010). These were due to a decrease in the RRP of synaptic vesicles and reduced vesicle recycling at inhibitory synapses (Saintot, 2010).

Network oscillations in the gamma range (30-100 Hz) are thought to underlie higher cognitive function such as encoding and retrieving episodic memory, attention and learning (Herrmann *et al*., 2004). Gamma oscillations have extensively been studied in the hippocampus (Bragin *et al*., 1995; Csicsvari *et al*., 2003), although they occur in all cortical regions (Gray and Singer, 1989; Buzsaki and Draguhn, 2004). Hippocampal gamma oscillations have been shown to be evoked during exploratory behaviour and spatial navigation (Jensen and Lisman, 1996; Buzsaki *et al*., 2003; Csicsvari *et al*., 2003) and require rhythmic synchronised neuronal activity (Bartos *et al*., 2007).

Models of gamma oscillations

In order to elucidate the underlying mechanisms of *in vivo* gamma oscillations, various methods can be used to evoke gamma oscillations *in vitro* such as chemical agonists which act on metabotropic glutamate receptors (mGluRs)(Whittington *et al*., 1995), muscarinic acetylcholine receptors (mAChRs)(Fisahn *et al*., 1998) and kainate receptors (KARs)(Fisahn *et al*., 2004), electrical stimuli such as tetanic stimulation (Traub *et al*., 1996; Traub *et al*., 1999), altering the ionic composition (e.g. application of high potassium solution (Lebeau *et al*., 2002) or removal of calcium ions (Traub *et al*., 2004)) or they can occur spontaneously (Pietersen *et al*., 2009). The various methods of inducing gamma oscillations pharmacologically differ in their reliance on excitatory and/or inhibitory synaptic transmission, depending on the synaptic connectivity and the distribution of receptors (Bartos *et al*., 2007). The agonists provide tonic activation of receptors which excite pyramidal cells and/or interneurons. Hippocampal oscillations have been most extensively (but not exclusively) studied in the CA3 region, which consists of a broader network of glutamatergic synapses than the CA1 which are required for phasic excitation. mGluRs and KARs are primarily located on interneurons whereas mAChR agonists act on principal neurons (Bartos *et al*., 2007).

The Kainate model of gamma oscillations

Previous studies investigating gamma oscillations in *Ophn1* mice used the kainate model to evoke gamma oscillations (Saintot, 2010). The kainate model of gamma oscillations is a commonly used method for generating CA3 gamma oscillations. Kainate is an excitatory amino acid which acts on KARs. Tonic activation of KARs evokes hippocampal and neocortical

gamma oscillations *in vitro* (Fisahn, 2005). Kainate receptors are extensively expressed at both pre- and postsynaptic sites of hippocampal pyramidal neurons and interneurons. These receptors consist of five subunits which are formed from glutamate subunits (GluR5-7) and kainate subunits (KA1-2)(Fisahn, 2005). Hippocampal CA3 neurons express high levels of KAR and activation of KARs directly increases the excitability of interneurons and pyramidal cells (Traub *et al*., 2004).

Gamma oscillations are dependent on inhibition mediated by $GABA_A$ receptors and inhibitory interneuron networks are thought to generate gamma oscillations (Bartos *et al*., 2007). Kainate-induced gamma oscillations rely solely on inhibition mediated by $GABA_A$ receptors as bicuculline, a $GABA_A$ receptor antagonist, completely abolishes gamma oscillations but the strength of the oscillations are unaffected by AMPA receptor antagonists (Fisahn *et al*., 2004). Parvalbumin expressing fast spiking basket cells have been shown to be important for gamma oscillation generation; these are abundant and form extensive networks of mutually connected interneurons (Bartos *et al*., 2007) Experimentally, this interneuronal network activation occurs due to excitatory drive, under physiological conditions the drive originates from pyramidal cells and these networks generate rhythmic synchronisation irrespective of rhythmicity of the excitatory drive (Fries *et al*., 2007). These types of basket cells also have wide branching contacts with many pyramidal cells, therefore they can impose inhibition onto the pyramidal cells as well as the local network of interneurons. Thus, inhibitory synapses between basket cells are able to synchronise the firing of action potentials within the interneuron network and basket-pyramidal cell inhibitory connections can enable distribution of this synchronised activity to the population

of pyramidal cells. Basket cells are also capable of firing ~1 action potential per gamma cycle which are phase locked to the gamma oscillations (Bartos *et al*., 2007). Pyramidal cells can only fire during the time window where inhibition is fading. Interneurons will fire with some phase delay, approximately several milliseconds after the pyramidal cells. The consequential network inhibition halts the firing of action potentials from pyramidal cells and interneurons, inhibiting the entire network and the following gamma cycle begins once inhibition has faded (Fries *et al*., 2007).

1.7 The neocortex and MR

Neocortical functional deficits have been reported in many MR models that also display behavioural deficits (Wijetunge *et al.*, 2013; Boggio *et al.*, 2010). Functional and behavioural deficits have been described in *Ophn1*-null mice, however neocortical function remains unexplored. Alterations in neocortical thickness have been implicated in *Ophn1* null mice and the impact of this on neocortical network function and how these translate to behavioural deficits is still unclear. Insight into the role of oligophrenin-1 in synaptic function in the neocortex could help explain its role in regulating aspects of normal cognitive function.

The neocortex is involved in higher level cognitive functions such as spatial reasoning, conscious thought and awareness, sensory processing, motor function and in humans, language. Its major role is to integrate and analyse sensory information via the thalamus, taking into account previous experiences together with planning and directing suitable

responses. It integrates simple functions and analyses the inter- and exteroreceptive environment (Kirkcaldie, 2012). The neocortex is organised into four large-scale lobes: frontal, parietal, temporal and occipital. Functionally, each of these regions are involved in motor, somatosensory, auditory and visual functions, respectively. However the function of each region goes beyond sensorimotor systems; there are various areas within the neocortex. For example, association cortices are involved in more complex functions including attention, emotion and memory (Crossman, 2005).

Composition of the neocortex

The neocortex is comprised of glia and neurons. Populations of neurons are extremely heterogeneous that can be categorised into one of two basic groups: spiny/excitatory and aspiny/inhibitory neurons. The former includes spiny stellate cells, and pyramidal cells which account for approximately 70-80% of neurons in the neocortex, receiving excitatory input with axons descending radially in the cortex (Connors and Gutnick, 1990). They are the major cells that project out of their local areas to other brain regions (DeFelipe and Farinas, 1992). Inhibitory interneurons are generally involved in local circuits (Markram *et al*., 2004), but some interneurons have long range axons projecting to other distant cortical areas in the ipsi- and contralateral hemisphere (Tamamaki and Tomioka, 2010).

Laminar organisation

The neocortex is organised into a laminar structure, comprising of six distinct layers which are underlined by white matter that is composed of glia and axons (fig 1.3). Layer I is the thin, outer layer of the cortex that resides below the pia, consisting of a few neurons which

are predominantly inhibitory and mainly synapse with dendrites of cells from deeper layers. This layer is sparsely populated with somas (Kirkcaldie, 2012) and is mostly composed of horizontal axons running across the cortex from within the cortex and thalamic projections (Rubio-Garrido *et al*., 2009). Layers II and III are treated as a single layer in mice and cells that reside here are predominantly involved in local circuits and connections between cortical regions (Kirkcaldie, 2012). Almost all cell types (spiny/excitatory and aspiny/inhibitory neurons) of the neocortex are found in this layer except cells exclusively located in layer I (e.g. Cajal Retzius interneurons) and excitatory spiny stellate neurons (Swanson, 2003; Markram *et al*., 2004), although layer II/III is mostly composed of small pyramidal cells. Layer IV, is the primary layer for receiving extra-cortical input mainly from the thalamus, as well as other subcortical structures such as the basal ganglia (Douglas and Martin, 2004). It has a range of inhibitory neurons and is the exclusive location of small excitatory spiny stellate cell (Markram *et al*., 2004). Layer V mainly consists of large pyramidal neurons, but also a selection of inhibitory neurons (Markram *et al*., 2004; Kirkcaldie, 2012). The pyramidal cells have axons projecting to numerous cortical and subcortical targets; the latter structures include the striatum, brainstem and spinal cord. Depending on the projections of layer V neurons, the layer is subdivided into Va, composed of corticostriatal pyramidal cells and Vb, comprising of corticospinal pyramidal cells (Molnar and Cheung, 2006). Layer VI is composed of various cells, principally large pyramidal neurons that have axons projecting back to the thalamus and in return have strong thalamic input. Pyramidal cells in this layer also receive input from all cortical layers (Thomson, 2010). Layer VI is also composed of (basket cell) interneurons that form an inhibitory network for excitatory cells within the layer (Kirkcaldie, 2012).

Layer V neurons and intracellular tracers

Layer V pyramidal cell apical dendrites extend into layers I-IV and basal dendrites ramify within layer V. Given that layer V pyramidal neurons span the majority of the thickness of the neocortex, these neurons are ideal to be able to relate neuronal morphology to function and neocortical thickness. Within layer V, a heterogeneous population of neurons are present which can be identified by their morphology. Intracellular tracers can be used to identify cell types and to study neuronal morphology. Tracers enable electrophysiological characterisation to be combined with morphological analysis. The ideal tracer for neuronal labelling needs to diffuse rapidly into the cell, survive histological processing and most importantly, not affect electrophysiological characteristics of the neurons; neurobiotin fulfils most of these criteria.

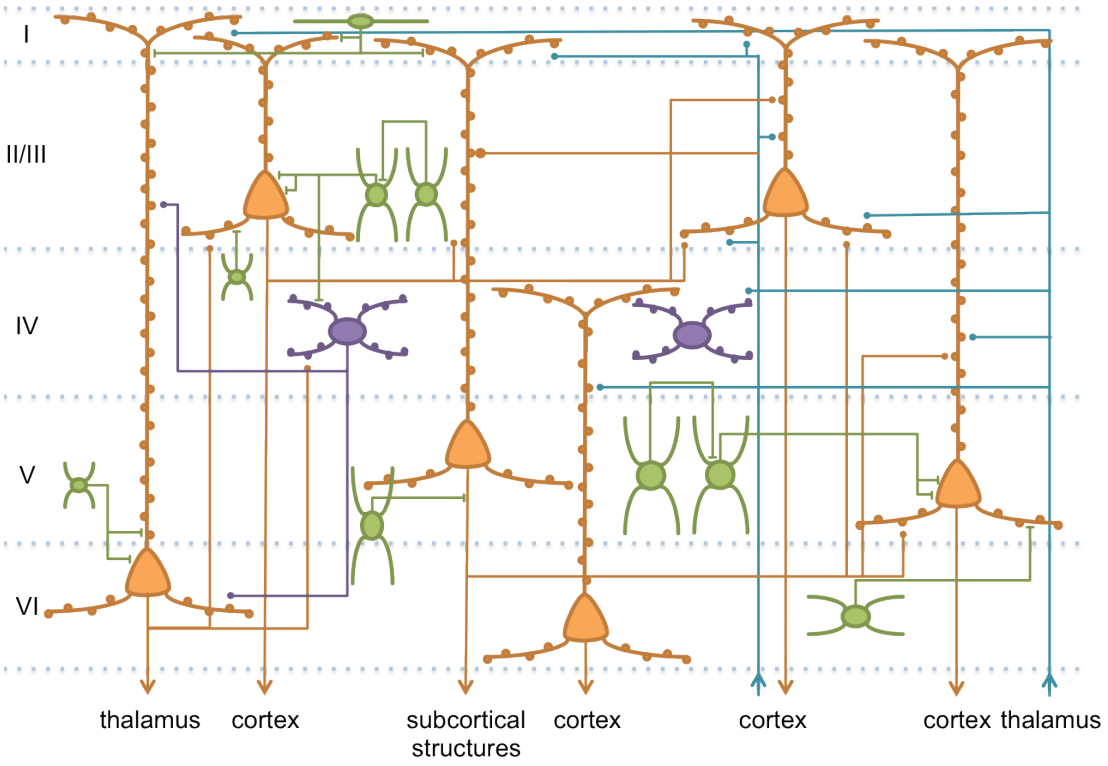

Figure 1.3 – Neocortical connections and circuits.

Schematic diagram outlining some of the known synaptic connections in the neocortex. Orange and purple lines are excitatory connections and green lines are inhibitory connections. Orange cells are spiny pyramidal, purple are spiny stellate and green are aspiny interneurons. Blue lines represent thalamocortical and corticocortical connections. Arrows pointing downwards indicate projections leaving the cortex and arrows pointing upwards represent afferent input to the cortex. Adapted from Kirkcaldie, 2012.

Unanswered questions

Alterations in synaptic activity (particularly excitatory) associated with reduced oligophrenin-1 expression are well documented in hippocampal neurons (Powell *et al.*, 2012; Saintot, 2010; Nadif Kasri *et al.*, 2009). However nothing is known about synaptic activity in the neocortex. The loss of neocortical tissue associated with the *Ophn1* model argues for investigating functional changes in the neocortex. A number of studies have described alterations in spine dynamics (Powell *et al.*, 2012; Khelfaoui *et al.*, 2007; Govek *et al.*, 2004), but only one study has addressed reduced dendritic morphology in *Ophn1* mice (Powell *et al.*, 2012). Dendritic arborisation of neocortical neurons is of interest as it could account for neocortical thinning.

Although it is essential for this study to examine neuronal morphology, there is some evidence that certain tracers (e.g. Lucifer yellow, neurobiotin) compromise electrophysiological recordings, namely, prolong action potential duration (Tasker *et al.*, 1991; Xi and Xu, 1996). It is not known whether lower concentrations of these tracers can minimise the effect on electrophysiological recordings without compromising morphology.

Expansion of the cerebral ventricles, typically associated with hydrocephalus, and apparent neocortical thinning has been reported in many *OPHN1* patients (Bergmann *et al.*, 2003) and *Ophn1* mice (Khelfaoui *et al.*, 2007). Despite the commonality of these phenotypes, no systematic study of brain morphology has been conducted, neither has the impact of altered ventricles and neocortex on the gross brain anatomy.

1.8 Hypotheses

The working hypothesis was that, similar to hippocampal neurons, a reduction in excitatory and inhibitory synaptic transmission in neocortical neurons would be associated with a reduced dendritic arborisation of layer V pyramidal neurons. Secondly, that *Ophn1* neuronal morphology could be examined using a lower concentration of neurobiotin that would not alter action potential duration and still enable morphological characterisation of neurons. Finally, that ventricular dilatation in *Ophn1* mice would alter brain morphology.

1.9 Aims

The aims of this study were four-fold; firstly, to examine whether loss of oligphrenin-1 in neocortical neurons affected synaptic activity and the dendritic complexity of neurons. Secondly, to determine whether alterations in dendritic arborisation could provide a link to alterations in gross anatomy. In order to answer these questions, a suitable intracellular tracer needed to be identified to combine electrophysiological characterisation of synaptic function with morphological analysis of the recorded neuron. Finally, to conduct a systematic analysis of brain anatomy in *Ophn1* mice to determine the impact of loss of oligophrenin-1 function on brain morphology.

To address these questions, whole-cell patch clamp recordings were made from layer V pyramidal neurons. Layer V pyramidal neurons were selected as they span the length of the neocortical thickness and thus were ideal to be able to relate neuronal morphology to

neocortical thickness. Initially, the impact of intracellular tracers on electrophysiological properties has been examined and a methodology has been established that enables neuronal identification and electrophysiological characterisation. Electrophysiology has been combined with morphology using intracellular tracers to address whether synaptic dysfunction was present in *Ophn*-$1^{-/y}$ neurons and if so, whether it was associated with altered dendritic arborisation. A comparative study has been conducted between neocortical neurons and hippocampal neurons using whole-cell patch clamp recordings and extracellular field potentials to compare phenotypes between the two regions. Finally, the gross anatomical phenotype has been examined in *Ophn1* mice using histological techniques.

Chapter 2: Materials and Methods

2.1 Experimental animals & slice preparation

Generation of Ophn1 knockout mice

Ophn-$1^{-/y}$ mice were produced as previously described (Khelfaoui *et al*., 2007). Briefly, *Ophn1* gene was constitutively inactivated by homologous recombination. Insertion of 100 base pair junk DNA within the coding sequence of exon 9 disrupts the open reading frame and leads to a premature STOP codon resulting in a frameshift mutation. Junk DNA was inserted after the BAR domain and before the PH and RhoGAP domains. Embryonic stem cells expressing homologous recombination constructs were implanted in females. Male chimeras were backcrossed for at least 8 generations.

Breeding

Ophn-$1^{+/y}$ and *Ophn*-$1^{-/y}$ mice were generated by breeding heterozygote females (*Ophn*-$1^{+/-}$ from C57/Bl6 background) with C57/Bl6 wild type males (*Ophn*-$1^{+/y}$), generating male progeny with an approximate ~50:50 *Ophn*-$1^{+/y}$:*Ophn*-$1^{-/y}$ ratio. Male mice were housed in litters (up to 8 per cage) regardless of genotype under standard conditions with water available *ad libitum*. C57/Bl6 wild type males were purchased from Charles River (Margate, UK). Breeding and experiments were performed under regulation by the Animals (Scientific Procedures) Act (1986) of the UK, and approved by institutional ethical review. Experiments and analysis were performed blind to genotype.

Genotyping

The genotype of mice were determined by polymerase chain reaction (PCR) analysis using DNA extracts from ear snips and were confirmed with post-mortem tail biopsies. To prepare DNA, tissue extracts were digested in 0.25 ml of lysis buffer comprising (in mM) 100 Tris (pH 8.5), 200 NaCl, 5 EDTA, 0.2% SDS and 1 µl proteinase K (0.1mg/ml) overnight at 55°C. Digested tissue was centrifuged (Thermo Scientific; Waltham, MA, USA) for 5 minutes at 13000 rpm at room temperature. The supernatant was removed and added to an equal volume of isopropanol and gently mixed, then centrifuged for 30 minutes at 13000 rpm. The supernatants were removed and the DNA pellet was washed with 100% ethanol. Ethanol was removed and DNA was dried for 15 minutes at ~55°C. DNA was reconstituted in 50 µl of nuclease-free water (Promega, Southampton, UK) and incubated at 50°C for 5 minutes. PCR reactions were carried out in 20 µl volume using 1 µl DNA, 1 µl forward primer (gcc cat gtt gtg agc aga gaa atc; Sigma-Aldrich; Poole, UK) and 1 µl reverse primer (gga agc tag agg atg acc ctg; Sigma-Aldrich) which flanked the *Sma*I position and 17 µl of PCR Reddymix Master Mix (comprising: 1.25 units thermoprime plus DNA polymerase, 0.2 mM of each dNTPs, 1.5 mM $MgCl_2$, 75 mM Tris-HCl pH 8.8, 20 mM $(NH_4)_2SO_4$, 0.2 mM Tween 20; Thermo Scientific).

Polymerase Chain Reaction

DNA was amplified in a PCR machine (Bio-Rad Laboratories, Hercules, CA, USA). An initial denaturation of DNA was carried out at 94°C for 3 minutes followed by 35 cycles of PCR as follows: denaturation at 94°C for 30 seconds, annealing at 55°C for 30 seconds, elongation at 72°C for 30 seconds; and a final elongation at 72°C for 5 minutes.

DNA samples were loaded onto a gel comprising 2% agarose in 1x tris-borate-EDTA (TBE) buffer (pH 8.4) and 1.5 µl of GelRed (Biotium; Hayward, CA, USA) per 100 ml of TBE, which stained nucleic acids. The gel was run in 1x TBE for 1 hour at constant voltage of 160 V. Samples were visualised by UV illumination using a Multi Genius Bio-Imaging System and GeneTools imaging software (Syngene; Cambridge, UK).

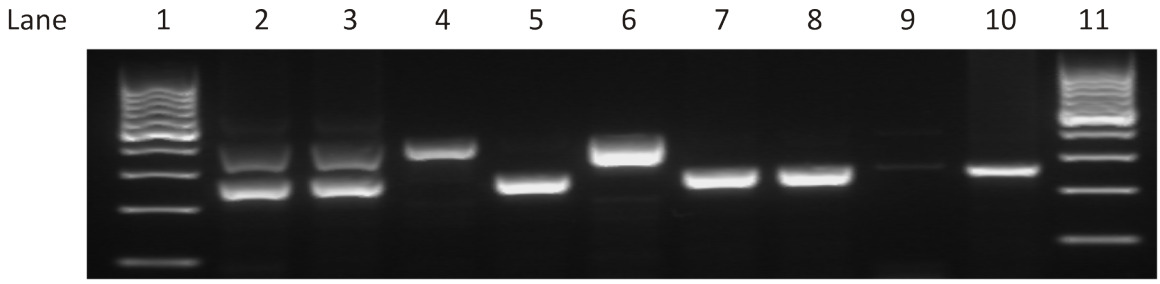

Figure 2.1 – Genotypes of *Ophn1* mice.

An example of the genotyping results for wild type (+/y), knockout (-/y) and heterozygote (+/-) mice. Lanes 1 and 11 are DNA ladders, lane 3 is a female and 4-8 are male. Lane 2 is a heterozygote control, lane 9 is a blank control (ddH_20) and 10 is a positive wild type control. Wild type mice consist of only lower band, knockout mice consist of only upper band and both bands represent heterozygotes.

Hippocampal and cortical slice preparation and maintenance

Ophn-$1^{+/y}$ and *Ophn*-$1^{-/y}$ mice (3-6 weeks) were anaesthetised with medetomidine (1mg/kg) and ketamine (76mg/kg) by intraperitoneal injection. Mice were intracardiacally perfused with ~5 ml of ice cold sucrose artificial cerebral spinal fluid (aCSF; composition in mM: 189 sucrose, 26 $NaHCO_3$, 2.5 KCl, 5 $MgCl_2$, 0.1 $CaCl_2$, 1.2 NaH_2PO_4, 10 glucose; gassed with

95%O_2-5%CO_2), at a flow rate of ~2.7 ml min^{-1}. Death was confirmed by cervical dislocation. Brains were removed and the dorsal surface was glued to the stage of the slicing chamber. The chamber contained ice cold (~1°C) sucrose aCSF, gassed with 95%O_2-5%CO_2. Horizontal slices (400 µm thick hippocampal slices for extracellular recordings, 300 µm thick cortical slices for whole-cell recordings) were cut from the ventral surface using a vibrating microtome (7000smz, Campden Instruments; Loughborough, UK). Slices containing the hippocampus and primary auditory cortex were selected; the appearance of the optic chiasm (OC) was used as a marker to localise the ventral hippocampus. This slice was denoted as OC and the subsequent slice D1, as it is more dorsal, then D2, D3, etc.). Slices were transferred into an interface storage chamber containing aCSF (composition in mM: 125 NaCl, 3 KCl, 1 $MgCl_2$, 2 $CaCl_2$, 1.2 NaH_2PO_4, 26 $NaHCO_3$, 10 glucose) bubbled with 95%O_2-5%CO_2 at room temperature. Slices were left in the interface storage chamber for at least 1 hr before use and were used up to 8 hr after slicing.

2.2 Electrophysiology: Extracellular recordings

Slices were placed in a Haas-type interface recording chamber and visualised using a stereo microscope (Leica MZ8, Micro Instruments; Long Hanborough, UK) and allowed to equilibrate for an hour prior to recording. The chamber was constantly perfused with 95%O_2-5%CO_2 oxygenated aCSF at a flow rate of ~4 ml min^{-1} at approximately 30-32°C. Extracellular microelectrodes were pulled from thick-walled borosilicate glass capillaries (1.2 mm O.D. x 0.69 mm I.D.; Harvard apparatus, Edenbridge, Kent, UK) using a P-97 puller (Sutter Instruments Co; Novato, CA, USA). Electrodes were filled with aCSF and had a typical

resistance of 2-4 MΩ. Extracellular field potentials were recorded using AC-coupled amplifiers (NL-104, Digitimer Ltd; Welwyn Garden City, UK) and were low pass Bessel filtered at 1 kHz (NL-125, Digitimer) prior to digitisation at 10 kHz by a micro1401 (CED Ltd, Cambridge, UK). Stimulation and data acquisition were controlled using Spike2 software (v6.12; CED) or Signal software (v3.12; CED). Data were stored onto a computer hard drive for subsequent off-line analysis using Spike2 or Signal.

Gamma oscillations

One recording electrode was placed in the stratum pyramidale of CA3c and another was placed in the stratum radiatum of CA3c (fig 2.2). Electrodes were advanced into the slices to a depth of ~150 μm using mechanical micromanipulators (Narishige; Japan).

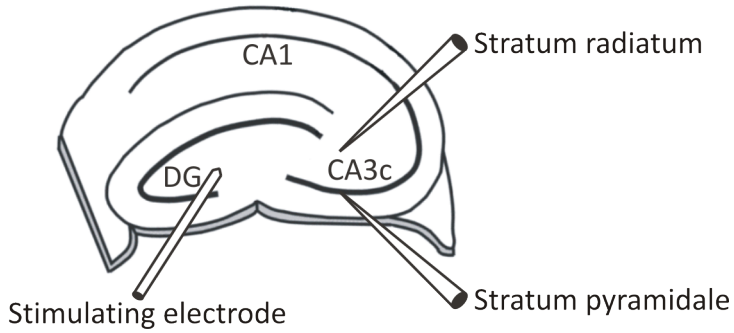

Figure 2.2 – Position of stimulating and recording electrodes in CA3c.

Schematic diagram of the hippocampal slice illustrating electrode placement. One recording electrode was placed in the stratum pyramidale of CA3c and the second was placed in the stratum radiatum of CA3c, approximately 150 μm away from the electrode in the stratum pyramidale. For evoked field potentials, a stimulus electrode was placed in the hilus.

Gamma oscillations were induced by bath application of 100 nM kainate for 60 minutes and were blocked by bath application of the $GABA_A$ antagonist, bicuculline (10 μM). Spontaneous gamma oscillations were recorded immediately after slicing or prior to addition of kainate; these were recorded for 60 minutes before application of kainate, or were evaluated as baseline recordings 5 minutes prior to kainate application.

Data analysis was performed using Spike2. The power of gamma oscillations were measured by performing fast Fourier transforms of 60 second epochs of data (Hanning window, FFT size 4096). Power spectra were generated which reveal how the strength of the signal is distributed across frequencies. The gamma band is in the frequency range 20-80 Hz and was quantified by peak frequency, peak power and summated power (fig 2.3). This band is lower than that used *in vivo* due to the low bath solution temperature used (~30-32°C) to ensure optimal slice viability. Spontaneous gamma oscillations were defined as present if summated power in the 25-35 Hz band was greater than summated power in the 10-20 Hz band (Pietersen *et al*., 2009).

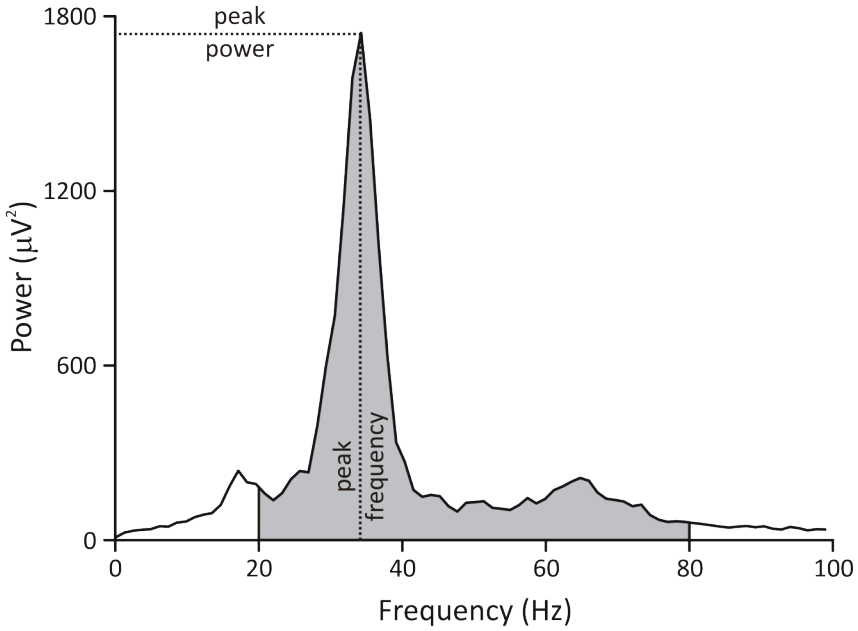

Figure 2.3 – Power spectrum of gamma oscillations.

Power spectrum generated from 60 second epochs of data following 60 min, 100 nM kainate application, illustrating how measurements were taken. Peak frequency was taken at the point where the power was the highest (peak power). Summated power corresponds to the area shaded in grey.

Evoked field potentials

The mossy fibre tract was stimulated using a nichrome concentric stimulating electrode (80% nickel/20% chromium, tip diameter 50 μm; Advent research materials; Oxford, UK) placed in the hilus. This pathway arises from the granule cells in the dentate gyrus and synapse with dendrites of CA3 neurons in stratum radiatum. Postsynaptic potentials (PSPs) were recorded from stratum radiatum in CA3c and population spikes were recorded from stratum pyramidale in CA3c. Figure 2.4 illustrates how the population spike amplitude and PSP slope were measured. Stimulus-response curves were generated to determine the half maximal

stimulus intensity values (20.8 ± 0.6 V, range 15-27 V, n=31). This intensity was used for subsequent paired pulse and high frequency stimulation recordings. PSP stimulus response curves were fitted using a Boltzmann function

$$(y = A_2 + (A_1\text{-}A_2)/(1 + \exp^{((x\text{-}0)/dx)})$$

where A_1 is the minimal value , A_2 the maximum response, x_0 the half maximal stimulus and *dx* the slope of the curve.

The paired pulse protocol consisted of two stimuli separated by a range of intervals (10-1500 ms). Pairs of stimuli were separated by 30 second intervals to allow sufficient recovery time (Bliss and Lomo, 1973). Paired pulse ratio (PPR) was calculated from the ratio of PSP_2 slope divided by PSP_1 slope. Figure 2.5 depicts how PSP slopes were measured from paired pulse recordings. High frequency stimulations were evoked by a train of 40 stimuli at 20 Hz, 33 Hz, 50 Hz and 100 Hz and PSP slopes were measured for the 1^{st}-10^{th}, 20^{th}, 30^{th} and 40^{th} response, and were normalised to the first response. Data analysis of postsynaptic potentials and population spikes were performed using Signal (v3.12; CED Ltd).

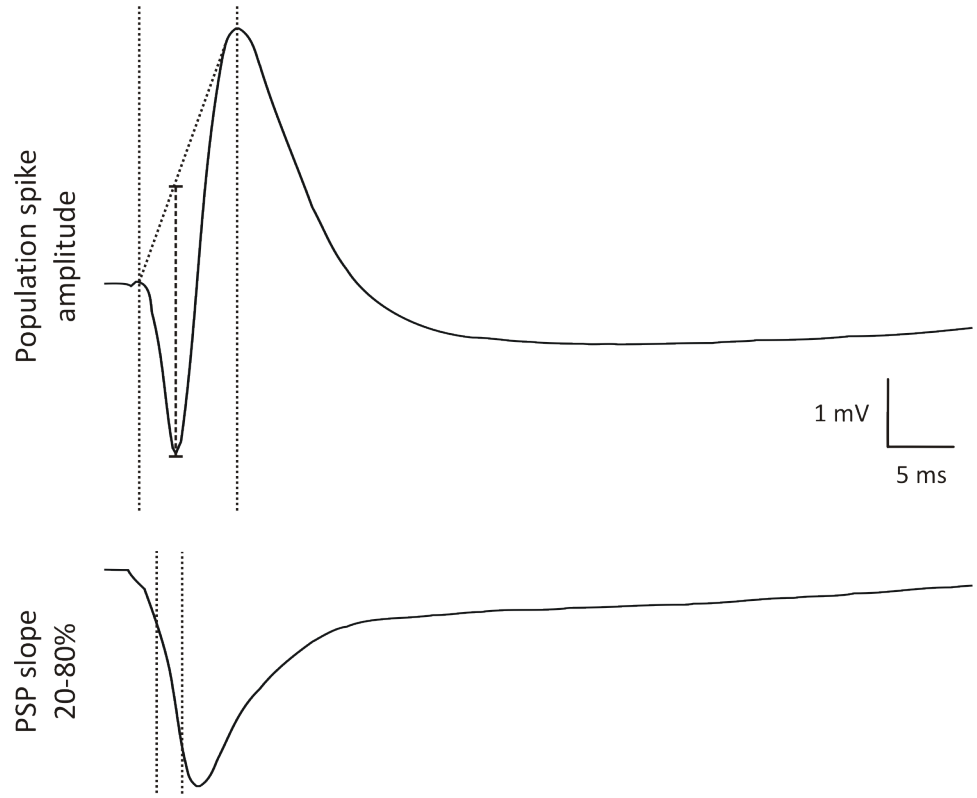

Figure 2.4 – Evoked field potential recordings from *Ophn*-1$^{+/y}$ slice.

Typical population spike recorded from the stratum pyramidale *(upper panel)* and PSP from the stratum radiatum *(lower panel)* in the CA3c region from an *Ophn*-1$^{+/y}$ slice. Dotted lines indicate where measurements were taken for the amplitude of the population spike and 20-80% PSP slope.

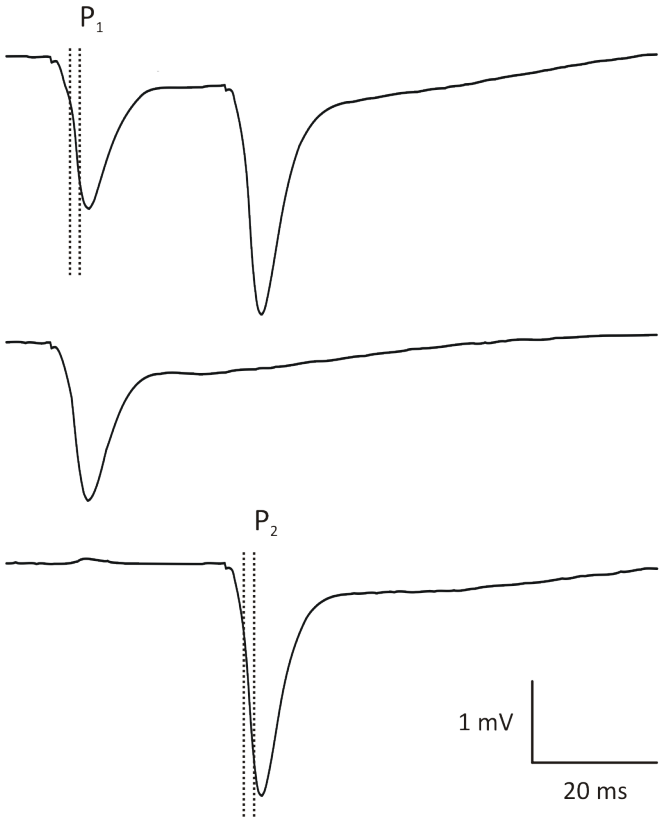

Figure 2.5 – Paired pulse recordings from *Ophn*-1$^{+/y}$ slice.

Unmodified trace *(upper panel)*, averaged trace *(middle panel)* and modified trace *(lower panel)* for PSPs recorded during paired pulse stimulation protocol. The dotted lines show where measurements were taken for PSP slopes. The unmodified trace shows the complete paired pulse response and the first PSP slope measured. The averaged trace was generated by averaging five consecutive responses to V_{50}. The modified trace was generated by subtracting the averaged trace from the unmodified trace, enabling the second PSP slope to be measured.

2.3 Electrophysiology: Whole-cell patch clamp recordings

Whole-cell patch clamp recordings were made from the somata of layer V pyramidal neurons in the primary auditory cortex (fig 2.6) or the upper/lower blade of the dentate gyrus, outer third molecular layer (as specified in the text) using infrared differential interference contrast (DIC; Olympus BX-51 upright microscope, fluorplan 40x, 0.8 NA water immersion lens; Micro Instruments). Slices were constantly perfused with 95%O_2-5%CO_2 oxygenated aCSF at a flow rate of ~4 ml min^{-1} at 30-32°C. Patch electrodes were pulled from borosilicate glass and typically had a resistance of 3-7 MΩ. Membrane potentials and currents were recorded using an NPI SEC-10L amplifier (Scientifica; Harpenden, UK) and were low-pass Bessel filtered at 1 kHz (NL-125 Digitimer Ltd) prior to digitisation at 10 kHz by a micro 1401 (CED). Stimulation and data acquisition were controlled using Signal software (v3.12; CED). Data were stored onto a computer hard drive for subsequent off-line analysis.

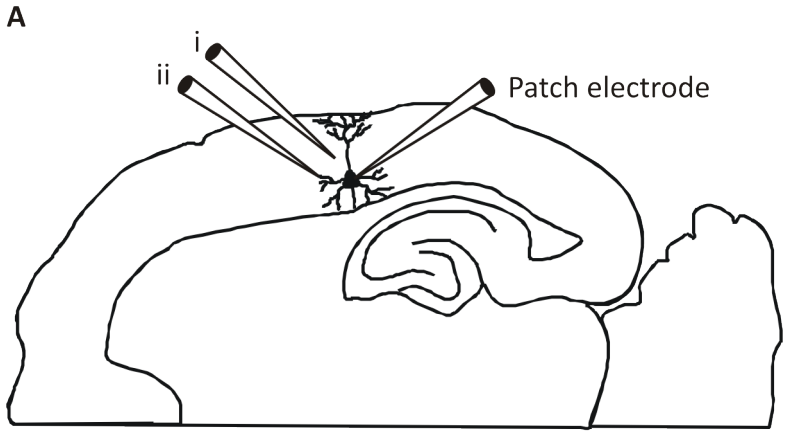

Figure 2.6 – Position of recording electrode and stimulating electrode in the neocortex.

Schematic diagram of horizontal cortical brain slice with patch recording electrode placed on the somata of a layer V neuron in the primary auditory cortex. For evoked recordings, the stimulating electrode was placed ~ 50 µm away from the soma (i) and for single synapse stimulation, 50 µm away from soma, next to an apical dendrite (ii).

Firing activity studies

To examine intrinsic properties of layer V neurons, the intracellular solution comprised (mM): 135 $KMeSO_4$, 8 NaCl, 2 Mg-ATP and 0.3 Na-GTP; pH 7.3 with 1 M KOH; osmolarity ~285 mosmol l^{-1}. Action potentials were elicited by a 200 ms 100-500 pA depolarising current injection, separated by 30 second intervals. Input resistance was measured by a 200 ms 10 pA hyperpolarising current injection. Action potential half widths, firing frequency and slow and fast afterhyperpolarisation (AHP) were measured (fig 2.7). Fast AHP was measured for the first action potential and slow AHP was measured as the potential 1 s after end of pulse. Cells were rejected if the action potential did not overshoot (peak amplitude less than

0 mV), had a high threshold (greater than -30 mV), input resistance changed by more than 20% or required more than 100 pA current injection to hold at -65 mV.

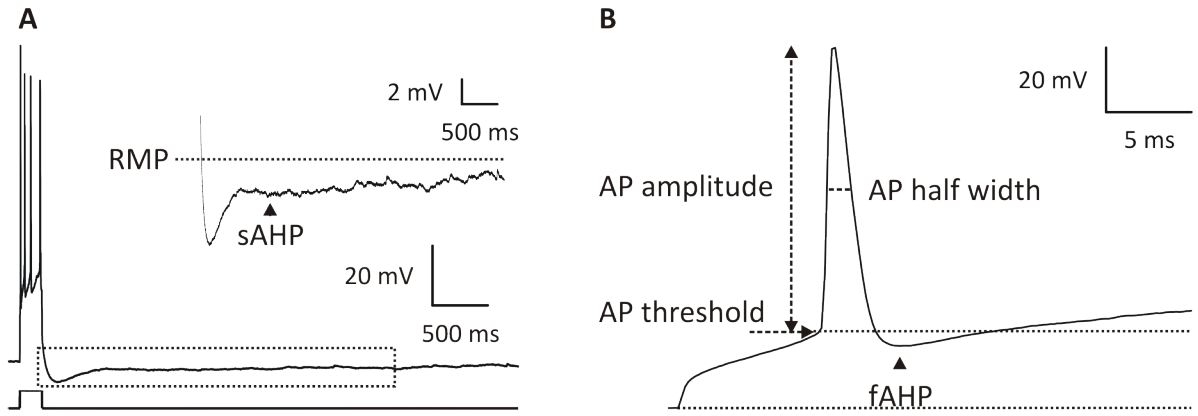

Figure 2.7 – Measurement of intrinsic properties of layer V neurons.

(A) Trace of action potentials evoked by 200 ms 300 pA depolarising current injection. Insert shows the slow afterhyperpolarisation (AHP) on expanded time scales. Slow AHP was measured as the potential difference between resting membrane potential *(dotted line)* and the point indicated. **(B)** First action potential on expanded time scale illustrating where fast AHP and action potential threshold, amplitude and half width were measured. Fast AHP was measured as the potential difference between the action potential threshold and the point indicated. RMP, resting membrane potential.

Spontaneous synaptic events

Spontaneous events (putative excitatory postsynaptic potentials, EPSPs) were recorded under whole-cell current clamp, between -63 to -67 mV. Events were identified using MiniAnalysis software (v6.0.3, Synaptosoft, Decatur, GA, US). Two minutes of recordings

were analysed from each viable cell. Events were automatically detected by the software and manually verified to ensure these were postsynaptic potentials; no difference was observed between the two ways of analysis. The amplitude and area detection threshold was set to five times greater than the root mean square of the baseline noise (typically 0.067 ± 0.002 mV^2, n=23).

Synaptic activity studies

Postsynaptic currents were recorded using whole-cell voltage clamp. For excitatory postsynaptic currents (EPSCs) the intracellular solution comprised (mM): 140 $CsMeSO_4$, 8 NaCl, 10 HEPES, 0.5 EGTA, 2 Mg-ATP, 0.3 Na-GTP and 5 QX-314; osmolarity ~285 mosmol l^{-1}; pH 7.3 with CsOH. EPSCs were recorded at -75 mV (the reversal potential of IPSCs). $GABA_A$ receptor antagonist picrotoxin (100 μM) was added to confirm isolation of EPSCs. These were blocked by NMDA receptor antagonist D-(-)-2-amino-5-phosphonopentanoic acid (D-APV, 25 μM) and AMPA receptor antagonist 2,3-dioxo-6-nitro-1,2,3,4-tetrahydrobenzo[f]quinoxaline-7-sulphonamide (NBQX, 20 μM). For IPSCs, the intracellular solution comprised (mM) 135 $CsCl_2$, 2 $MgCl_2$, 10 HEPES, 1 EGTA, 2 Mg-ATP, 0.3 Na-GTP and 5 QX-314; osmolarity ~285 mosmol l^{-1}; pH 7.3 with CsOH. IPSCs were recorded at -80 mV. The high chloride shifted the reversal potential to 0 mV, resulting in inward IPSCs at -80 mV. D-APV (25 μM) and NBQX (20 μM) were added to the external solution to isolate IPSCs. These were blocked by bicuculline (10 μM). Miniature IPSCs were isolated by superfusion of tetrodotoxin (TTX, 1 μM) to the aCSF.

Access resistance was measured by a 200 ms 10 mV hyperpolarising current injection. Cells were rejected if access resistance or holding current changed by more than 20% of the initial value after establishing the whole-cell configuration. Five minutes of data were analysed from each viable cell. Postsynaptic currents were manually detected using MiniAnalysis software (Synaptosoft). The amplitude and area detection threshold was set to five times greater than the root mean square of the baseline noise.

Evoked postsynaptic currents

Cells were stimulated using a patch electrode filled with aCSF. The stimulating electrode was placed 50 µm away from the soma, parallel to long axis of the cell, 20 µm deep from the slice surface. The amplitude of the evoked EPSCs were measured (fig 2.8) and a stimulus response curve was produced. The data were fitted to a sigmoid curve

$$y = A1 + (A2-A1)/(1+10^{((LOGx0-x)*p)}$$

where A1 is the maximum amplitude, A2 the minimal value, p is the slope and $\log_{x0}$ is the V_{50}. The V_{50} value was determined for each slice and used for subsequent paired pulse and frequency following experiments. Paired pulse experiments consisted of two stimuli delivered at inter-pulse intervals between 10-1500 ms, separated by 30 second intervals. To determine the amplitude of the second evoked postsynaptic current, digital subtraction was performed as described in figure 2.5 and paired pulse ratio was estimated as described for extracellular evoked recordings (see section 2.2 *evoked field potentials*). High frequency stimulation protocol consisted of a train of 10 stimuli at 10 Hz, 20 Hz, 33 Hz, 50 Hz and 100 Hz. The amplitude of individual evoked postsynaptic currents were measured and normalised to the first response.

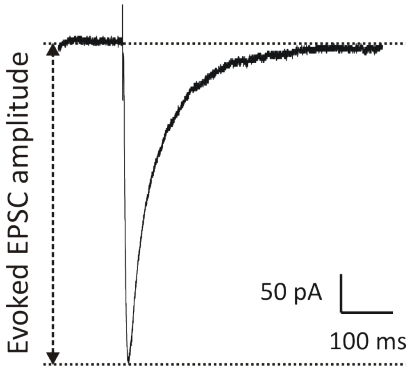

Figure 2.8 – Measurement of evoked EPSC.

Trace of evoked EPSC from a layer V pyramidal neuron, following a 30 V stimulus. The stimulating electrode was placed 50 µm away from the soma, parallel to long axis of the cell, 20 µm deep from the slice surface. Dotted lines indicate where the amplitude was measured.

Evaluation of RRP vesicle dynamics

Synaptic vesicle dynamics were assessed using a repetitive stimulation protocol (Schneggenburger *et al*., 1999; Powell *et al*., 2012). The stimulating electrode (patch pipette filled with aCSF) was placed near the dendritic tree, approximately 50 µm from soma. Alexa 488 (100 µM; Molecular Probes; Eugene, OR, USA) was included in the patch pipette and the stimulating electrode to enable the dendritic arbor to be visualised and aid placement of stimulating electrode in relation to the dendrite. Fluorescent dendrites were visualised using a xenon arc lamp (Caim Research, Faversham, Kent, UK). Stimulus intensity was varied and stimulus-response curves were generated to determine the minimal stimulus threshold value that activated as few synapses as possible. Responses were accepted as evoked IPSCs if the latency was less than 15 ms after stimulus artefact. Stimulation was accepted as

minimal if (1) it successfully evoked an IPSC and failed on numerous attempts, (2) a 10% reduction in stimulus intensity resulted in failure to evoke IPSC and (3) a 10% increase resulted in no change in amplitude. The stimulus intensity required for minimal stimulation was 3-14 V and did not differ between genotypes. The RRP was depleted using a train of stimuli (40 at 20 Hz). The minimal stimulation protocol was repeated five times and these responses were averaged. Measurements were made from the averaged trace. The amplitudes were measured for all IPSCs and the cumulative amplitude was plotted. The last 20 data points were fitted with a linear regression and back-extrapolated to time 0 to estimate the size of the RRP (fig 2.9).

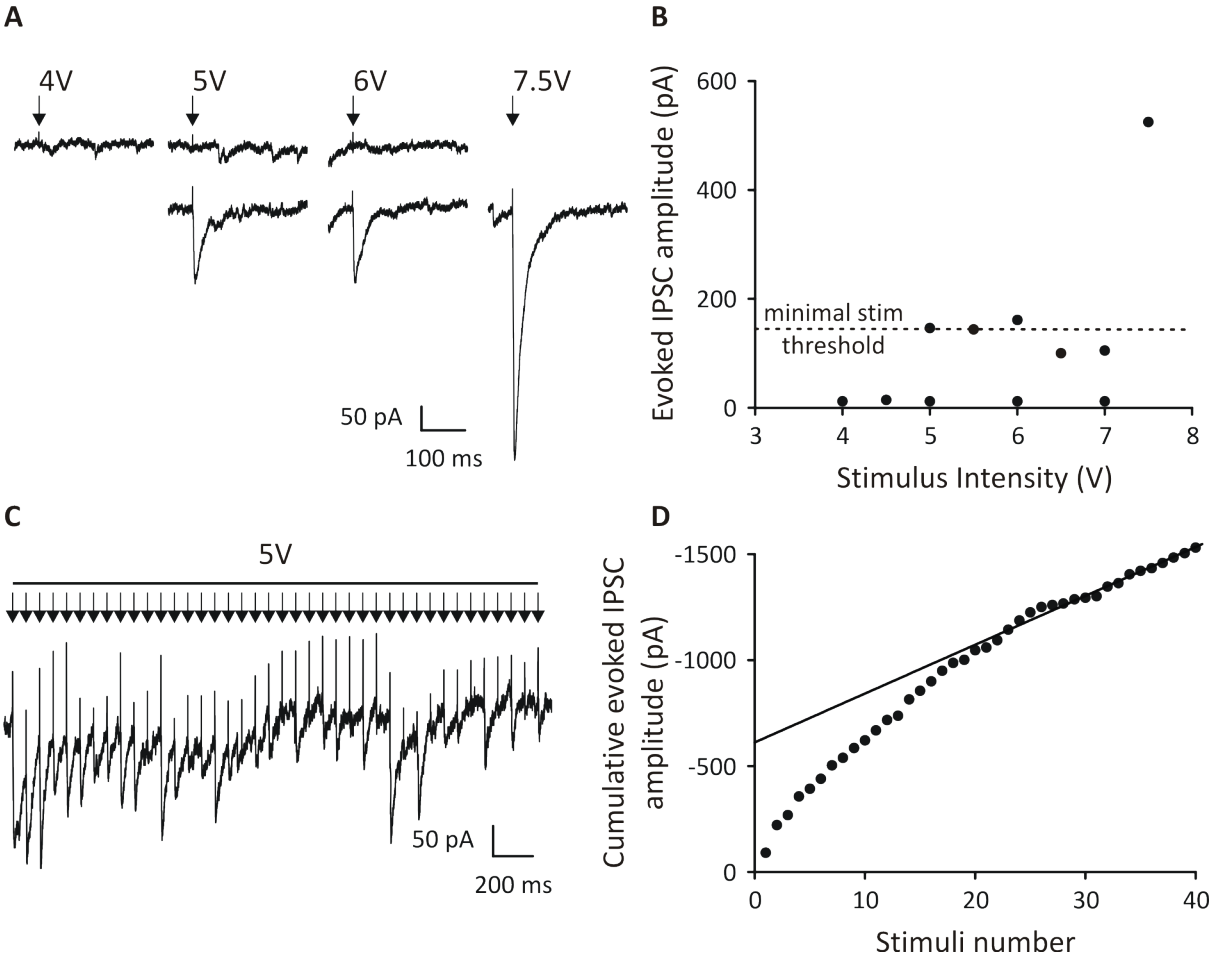
A
4V
5V
6V
7.5V
50 pA
100 ms
B
Evoked IPSC amplitude (pA)
600
400
200
0
minimal stim
threshold
3
4
5
6
7
8
Stimulus Intensity (V)
C
5V
50 pA
200 ms
D
Cumulative evoked IPSC amplitude (pA)
-1500
-1000
-500
0
0
10
20
30
40
Stimuli number

Figure 2.9 – Measurement of readily releasable pool size in an *Ophn*-1$^{+/y}$ neuron.

(A) Traces of evoked IPSCs at different stimulus intensities to achieve minimal stimulation (activation of single synapse). Top panel shows failure to evoke IPSCs and bottom panel shows successfully evoked IPSCs. A 5V stimulus evoked an ~ 150 pA IPSC, a reduction in stimulus intensity to 4V resulted in failure and an increase to 6V did not alter the amplitude of the IPSC. A number of stimuli resulted in failures at 5 and 6V. **(B)** Input-output relationship of stimulus intensity and evoked IPSC amplitude, which suggests minimal stimulus threshold (dotted line) activates a single synapse. **(C)** Evoked IPSCs elicited by a train of 40 stimuli at 20 Hz. The trace represents an average of the response to 5 individual trains of repetitive stimuli. **(D)** Cumulative amplitude plot to the corresponding 40 stimuli in **(C)**. Data points between 20-40th stimuli were fitted with a linear regression and back-extrapolated to time 0 where it intercepts the *y*-axis to determine the readily releasable pool size.

2.4 Histology

Neurobiotin cytochemistry

To examine cortical neuron arborisation, neurons were filled with neurobiotin (0.5%, 0.25%, 0.1% or 0.05%) via the internal solution in the patch electrode. Following electrophysiological characterisation, slices were fixed overnight in 4% paraformaldehyde in 0.1 M phosphate buffer at pH 7.4 at 4°C. Sections were washed (3 x 10 min) in 0.1 M phosphate buffer (PB) followed by permeabilisation with 0.5% Triton X-100 in 0.05 M tris buffered saline (TBS) at pH 7.4 for 1 hr at room temperature. Sections were incubated with avidin/biotinylated enzyme complex (ABC) peroxidase system (1:200 dilution; Vector

Laboratories; Peterborough, UK) for 4 hrs at room temperature. Peroxidase activity was detected by incubating sections with 3'-3'-diaminobenzidine nickel solution (DAB-Ni; comprised in mM: 10 PB, 2.5 $NiNH_4SO_4$, 6.9 NH_4Cl and 1.4 DABN) for 20 min in the dark at room temperature. Hydrogen peroxide (0.03%) was added to the DAB-Ni solution to start the reaction, which was stopped by washing (2 x 10 min) with 0.1 M PB when a black chromogen product was observed.

Alexa immunohistochemsitry

Neurons were filled with Alexa Fluor488 (100 µM) via the internal solution in the patch electrode. Following electrophysiological characterisation, slices were fixed overnight in 4% paraformaldehyde in 0.1 M phosphate buffer at pH 7.4 at 4°C. Sections were washed (3 x 10 min) in 0.1 M PB followed by permeabilisation with 0.5% Triton X-100 in 0.05M PB for 2 x 15 min at room temperature. Sections were first incubated with rabbit anti-Alexa Fluor 488 (1:500 dilution in 0.05 M PB with 0.5% Triton X-100; Molecular Probes) for 4 days at 4°C. After washing 3 x 10 min with 0.1 M PB, the sections were incubated with biotinylated goat anti-rabbit IgG (1:1000 dilution in 0.1 M PB; Vector Laboratories) for 3 days at 4°C. After washing 3 x 10 min with 0.1 M PB, sections were incubated with ABC peroxidase system (1:200 dilution) as described for neurobiotin, however TBS was substituted for PB to avoid the potential interference of tris amines with ester moieties in Alexa Fluor dye.

Embedding

Sections were dehydrated in graded ethanols (1 x 10 min in each of 50, 70, 90 and 100% ethanol), followed by propylene oxide (2 x 5 min) to absorb residual ethanol and then

immersed in Durcupan (Sigma-Aldrich) overnight at room temperature. Sections were mounted onto slides with Durcupan as this improves 3D neuronal reconstruction, coverslipped and left to dry at 56°C for 2 days. Sections were imaged using an upright confocal microscope (Olympus BX-51 FV1000, fluorplan 40x, 1.3 NA oil immersion lens; Olympus KeyMed House, Southend-on-Sea, UK). Images were acquired using Fluoview (v3.1; Olympus). Image stacks were generated for both apical and basal domains to optimise visualisation of the full extent of dendritic ramifications.

Sholl analysis

The complexity of dendritic arborisation was studied using Sholl analysis (Sholl, 1953; 1956). Sholl analysis was used as it quantifies the dendritic branching as a function of distance from the soma. Concentric rings were placed centred around the soma at 10 µm intervals (fig 2.10A) and the number of dendrites intersecting each concentric ring were counted (fig 2.10B). Dendritic branching was quantified for the basal and apical compartment.

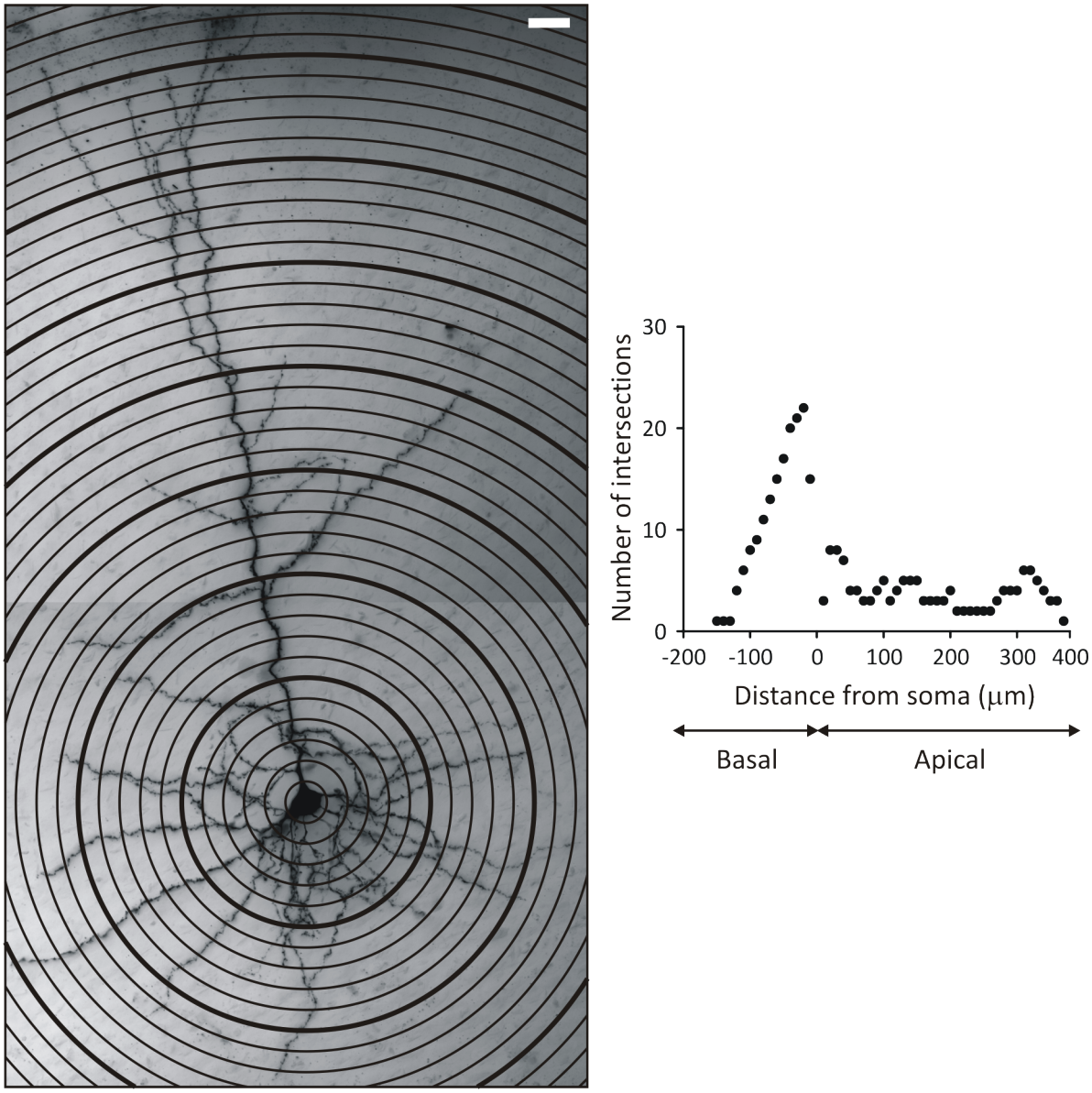

Figure 2.10 – Sholl analysis.

(A) Photomicrograph of layer V pyramidal neuron patched using an internal solution containing 0.5% neurobiotin, followed by immunohistochemical staining. An overlay of concentric rings centred around the soma, in 10 μm intervals (darker lines, 50 μm intervals) for Sholl analysis. Scale bar, 20 μm. **(B)** Graph illustrating number of dendritic intersections with distance from soma for this neuron.

Spine analysis

Images for dendritic spine analysis were acquired using an upright brightfield microscope (Olympus BX-61, fluorplan 100x, 1.4 NA oil immersion lens; Olympus) equipped with a digital black and white EXi blue camera (QImaging; Surrey, Canada). Images were acquired with a *Z* resolution of 0.5 µm, using ImagePro Plus (v7, Media Cybernetics Inc; Rockville, MD, USA). Dendritic protrusions (spines and filopodia) were measured along separate 20 µm stretches, approximately 100 µm away from the soma, along the basal dendrites and the apical dendrites. All protrusions extending from the dendritic shaft were counted by manually scrolling through individual frames of the *z*-stack. Spine density was calculated by counting the total number of spines per 20 µm stretch and dividing the value by the distance. The average spine density was calculated per neuron from three 20 µm segments for basal dendrites and three 20 µm segments for apical dendrites.

Gross brain morphology preparation

Anaesthetised mice (6 and 12-14 weeks) were intracardically perfused with ice cold 0.9% (w/v) saline, followed by ~ 50 ml ice cold 4% paraformaldehyde in 0.1 M phosphate buffer at pH 7.4. Brains were postfixed in 4% paraformaldehyde in 0.1 M phosphate buffer at pH 7.4 at 4°C for 1 week prior to being washed with 0.1 M PB (3 x 24 hr). After fixation brains were stored long term in cryoprotective solution comprised (mM): 5.1 $NaH_2PO_4x2H_2O$, 38.2 Na_2HPO_4, 30% ethylene glycol, 20% glycerol at -20°C. Brains were washed with 0.1 M PB (3 x 1 hr) prior to sectioning. The cerebellum was partly removed ensuring that the cut surface was perpendicular to the long axis of the brain and the dissected surface of the brain was glued to the stage of the slicer. Brains were embedded in 6% agar (low melting point) with

0.9% (w/v) saline using a 12.5 mm specimen embedding tube. Coronal sections (100 µm) were cut with a Compresstome slicer (Precisionary Instruments; San Jose, CA, USA) in 0.1 M PB. Sections were mounted onto slides with 0.1 M PB and temporarily cover-slipped. Images of slices were captured after sectioning on a stereo microscope (Leica MZ8; Micro Instruments) using a digital camera (Deltapix, Maalov, Denmark) and slices were kept in 0.1 M PB with thimerosal (10% w/v; 1:1000) at 4°C for future histological analysis.

Gross brain morphological analysis

Ventricular volume, cortical thickness and brain area were analysed using Image J (v1.45s NIH, USA; http://rsbweb.nih.gov/ij/). Greyscale images (8-bit) were converted into binary images. Ventricular area outline was selected using the wand selection tool. The area of the ventricles was measured per slice, multiplied by the thickness (0.1 mm), and sum of all ventricular areas was used to approximate ventricular size. Areas were taken for lateral and third ventricles (fig 2.11). Cortical thickness was measured in sections containing motor, somatosensory and auditory cortices. The regions were located as indicated in figure 2.12. Six measurement were taken per section, three from each hemisphere; the mean of these values were used per region, per brain. Measurements were taken at approximately the same coronal plane for both genotypes.

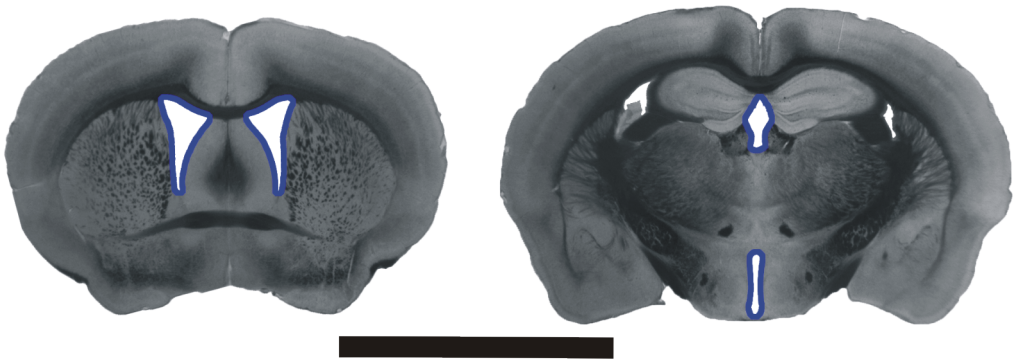

Figure 2.11 – Measurement of ventricular volume.

Bright field images of 100 µm thick coronal brain sections showing regions of analysis. Blue lines indicate area measured for lateral ventricles *(left panel; ~bregma 0.1 mm)* and third ventricle *(right panel; ~bregma -1.4 mm)*. Scale bar, 5 mm.

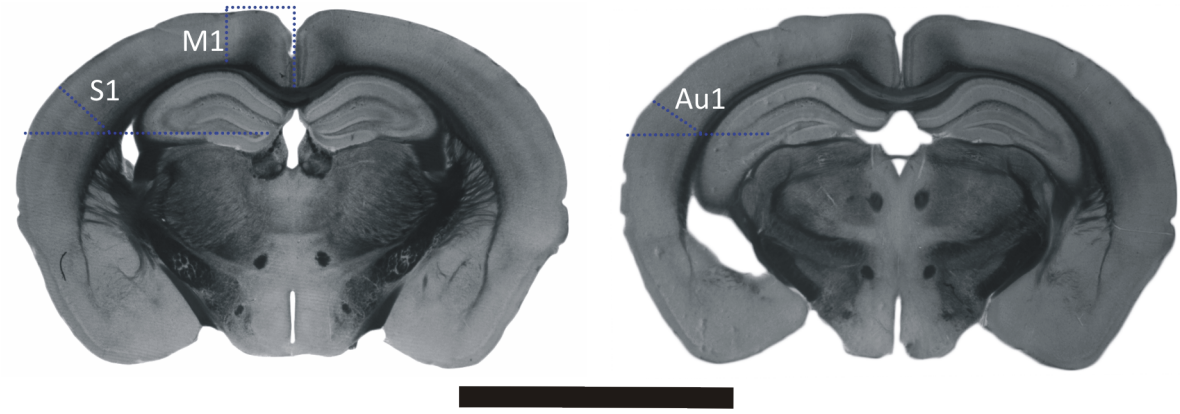

Figure 2.12 – Measurement of cortical thickness.

Bright field images of 100 µm thick coronal brain sections showing regions of analysis. The primary somatosensory (S1) region was located by drawing a horizontal line from the crest of the dentate gyrus, across the cortex to the pia. The primary motor (M1) region was located by drawing a vertical line from the centre of the corpus callosum to the pia, followed by a 1 mm perpendicular line across *(left panel; ~bregma -1.5 mm)*. The primary auditory (Au1) region was located by drawing a horizontal line from the tip of the suprapyramidal blade of the dentate gyrus, to the pia *(right panel; ~bregma -2.3 mm)*. Three measurements were made in each area, in each hemisphere. Scale bar, 5 mm.

2.5 Statistical analysis

Statistical analysis was performed using Origin software (v8.0, Silverdale Scientific; Stoke Mandeville, UK) or PASW Statistics (v18.0). Data were tested for normality using a Shapiro-Wilk test; significant criterion was α=0.05. Student's t-test was used for independent samples and ANOVA was used for multiple comparisons on normally

distributed data. Paired t-test with Bonferonni correction for multiple comparisons was used on related samples. For data that did not follow a normal distribution, a Mann-Whitney U test was used. For non-normally distributed data for multiple comparisons, data was ranked; smallest values were denoted by rank 1 and analysis of variance was used to test for significance (Kruskal-Wallis test). Fisher's exact test was used for categorical data. Significant criterion was α=0.05 unless stated otherwise. All data is expressed as mean ± S.E.M. N numbers in text refer to number of cells. Cells were taken from 4-7 mice for each genotype unless stated otherwise.

2.6 Software and chemicals

Graphs were produced using Origin and formatted with CorelDRAW (v12.0). Images were edited for display purposes using Adobe Photoshop CS6 (v13.0, Adobe System; San Jose, CA). Editing involved subtraction of image background. All chemicals were purchased from Fisher Scientific (Loughborough, UK) unless otherwise stated.

Chapter 3: Characterisation of *Ophn1* Layer V Neurons Using Intracellular Tracers

3.1 Aims

The aims of this study were two-fold. Firstly, to identify layer V pyramidal neurons to ensure consistent comparisons are made between genotypes. Secondly, to optimise a suitable technique to study the dendritic arborisation of *Ophn1* layer V pyramidal neurons. Powell and colleagues (2012) reported dendritic arborisation is reduced in *Ophn*-$1^{-/y}$ dentate gyrus granule neurons. Alterations in dendritic complexity in neocortical neurons could provide a link to neocortical thinning. In order to examine arborisation, a suitable tracer needed to be identified that does not affect electrophysiological properties of layer V pyramidal neurons, whilst giving complete neuron labelling. It is known that some tracers (e.g. Lucifer Yellow and neurobiotin) prolong the duration of action potentials (Tasker *et al.*, 1991; Xi and Xu, 1996). In the case of neurobiotin, the affect appeared to be concentration dependent and it is not known whether lower concentrations of neurobiotin can minimise the impact on electrophysiological properties and still enable neuronal labelling. Whole-cell patch clamp recordings combined with immunohistochemical labelling have been used to study the impact of intracellular tracers, namely neurobiotin and Alexa 488, on the intrinsic properties and synaptic currents of layer V pyramidal neurons. A methodology has been established that enables neuronal identification and electrophysiological characterisation.

3.2 Distinction of pyramidal and non pyramidal neurons

Layer V neocortical neurons consists of a heterogeneous population of neurons which vary immensely in their intrinsic electrophysiological properties (Connors and Gutnick, 1990). It was important to examine the intrinsic membrane and firing properties as a tool to ensure consistent comparisons between layer V pyramidal cells in the two genotypes. Initially, pyramidal cells were identified using DIC optics, however subsequent morphology studies proved that use of this method alone was inadequate to identify pyramidal cells and were therefore characterised based on electrophysiological characteristics in addition to soma discrimination. Whole-cell patch clamp recordings were made in current clamp from the somata of layer V neurons. Cells were depolarised with current injections (200 ms duration; intensity range: 0.05-0.5 nA), which elicited action potential firing at various frequencies. Input-output plots were generated which demonstrated heterogeneity in firing frequency (fig 3.1 A,B).

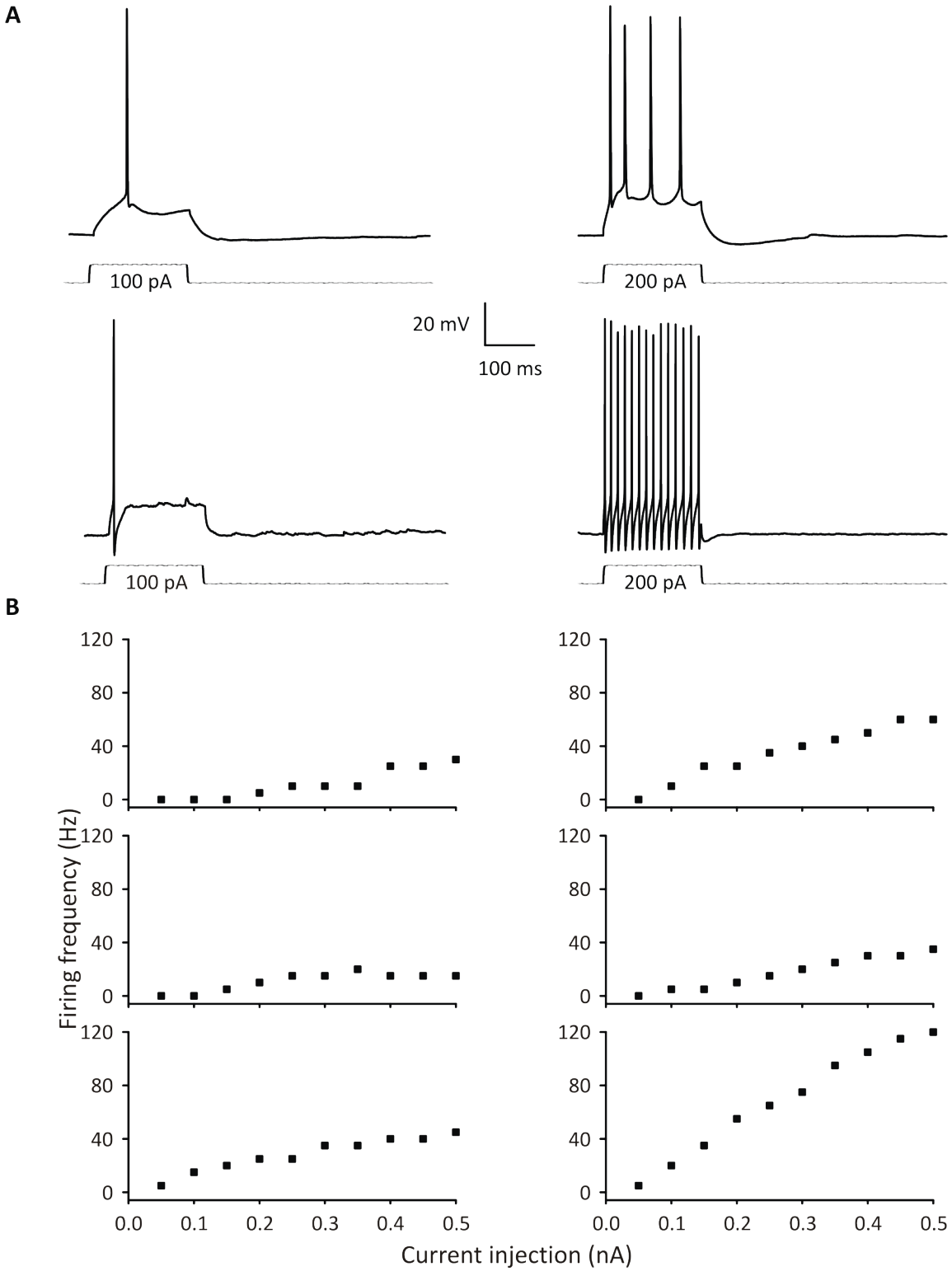
A
100 pA
200 pA
20 mV
100 ms
100 pA
200 pA
B
Firing frequency (Hz)
120
80
40
0
0.0
0.1
0.2
0.3
0.4
0.5
Current injection (nA)

Figure 3.1 – Firing patterns of *Ophn*-1$^{+/y}$ layer V neurons.

(A) Representative trace of action potential firing in putative pyramidal cell *(upper panels)* and putative non pyramidal cell *(lower panels)* upon 200 ms, 100 pA *(left panels)* and 200 pA *(right panels)* current injection. **(B)** Input-output plots of individual pyramidal and non pyramidal cells demonstrating variability in neuronal firing in layer V neurons.

Interneurons have been extensively shown to have shorter action potential half widths, higher firing frequencies and larger fast AHPs than pyramidal cells (Beierlein *et al*., 2003). The intrinsic properties (firing frequency, fast AHP, action potential half width and membrane resistance) were measured in an attempt to categorise the recorded neurons. Each of these electrophysiological parameters were plotted against all others to provisionally distinguish non pyramidal from pyramidal cells (fig 3.2), however there was no clear demarcation to enable identification of neuronal subtypes. These properties were then plotted onto a three-dimensional plot to identify any boundaries (fig 3.3). There was no clear division of neuronal subtypes.

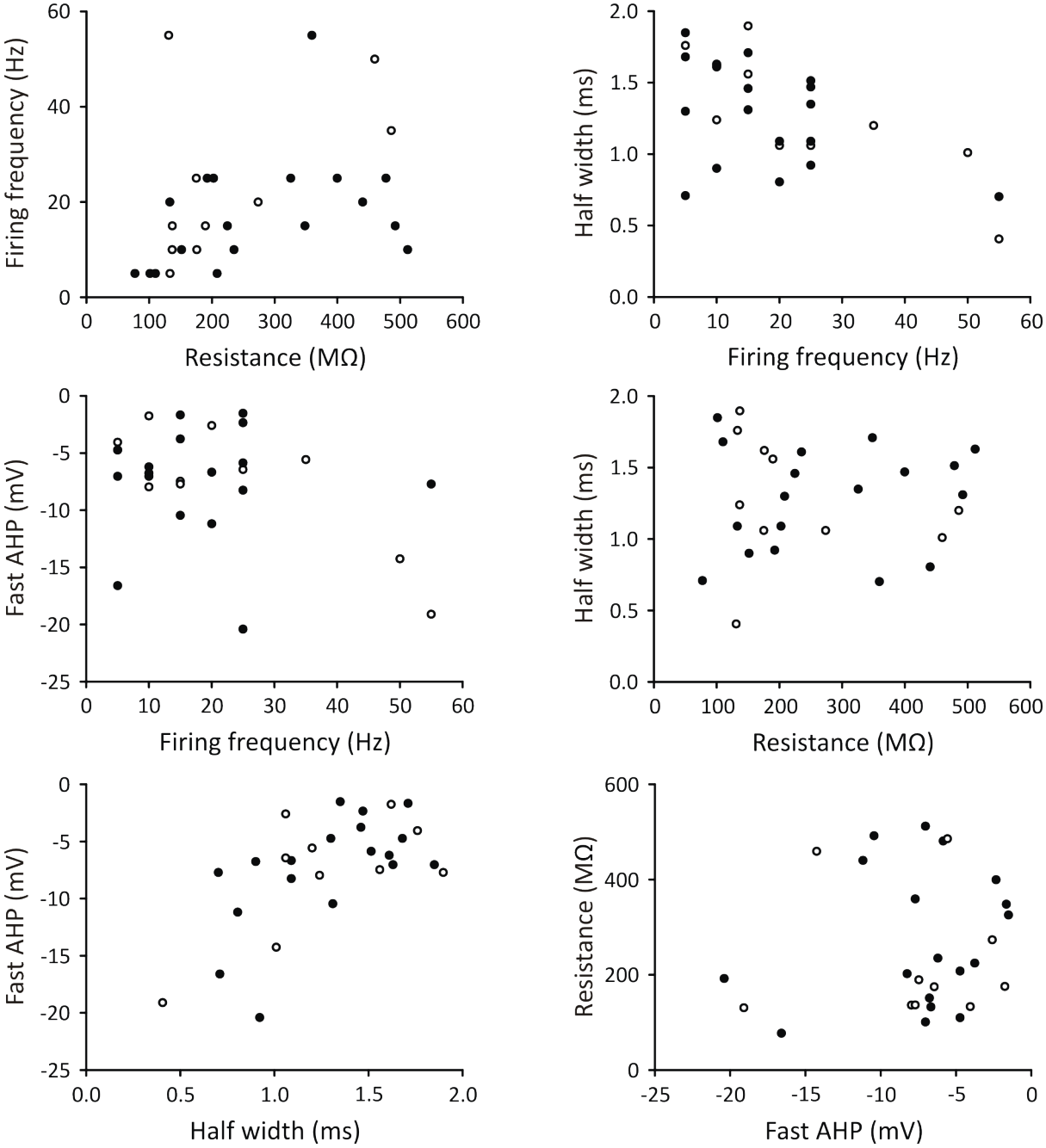
Firing frequency (Hz)
Resistance (MΩ)
Half width (ms)
Firing frequency (Hz)
Fast AHP (mV)
Firing frequency (Hz)
Half width (ms)
Resistance (MΩ)
Fast AHP (mV)
Half width (ms)
Resistance (MΩ)
Fast AHP (mV)

Figure 3.2 – Characterisation of neuronal subtypes in layer V.

Action potential firing frequency is plotted against fast AHP, half width and resistance. Half width is plotted against fast AHP and resistance and fast AHP is plotted against resistance. Intrinsic properties were recorded from a 200 ms, 200 pA current injection. Each symbol represents one cell (*Ophn*-$1^{+/y}$ *filled circles,* 18 cells from 13 mice and *Ophn*-$1^{-/y}$ *open circles*, 10 cells from 6 mice).

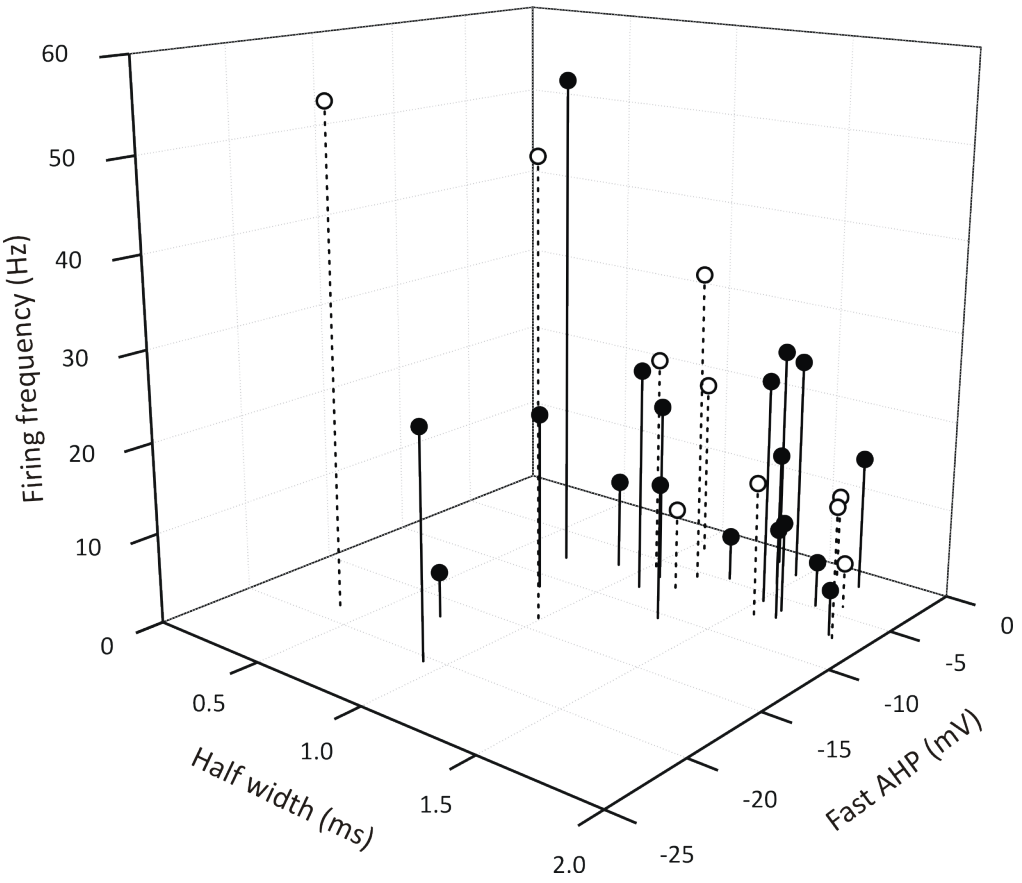

Figure 3.3 – Classification of layer V neurons.

Three-dimensional scatter plot of action potential half width, fast AHP and firing frequency. Intrinsic properties are recorded from a 200 ms, 200 pA current injection. Each symbol represents one cell (*Ophn*-1$^{+/y}$ *filled circles,* 18 cells from 13 mice and *Ophn*-1$^{-/y}$ *open circles*, 10 cells from 6 mice).

Previous reports have investigated the firing properties of various layer V neocortical neuron types, however characterisation based solely on electrophysiological recordings is problematic due to heterogeneity among pyramidal and non pyramidal neurons and thus were characterised only after morphological identification (Kawaguchi, 1993; Hattox and

Nelson, 2007). As recordings have been made from a heterogeneous population of neurons in this study, it is important to distinguish between these two different groups in order to make valid comparisons between genotypes. Thus electrophysiological properties of pyramidal neurons were correlated with morphological identification. More importantly, the morphology of hippocampal neurons has been suggested to be altered in *Ophn*-$1^{-/y}$ animals (Powell *et al*., 2012); similar alterations in the neocortex may be sufficient to explain the cortical thinning associated with this model (Khelfaoui *et al*., 2007) (see chapters 4 and 5). To study morphology, neurobiotin was used, an intracellular tracer substance which enables investigation of neuronal morphology following electrophysiological characterisation (Kita and Armstrong, 1991).

3.3 Impact of neurobiotin on electrophysiology properties

There is some evidence that 3% neurobiotin affects electrophysiological properties of neurons, namely, the action potential half width (Xi and Xu, 1996). It is not known whether lower concentrations can minimise the effect on electrophysiological recordings and still enable neuronal labelling suitable for morphological analysis. It was necessary to ensure that neurobiotin did not impact electrophysiological recordings to confirm that if differences arise between genotypes, they were not due to this factor. Preliminary experiments were conducted to determine whether neurobiotin affected the electrophysiological properties of layer V neocortical neurons. Neurobiotin was added to the internal solution at a concentration of 0.5% (w/v). Cells were depolarised with a 200ms, 200pA current injection at 30 second intervals for 30 minutes, eliciting a train of action potentials. In the absence of

neurobiotin, there was no change in action potential firing frequency or the shape of individual spikes over the recording period after establishment of whole-cell configuration (fig 3.4A). In the presence of neurobiotin, at 1 minute, the action potential half width was 1.9 ± 0.1 ms (n=6); after 10 minutes, there was a pronounced change in shape of individual spikes (2.1 ± 0.2, n=6; p=0.005; fig 3.4A,B,C). Action potential half width increased linearly as a function of time ($p<0.001$, $r^2=0.9$; fig 3.4D). Neurobiotin did not alter the firing frequency; nor was there a difference observed on other intrinsic properties measured (fig 3.4E). An observation of note, neurobiotin appeared to have little impact on the action potential half width of (fast spiking) non pyramidal cells (data not shown), however there were insufficient cell numbers to draw firm conclusions.

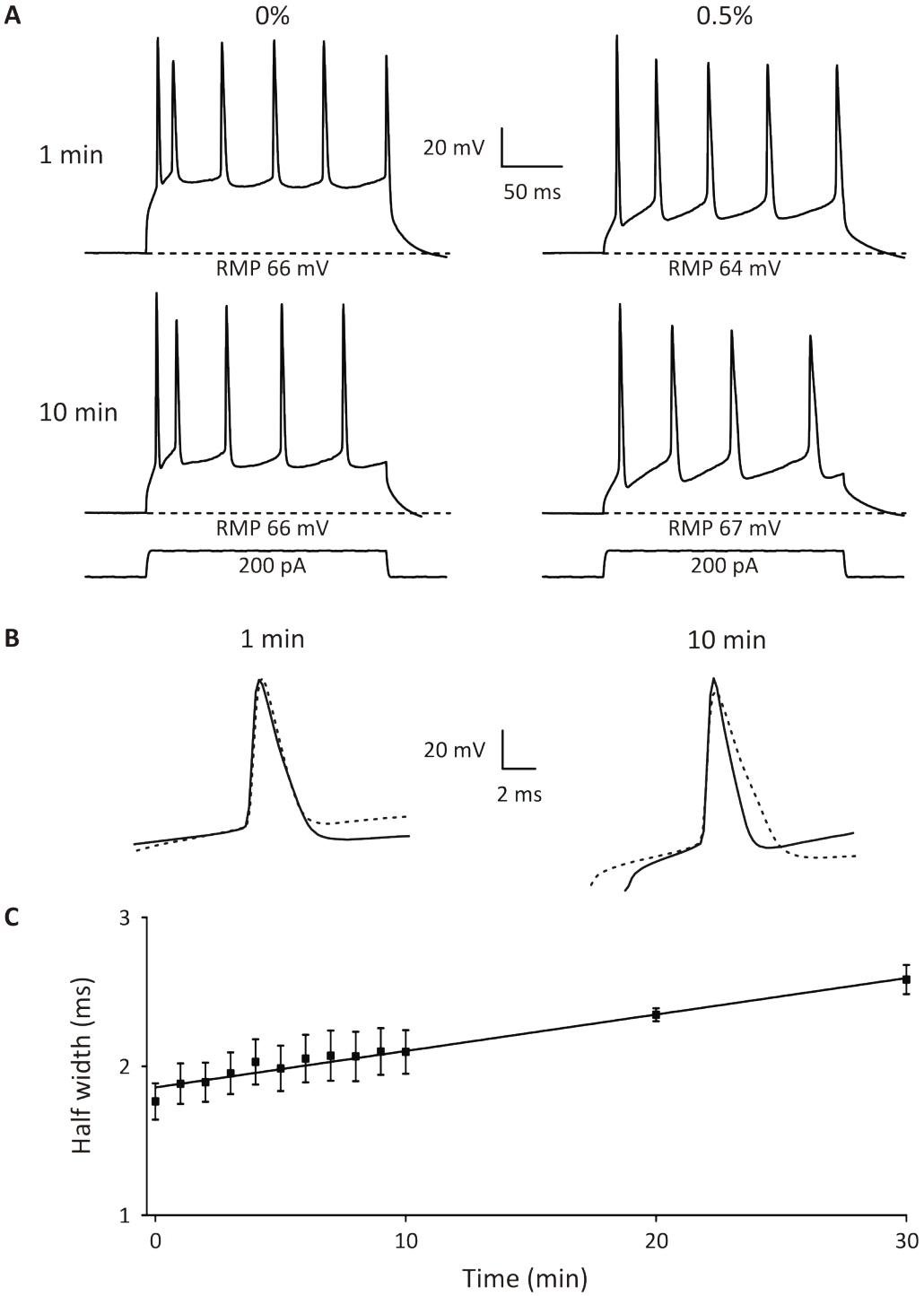

D

	1 min	10 min	p value
Input resistance (MΩ)	291.7 ± 49.3	276.4 ± 25.7	0.7
Half width (ms)	1.9 ± 0.1	2.1 ± 0.2	0.005
Firing frequency (Hz)	17.5 ± 3.6	14.2 ± 2.4	0.1
Fast AHP (mV)	-8.4 ± 1.6	-9.5 ± 1.6	0.5
Slow AHP (mV)	-3.1 ± 0.7	-1.9 ± 0.5	0.04
Threshold (mV)	-42.0 ± 2.0	-42.2 ± 2.2	0.8

Figure 3.4 – Effect of neurobiotin on intrinsic properties.

(A) Representative trace of action potential firing evoked by 200 ms, 200 pA current injection in the absence of neurobiotin and 0.5% neurobiotin at 1 minute and 10 minutes after establishment of whole-cell configuration. **(B)** Representative trace of first action potential evoked by 300 pA current injection without neurobiotin neuron *(black trace)* superimposed on the first action potential from a 0.5% neurobiotin filled neuron *(dotted line)* at 1 minute and 10 minutes. **(C)** Time course of the effect of 0.5% neurobiotin on action potential half width (6 cells from 3 mice). Data were fitted by linear regression. Action potential half width increased with recording duration. **(D)** Effect of neurobiotin on intrinsic properties of layer V pyramidal neurons. Paired t-test with Bonferonni correction (α=0.008); half width $p<0.008$. RMP, resting membrane potential.

As the magnitude of the effect of neurobiotin progressed with time, this suggests a concentration dependent effect. This is problematic for *Ophn1* experiments as the average recording period per cell was 30 minutes and it would be difficult to identify that if changes in intrinsic properties occur, whether they are due to neurobiotin or knockout of *Ophn1.* Therefore, it is important to ensure the intracellular tracer does not impact electrophysiological recordings. Reduced concentrations of neurobiotin (0.25%, 0.1% and 0.05%) were used to determine an optimal concentration whereby immunohistochemical staining could be obtained without compromising the electrophysiological characterisation. Action potential half width was the only parameter examined for lower concentrations as this was the only property that was affected by 0.5% neurobiotin. Within a period of 10 minutes, action potential duration increased at 0.25% (p=0.005, paired t-test) and 0.1%

(p=0.03, paired t-test; fig 3.5); however no significant difference was observed at 0.05% (p=0.2, paired t-test). However by 30 minutes after establishment of whole-cell configuration, the action potential duration was significantly prolonged by 0.05% neurobiotin (p=0.03, r^2=0.9; fig 3.5C).

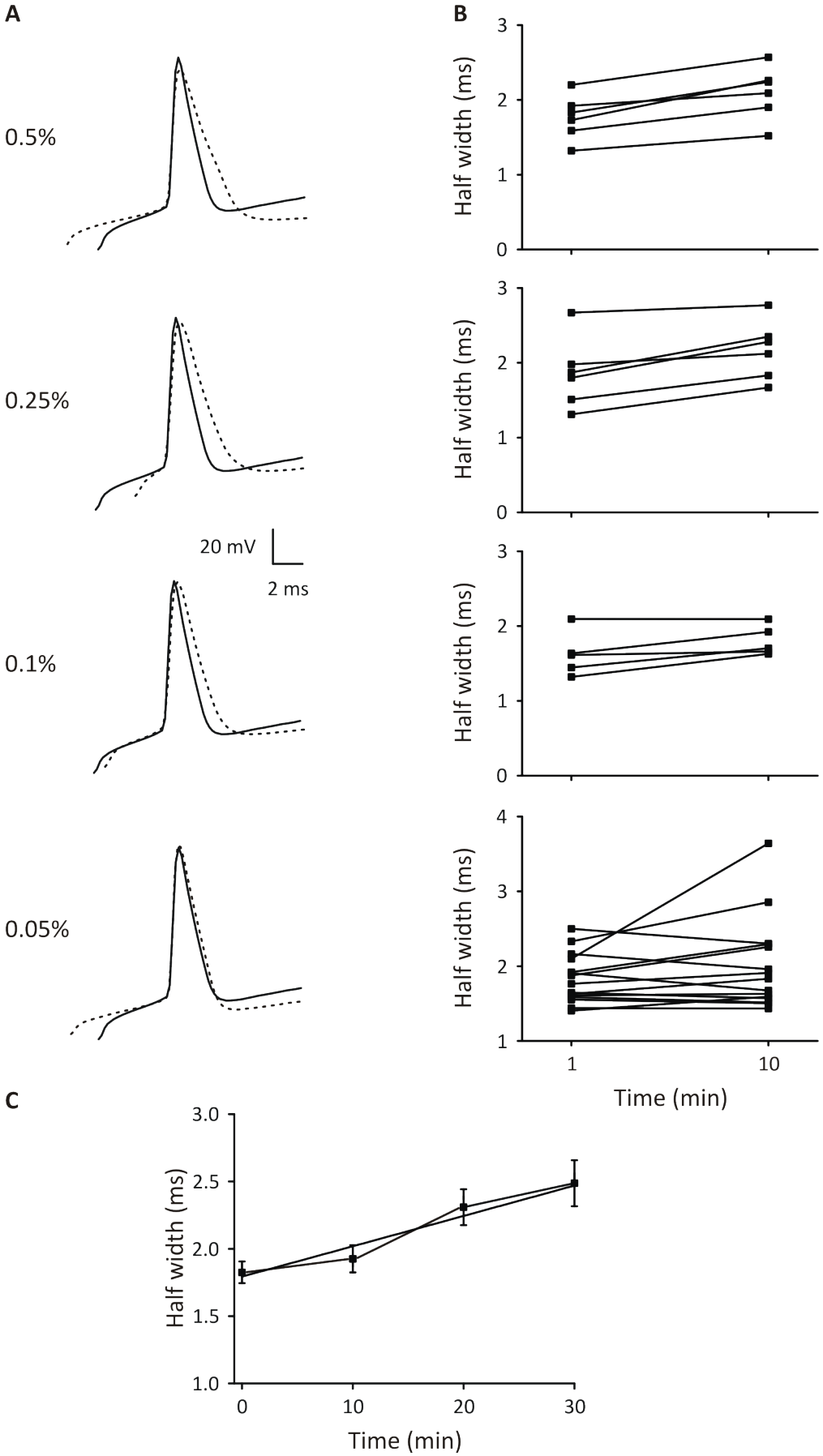
A
0.5%
0.25%
20 mV
2 ms
0.1%
0.05%
B
Half width (ms)
Time (min)
C
Half width (ms)
Time (min)

Figure 3.5 – Concentration dependent effect of neurobiotin on action potential half width.

(A) Representative traces of first action potential evoked by 300 pA current injection at 1 minute *(black traces)* superimposed on the first action potential from a 0.5%, 0.25%, 0.1% and 0.05% neurobiotin filled neuron *(dotted lines)* at 10 minutes. **(B)** Changes in action potential half width in each cell over 10 minutes for each concentration of neurobiotin (0.5%: 6 cells from 3 mice, 0.25%: 6 cells from 3 mice, 0.1%: 5 cells from 3 mice, 0.05%: 16 cells from 4 mice). Pairs of symbols represent one cell. **(C)** Time course of the effect of 0.05% neurobiotin on action potential half width. Data were fitted by linear regression.

Before further lowering the concentration of neurobiotin in an attempt to minimise the impact on the electrophysiological properties, it was important to examine if the staining of the neuronal architecture was comparable to more conventionally used concentrations of neurobiotin. Filled neurons from 0.5% and 0.05% neurobiotin were fixed with paraformaldehyde and stained for neurobiotin. Pyramidal neurons were identified by their pyramidal shaped somata, long apical dendrite and basal dendrites emerging from the base of the soma. Neurons filled with 0.5% neurobiotin had darkly stained somata, dendrites and clearly identifiable dendritic spines (fig 3.6A, 3.9). In contrast, cells labelled with 0.05% had lightly stained somata and dendritic trees, with few arborisations and dendritic spines could not be clearly identified (fig 3.6A, 3.9). Sholl analysis (Sholl, 1953; 1956) confirmed the number of dendrites stained with 0.05% neurobiotin was lower than those stained with 0.5% (fig 3.6B). The total number of intersections was reduced four-fold with 0.05% neurobiotin than 0.5% neurobiotin (55 ± 10, n=14 and 220 ± 20, n=9; respectively; Mann-Whitney U test

$p<0.001$). Therefore, lower concentrations of neurobiotin were undesirable for morphological analysis as histological staining was compromised.

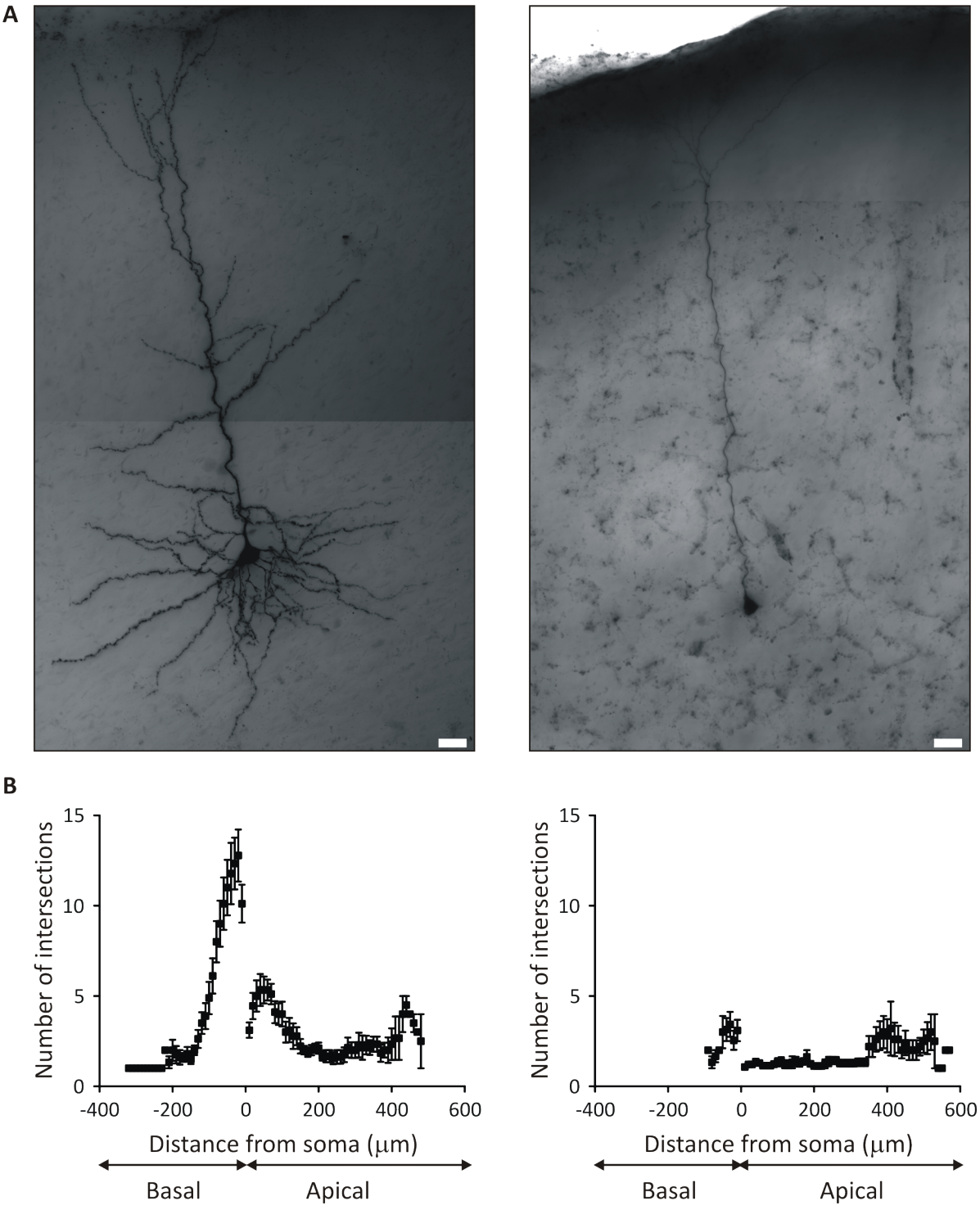
A
B
Number of intersections
15
10
5
0
-400
-200
0
200
400
600
Distance from soma (μm)
Basal
Apical
Number of intersections
15
10
5
0
-400
-200
0
200
400
600
Distance from soma (μm)
Basal
Apical

Figure 3.6 – Lower concentration of neurobiotin compromises morphological analysis.

(A) Photomicrograph of layer V pyramidal neurons recorded using the whole-cell configuration with an internal solution containing 0.5% neurobiotin *(left panel)* and 0.05% neurobiotin *(right panel)* to show quality of histology. Scale bar, 20 µm. **(B)** Sholl analysis of the number of dendritic intersections per concentric ring at increasing distances from the soma in both the basal and apical direction in 0.5% *(left panel)* and 0.05% *(right panel)* neurobiotin labelled neurons (0.5%: 9 cells from 3 mice and 0.05%: 14 cells from 3 mice). Sholl analysis revealed that the number of dendrites stained is fewer with the lower concentration of neurobiotin. Mann-Whitney U test ($p<0.001$).

3.4 Neuronal tracing using Alexa 488

An alternative method for studying electrophysiology combined with morphology is using fluorescent tracers. Alexa 488 (100 µM) was added to the internal solution and cells were depolarised with a 200ms, 200pA current injection at 30 second intervals for 10 minutes, followed by varying intensities of current injections for the subsequent 20 minutes, eliciting trains of action potentials. No significant difference was observed in the action potential half width throughout the 30 minute recording period ($p=0.1$ and $r^2=0.5$; fig 3.7A); nor was there a significant difference in the intrinsic properties of layer V neurons (fig 3.7B).

A

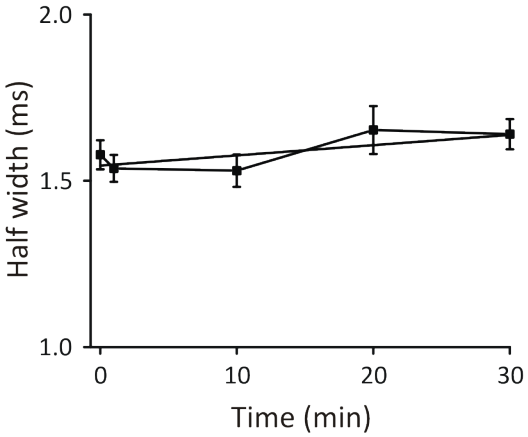

B

	1 min	10 min	p value
Input resistance (MΩ)	308.2 ± 36.5	283.5 ± 28.6	0.5
Half width (ms)	1.5 ± 0.1	1.5 ± 0.1	0.9
Firing frequency (Hz)	17.5 ± 2.7	14.4 ± 2.0	0.1
Fast AHP (mV)	-2.5 ± 1.2	-8.1 ± 1.9	0.03
Slow AHP (mV)	-3.3 ± 0.4	-2.9 ± 0.8	0.7
Threshold (mV)	-41.1 ± 1.9	-38.6 ± 0.9	0.1

Figure 3.7 – Alexa 488 does not affect intrinsic properties of layer V pyramidal neurons.

(A) Time course of the effect of Alexa 488 on action potential half width. Data were fitted by linear regression. Action potential half width does not change with recording duration of 30 minutes. **(B)** Effect of Alexa 488 on the intrinsic properties of layer V neurons (18 cells from 9 mice). Paired t-test with Bonferonni correction (α=0.008).

Having shown Alexa 488 does not impact the intrinsic properties of layer V pyramidal cells, the next step was to determine if *post hoc* non-fluorescent neuronal labelling was possible. Filled neurons were fixed with paraformaldehyde (4%) and stained with an anti-Alexa Fluor 488 antibody followed by a biotinylated secondary antibody and visualised with DAB. These

were compared with neurobiotin (0.5%) labelled neurons to assess the quality of histology, as neurobiotin stained neurons were strongly labelled. Neuronal labelling was visible with Alexa 488 (fig 3.8A) and fine dendrites and spines could also be resolved (fig 3.9). Sholl analysis revealed the number of dendrites stained with Alexa 488 was fewer than those stained with 0.5% neurobiotin at all distances from the soma (fig 3.8B). Furthermore, the total number intersections were significantly less with Alexa 488 than 0.5% neurobiotin (111 ± 11, n=23 and 220 ± 20, n=9; respectively; $p<0.001$; fig 3.8C). Alexa 488 labels neurons, albeit not as effectively as neurobiotin, it is suitable to distinguish between pyramidal and non pyramidal cells.

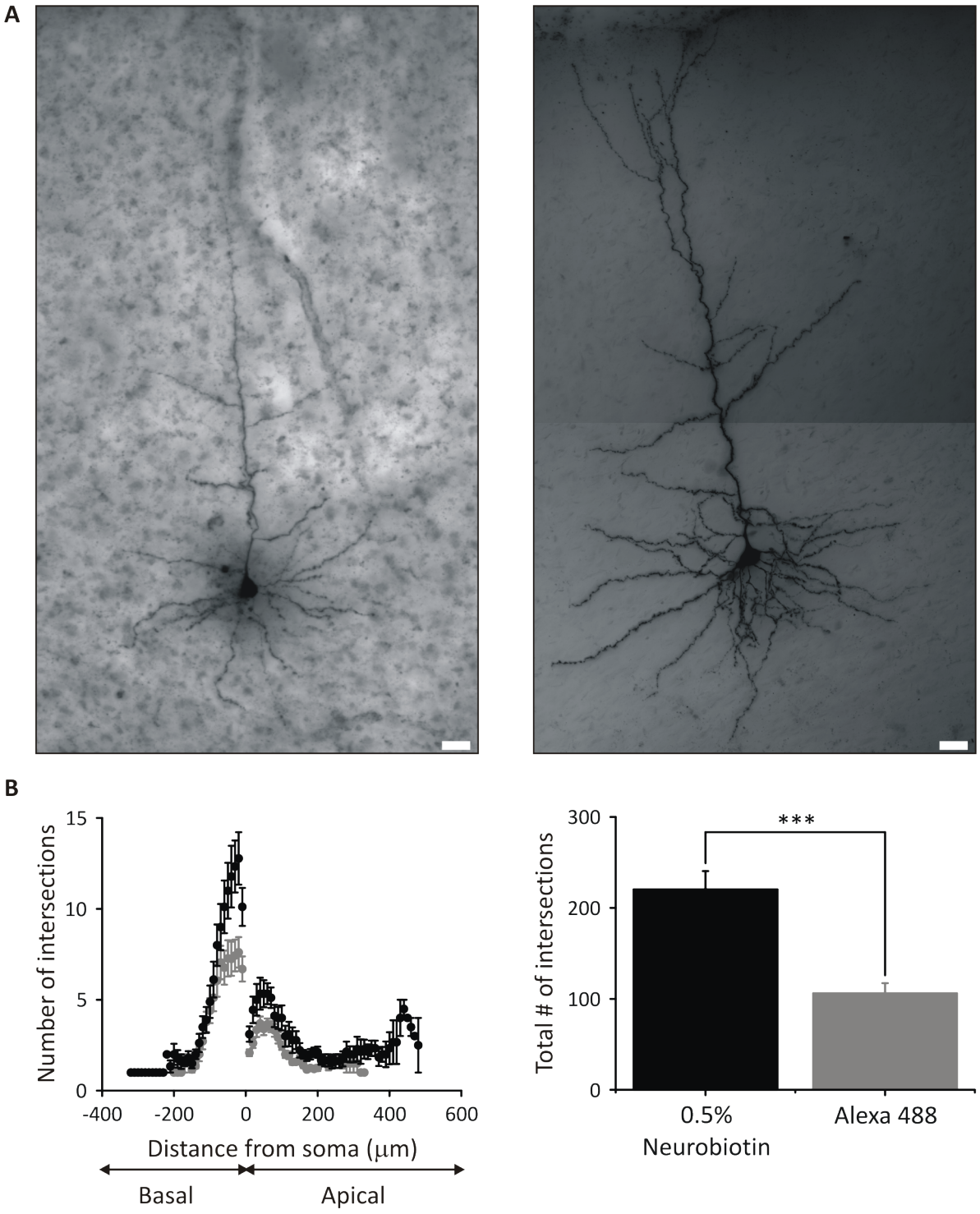
A
B
Number of intersections
15
10
5
0
-400
-200
0
200
400
600
Distance from soma (μm)
Basal
Apical
Total # of intersections
300
200
100
0
***
0.5%
Neurobiotin
Alexa 488

Figure 3.8 – Alexa 488 compromises morphological analysis.

(A) Photomicrograph of layer V pyramidal neurons patched using an internal solution containing Alexa 488 *(left panel)* and 0.5% neurobiotin *(right panel)*. The cell body and dendritic tree were more darkly stained with 0.5% neurobiotin than Alexa 488. Scale bar, 20 µm. **(B)** Sholl analysis of the number of dendritic intersections per concentric ring at increasing distances from the soma in both the basal and apical direction in Alexa 488 (*grey symbols,* 23 cells from 11 mice) and 0.5% neurobiotin (*black symbols,* 9 cells from 3 mice) labelled neurons. **(C)** The total number of intersection was lower in Alexa 488 stained neurons. Student's t-test ***=$p<0.001$.

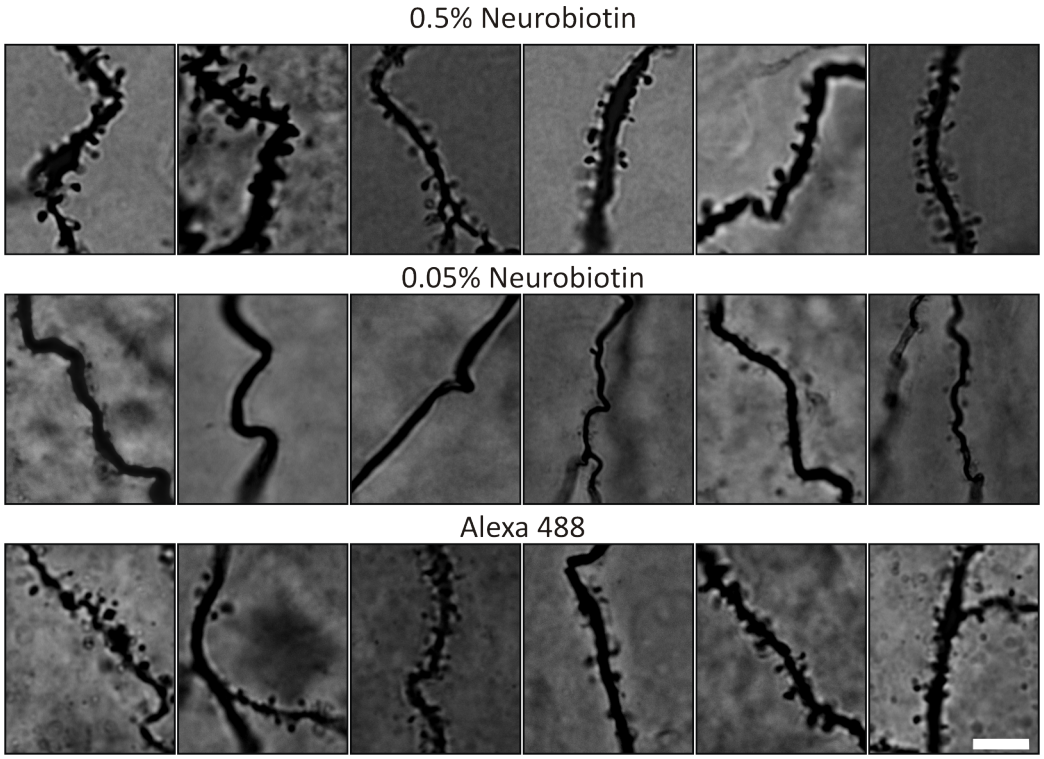

Figure 3.9 – Dendritic spines stained with neurobiotin and Alexa 488.

Photomicrographs of layer V pyramidal neuron dendritic spines. Fine dendrites and spines were darkly stained and densely populated at 0.5% neurobiotin, but this microstructure was lightly stained and sparse with 0.05% neurobiotin. Dendritic spines can be observed with Alexa 488 stained neurons. Different spine types can be differentiated with 0.5% neurobiotin and Alexa 488, but not with 0.05% neurobiotin. Scale bar, 5 µm.

Having identified a tracer that does not impact the intrinsic properties and enables identification of cell types, Alexa 488 was used to characterise layer V pyramidal cells. Figure 3.10 shows the distribution of pyramidal, non pyramidal and unknown cell types in *Ophn*-$1^{+/y}$ and *Ophn*-$1^{-/y}$ neurons; illustrating no distinct difference between cell types based on these intrinsic properties. These properties have been characterised between *Ophn*-$1^{+/y}$ and *Ophn*-$1^{-/y}$ neurons in chapter 4 using Alexa 488 to identify layer V pyramidal neurons.

A

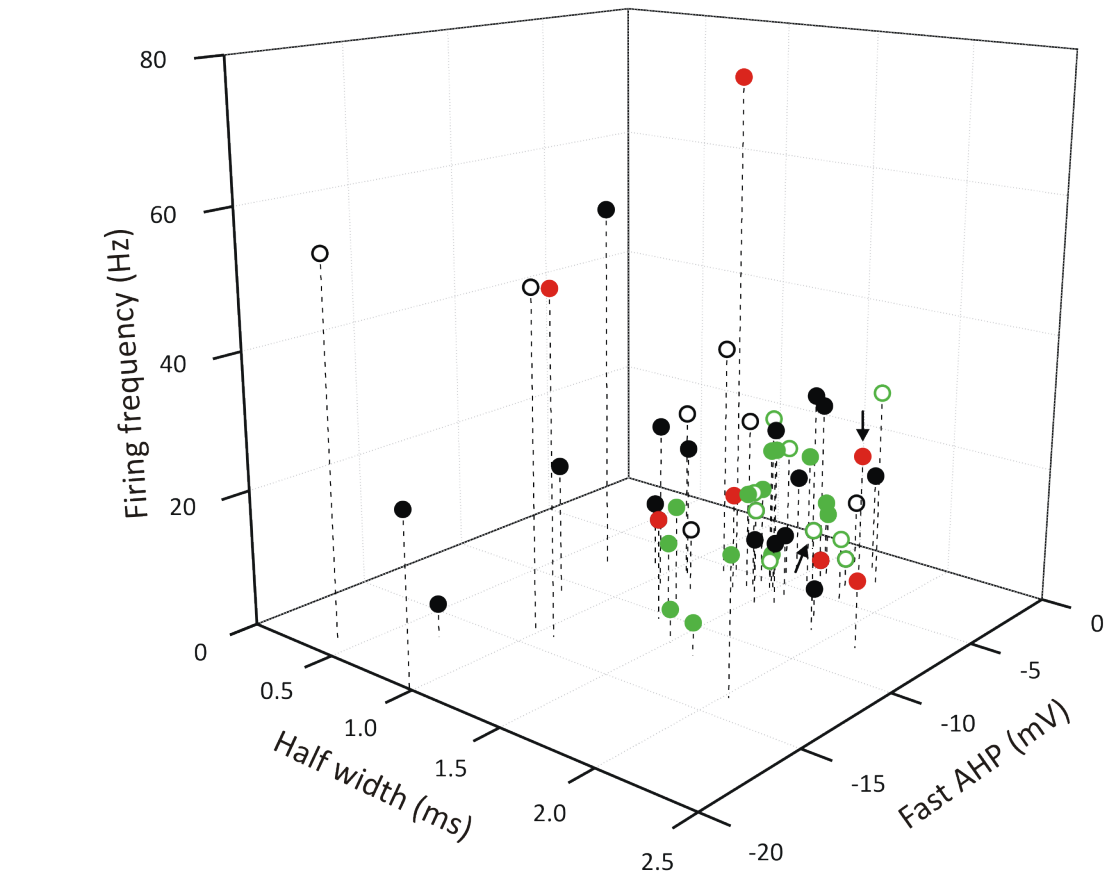
80
60
40
20
0
Firing frequency (Hz)
0
0.5
1.0
1.5
2.0
2.5
Half width (ms)
0
-5
-10
-15
-20
Fast AHP (mV)

B

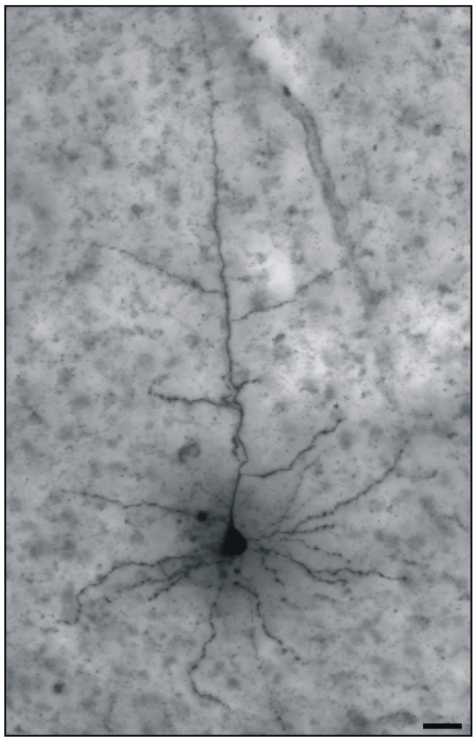

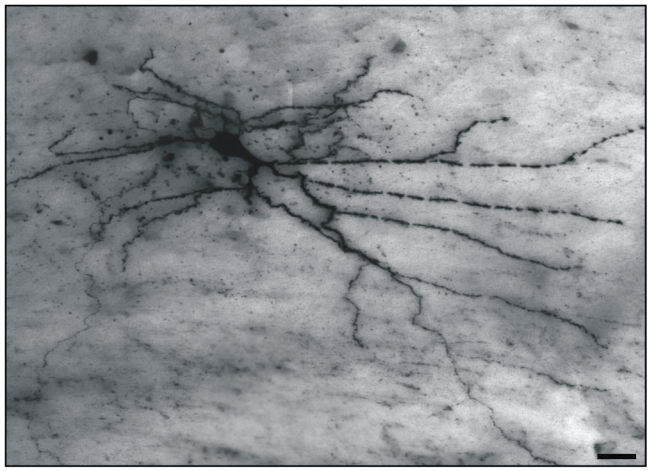

Figure 3.10 – Characterisation of intrinsic properties of layer V neurons.

(A) Three-dimensional scatter plot of action potential half width, fast AHP and firing frequency recorded from a 200 ms, 200 pA current injection. Each symbol represents one cell (*Ophn*-$1^{+/y}$ *filled circles*, 37 cells from 19 mice and *Ophn*-$1^{-/y}$ *open circles*, 19 cells from 9 mice). Green symbols represent cells that have been confirmed as pyramidal neurons from morphology, red symbols are non pyramidal neurons and black symbols represent unknown cell types. Note the overlap of intrinsic properties between pyramidal and non pyramidal neurons. **(B)** Photomicrograph of layer V pyramidal cell *(left panel)* and layer V non pyramidal cell *(right panel)* labelled with anti Alexa 488, then stained with biotinylated secondary antibody and visualised with DAB. Intrinsic properties of these neurons are indicated by arrows in **(A)**. Scale bar, 20 µm.

3.5 Impact of intracellular tracers on postsynaptic currents

The observation that neurobiotin increased action potential half width raised the question whether it alters postsynaptic currents; this remains unknown. This was of interest, as synaptic physiology would be investigated in *Ophn*-$1^{-/y}$ mice. Neurobiotin did not change the amplitude of spontaneous excitatory and inhibitory postsynaptic currents; neither the rise time, nor the decay time were affected (fig 3.11).

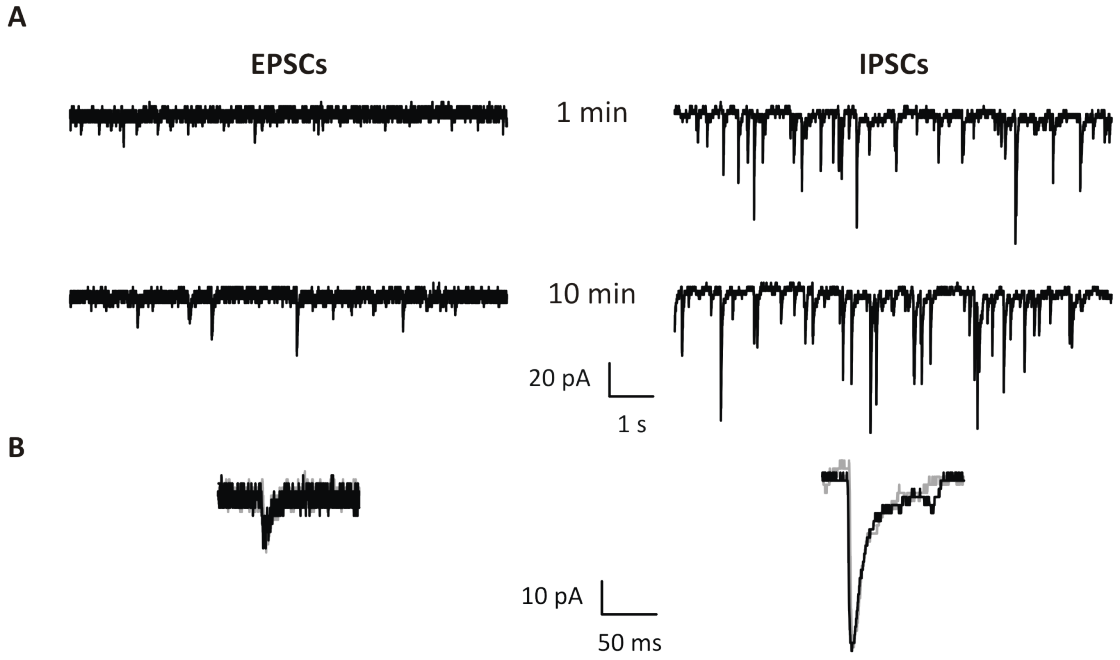

C

		1 min	10 min	p value
EPSC	Amplitude (pA)	13.8 ± 1.0	13.7 ± 1.3	0.9
	10-90% rise (ms)	3.4 ± 0.5	4.0 ± 0.2	0.3
	Decay (ms)	22.5 ± 1.0	25.7 ± 1.9	0.1
IPSC	Amplitude (pA)	56.8 ± 2.9	67.6 ± 9.8	0.2
	10-90% rise (ms)	2.5 ± 0.1	2.4 ± 0.1	0.3
	Decay (ms)	29.3 ± 2.0	33.2 ± 4.5	0.4

Figure 3.11 – Spontaneous postsynaptic currents were unaltered in 0.5% neurobiotin.

(A) Representative traces of EPSCs and IPSCs at 1 minute *(upper panels)* and 10 minutes *(lower panels)* in layer V pyramidal neurons. **(B)** Overlay of EPSC *(left panel)* and IPSC *(right panel)* at 1 minute *(black trace)* and 10 minutes *(grey trace)*. **(C)** The kinetics of PSCs were not altered by neurobiotin (EPSCs: 7 cells from 3 mice and IPSCs: 5 cells from 3 mice). Paired t-test with Bonferonni correction (α=0.02).

Despite that Alexa 488 did not alter intrinsic properties, it was important to ensure it did not impact postsynaptic currents. Alexa 488 did not change the amplitude of spontaneous excitatory and inhibitory postsynaptic currents; neither the rise time, nor the decay time were affected (fig 3.12). As Alexa 488 did not affect the intrinsic properties or postsynaptic currents and gave reasonable neuronal staining and enabled dendritic spines to be studied, it was used for subsequent *Ophn1* studies relating neocortical physiology to morphology (see chapter 4).

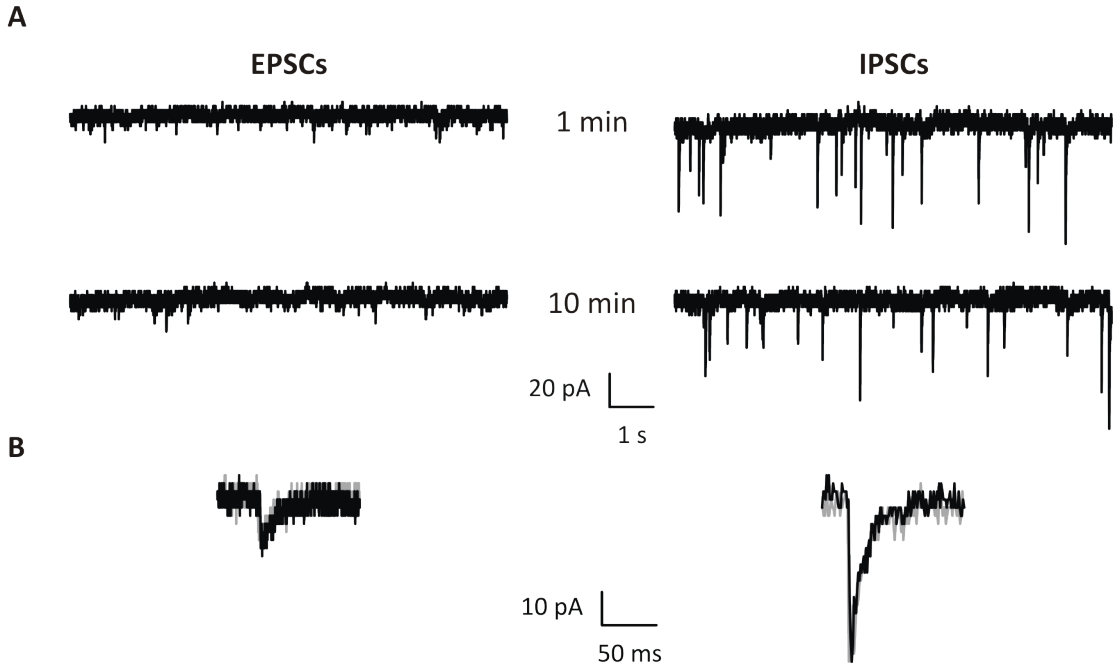

C

		1 min	10 min	p value
EPSC	Amplitude (pA)	13.8 ± 1.2	14.6 ± 1.3	0.3
	10-90% rise (ms)	2.7 ± 0.3	2.6 ± 0.3	0.8
	Decay (ms)	20.2 ± 2.8	21.1 ± 3.1	0.8
IPSC	Amplitude (pA)	34.9 ± 5.3	38.9 ± 4.2	0.4
	10-90% rise (ms)	1.5 ± 0.3	1.2 ± 0.2	0.2
	Decay (ms)	16.4 ± 1.4	17.1 ± 1.3	0.2

Figure 3.12 – Spontaneous postsynaptic currents were unchanged in Alexa 488.

(A) Representative traces of EPSCs and IPSCs at 1 minute *(upper panels)* and 10 minutes *(lower panels)* in layer V pyramidal neurons. Overlay of EPSC *(left panel)* and IPSC *(right panel)* at 1 minute *(black trace)* and 10 minutes *(grey trace)*. **(B)** The kinetics of PSCs were not altered by Alexa 488 (EPSCs: 5 cells from 4 mice and IPSCs: 6 cells from 3 mice). Paired t-test with Bonferonni correction (α=0.02).

3.6 Summary

Layer V pyramidal cells have heterogeneous intrinsic properties that overlap with non pyramidal cells, thus were difficult to characterise without morphological identification. The morphology of neurons has been studied using neurobiotin and Alexa 488. Neurobiotin affected electrophysiological recordings, namely the duration of the action potential, in a concentration dependent manner. A lower concentration of neurobiotin (0.05%) prolonged action potential duration and compromised histological staining. Alexa 488 did not alter the intrinsic properties, however histology was compromised compared to 0.5% neurobiotin; but dendritic spines could be resolved and Alexa 488 was sufficient for pyramidal cell identification. Neither neurobiotin (0.5%) nor Alexa 488 altered the kinetics or amplitude of postsynaptic currents, suggesting either were suitable for studying synaptic currents combined with neuronal labelling. Having identified that Alexa 488 does not alter any of the measured electrophysiological properties of layer V pyramidal neurons, this tracer was used to characterise layer V pyramidal neuron intrinsic properties and synaptic currents in *Ophn1* neurons. Despite the limitations of Alexa 488 labelling (i.e. less extensive labelling), this is unlikely to contribute to genotype comparisons of arborisation.

Chapter 4: Characterisation of Neocortical Physiology in *Ophn*-1$^{-/y}$ mice

4.1 Aims

Previous studies have shown alterations in spine dynamics, synaptic function and neuronal arborisation in *Ophn1* deficient hippocampal neurons (Govek *et al.,* 2004; Khelfaoui *et al.*, 2007; Powell *et al.*, 2012). Whilst several studies have looked at the function of oligophrenin-1 in the hippocampus, nothing is known about loss of function of oligophrenin-1 in neocortical neurons. The apparent loss of neocortical tissue argues for investigating functional changes in the neocortex as loss of neuropil could result from synaptic dysfunction. The aims of this study were to explore whether neocortical synaptic function was altered and if it was combined with deficits in spine dynamics and dendritic morphology. Whole-cell patch clamp recordings have been made from layer V pyramidal neurons. Initially, the intrinsic properties of layer V pyramidal neurons have been characterised between *Ophn*-1$^{+/y}$ and *Ophn*-1$^{-/y}$ neurons. Excitatory and inhibitory spontaneous and evoked synaptic transmission has been examined to study basal transmission whereas repetitive stimulation at high frequencies has been employed to explore vesicle dynamics to identify whether oligophrenin-1 regulates synaptic vesicles in neocortical neurons. Finally, Alexa 488 has been used to study neuronal morphology and dendritic spine density of the recorded neurons from excitatory synaptic current studies.

4.2 Intrinsic properties of layer V pyramidal neurons

Alterations in neuronal intrinsic properties have been shown to play a role in some CNS disorders, e.g. contributing to hyperexcitability in models of epilepsy (Beck and Yaari, 2008). Intrinsic properties were examined to assess whether changes were present in *Ophn*-$1^{-/y}$ mice. Whole-cell patch clamp recordings were made from layer V pyramidal neurons using the current clamp mode. Alexa 488 (100 µM) was added to the internal solution to enable *post hoc* neuronal staining to confirm pyramidal cells. No difference was observed in any intrinsic property measured between *Ophn*-$1^{+/y}$ and *Ophn*-$1^{-/y}$ neurons (fig 4.1C).

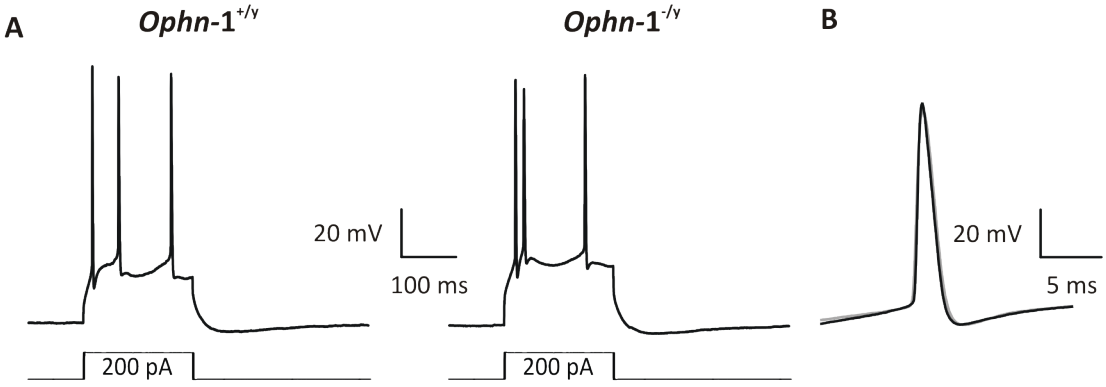

C

	Ophn-1$^{+/y}$	*Ophn*-1$^{-/y}$	p value
Input resistance (MΩ)	275.5 ± 26.5	232.1 ± 35.4	0.3
Half width (ms)	1.5 ± 0.1	1.6 ± 0.1	0.2
Firing frequency (Hz)	14.4 ± 2.0	15.6 ± 2.8	0.7
Fast AHP (mV)	-7.4 ± 1.3	-5.4 ± 0.5	0.2
Slow AHP (mV)	-2.9 ± 0.7	-2.6 ± 0.7	0.8
Threshold (mV)	-38.4 ± 0.9	-42.4 ± 2.1	0.1
RMP (mV)	-51.0 ± 3.6	-55.5 ± 2.2	0.4

Figure 4.1 – Intrinsic properties were unchanged in *Ophn*-1$^{-/y}$ layer V pyramidal neurons.

(A) Trace of action potential firing, evoked by 200 ms, 200 pA current injection in *Ophn*-1$^{+/y}$ *(left panel)* and *Ophn*-1$^{-/y}$ neuron *(right panel)*. **(B)** Overlay of the first action potential from *Ophn*-1$^{+/y}$ *(black trace)* and *Ophn*-1$^{-/y}$ neuron *(grey trace)*. **(C)** Intrinsic properties were unaltered between *Ophn*-1$^{+/y}$ (9 cells from 3 mice) and *Ophn*-1$^{-/y}$ neurons (9 cells from 5 mice). Student's t-test with Bonferonni correction α=0.007.

Having characterised the intrinsic properties of layer V pyramidal neurons, spontaneous and evoked excitatory input to these neurons was investigated.

4.3 Putative excitatory postsynaptic potentials

Spontaneous EPSCs have shown to be reduced in dentate gyrus granule cells in acute slices from the *Ophn1* mouse model (Powell *et al*., 2012) and also in siRNA knockdown experiments in organotypic slice cultures in CA1 pyramidal neurons (Nadif Kasri *et al*., 2009). During examination of action potential activity using the current clamp mode, spontaneous activity was observed (fig 4.2A). Analysis of these spontaneous events revealed they occurred at a significantly lower frequency in *Ophn*-$1^{-/y}$ than *Ophn*-$1^{+/y}$ neurons (3.0 ± 0.5 Hz, n=10 and 4.5 ± 0.3 Hz, n=13, respectively; p=0.01; fig 4.2C). These events are likely to be excitatory postsynaptic potentials as they were recorded at a membrane potential close to the reversal potential of IPSCs (*Ophn*-$1^{+/y}$ -66.2 ± 0.4 mV, n=13 and *Ophn*-$1^{-/y}$ -65.5 ± 0.3 mV, n=10; respectively; p=0.2, Mann-Whitney U test). Furthermore, these events resulted in membrane depolarisation. These data are suggestive of alterations in excitatory synaptic transmission. A major weakness of using current clamp to study postsynaptic currents is that accurate measurements cannot be made. For example, fluctuations in membrane potential could result in membrane depolarisation leading to imprecise measurements of spontaneous EPSPs. Additionally, superimposition of IPSPs onto EPSPs could attenuate the size of the EPSPs leading to underestimation of amplitude and frequency. Voltage-clamp should be used to hold the membrane potential at -75mV (the reversal potential of IPSCs) and addition of $GABA_A$ antagonists such as picrotoxin will confirm the identity of EPSCs.

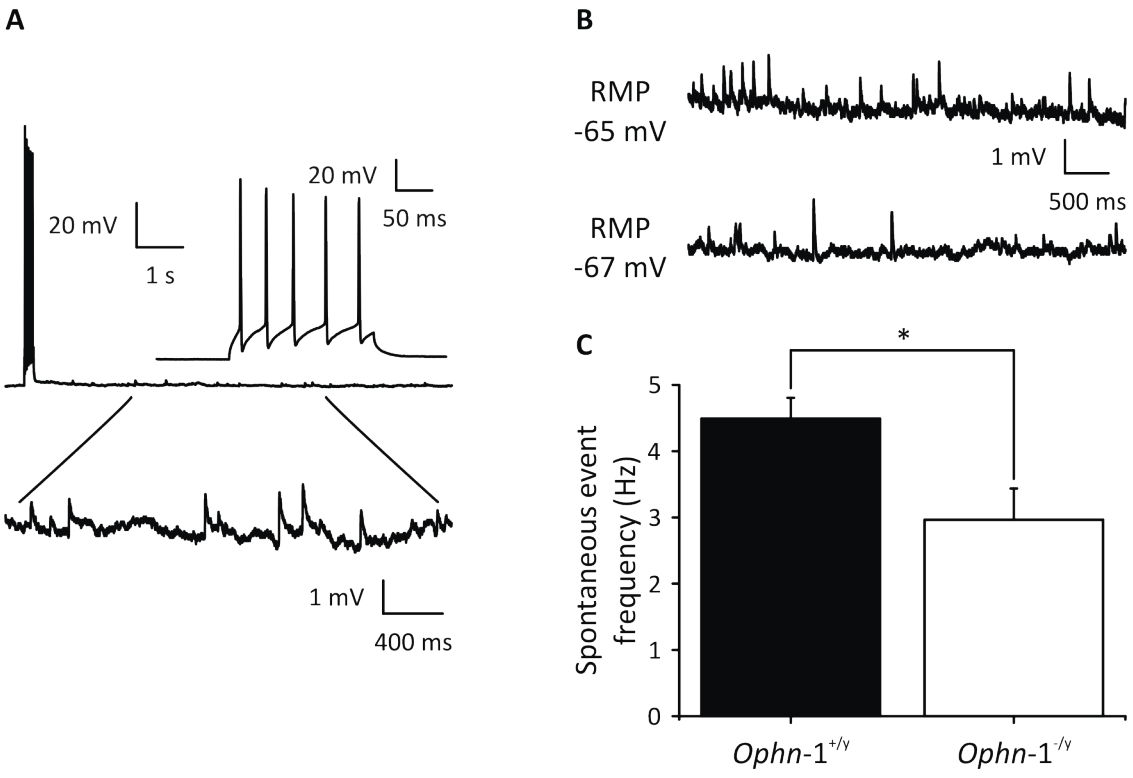

Figure 4.2 – The frequency of spontaneous events were reduced in *Ophn*-1$^{-/y}$ neurons.

(A) Train of action potentials recorded from a layer V pyramidal neuron using current clamp at approximately -65 mV. Action potentials were evoked by 300 pA, 200 ms current injection. Inset shows action potentials *(upper panel)* and spontaneous baseline activity *(lower panel)* on an expanded time scale. **(B)** Representative spontaneous events in *Ophn*-1$^{+/y}$ *(top panel)* and *Ophn*-1$^{-/y}$ *(bottom panel)*. **(C)** The frequency of these events was reduced in *Ophn*-1$^{-/y}$ neurons (10 cells from 3 mice) than *Ophn*-1$^{+/y}$ neurons (13 cells from 6 mice). Student's t-test (*=p<0.05). RMP, resting membrane potential.

4.4 Spontaneous EPSCs

To accurately determine if spontaneous transmission was altered in the neocortex, spontaneous EPSCs were recorded from layer V pyramidal cells using a more controlled setup. Cells were voltage clamped at -75 mV using an internal solution containing caesium ions, a potassium channel blocker that improves voltage clamp by blocking leak currents. To confirm isolation of EPSCs, the $GABA_A$ receptor antagonist picrotoxin (100 μM), was added to the bath solution. Furthermore, EPSCs were recorded as inward deflections at -75 mV which reversed polarity at 0 mV (data not shown). Figure 4.3A depicts typical spontaneous EPSCs recorded from a layer V neuron which were abolished following bath application of NBQX (20 μM) and D-APV (25 μM). The spontaneous EPSC amplitude of *Ophn*-$1^{+/y}$ neurons was comparable to *Ophn*-$1^{-/y}$ neurons (15.5 ± 0.8 pA, n=22 and 13.7 ± 0.6 pA, n=9; respectively; p=0.2; fig 4.3C). No significant difference was observed in the frequency of EPSCs between *Ophn*-$1^{+/y}$ and *Ophn*-$1^{-/y}$ neurons (3.5 ± 0.8 Hz, n=22 and 1.9 ± 0.3 Hz, n=9; p=0.3; fig 4.3C).

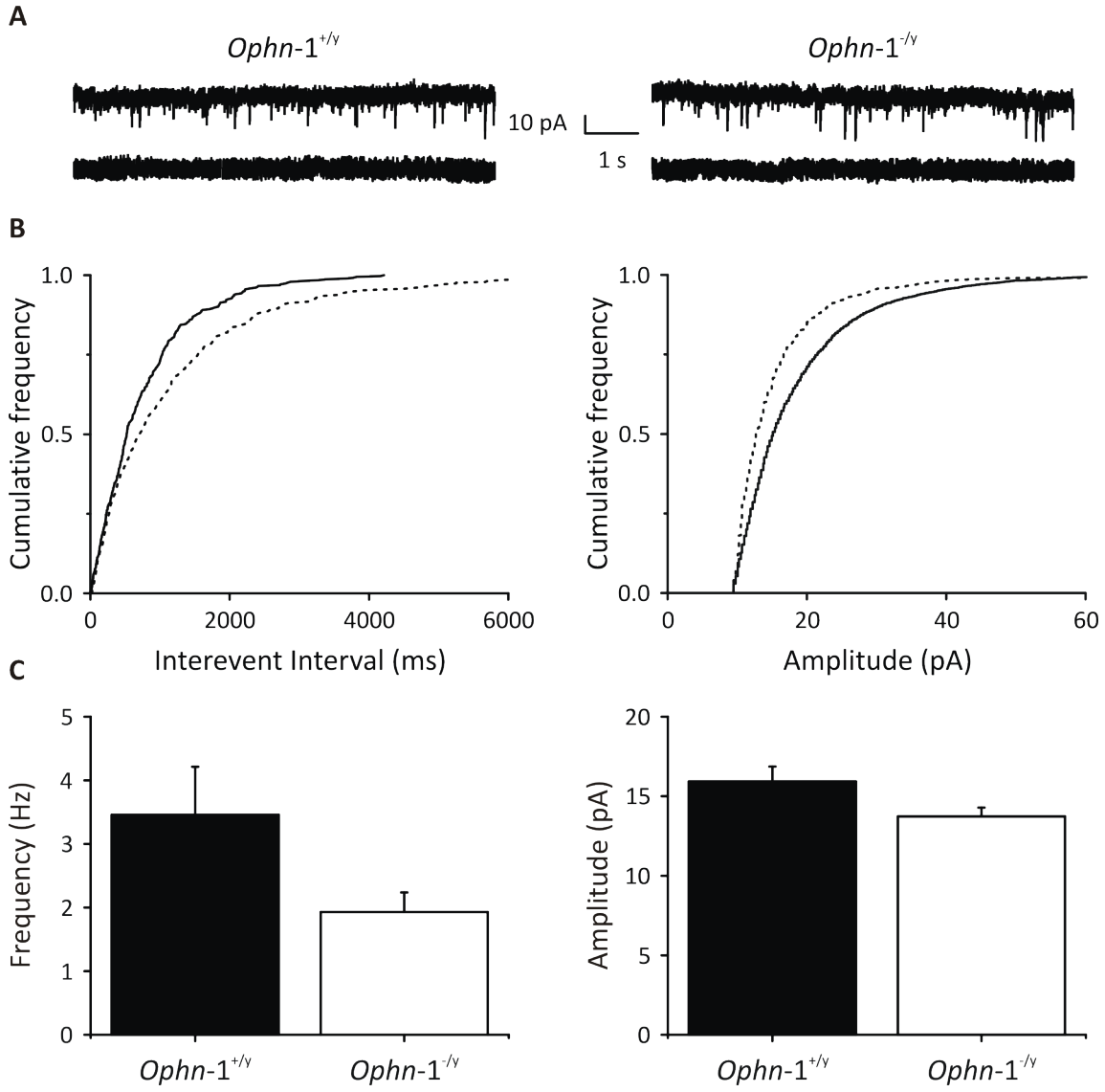

Figure 4.3 – Spontaneous EPSCs were unaltered in *Ophn*-1$^{-/y}$ neurons.

(A) Representative trace of spontaneous EPSCs *(upper panel)* in *Ophn*-1$^{+/y}$ *(left panel)* and *Ophn*-1$^{-/y}$ *(right panel)* neurons. These were abolished in the presence of NBQX (20 µM) and D-APV (25 µM; *lower panels*). **(B)** Representative cumulative frequency plots of spontaneous EPSC frequency and amplitude in *Ophn*-1$^{+/y}$ *(solid line)* and *Ophn*-1$^{-/y}$ *(dotted line)* neuron. **(C)** Mean of the median frequency and amplitude of spontaneous EPSCs (*Ophn*-1$^{+/y}$ 22 cells from 12 mice and *Ophn*-1$^{-/y}$ 9 cells from 5 mice). Mann-Whitney U test ($p>0.05$).

4.5 Evoked EPSCs

To study evoked EPSCs, presynaptic axons were stimulated using an aCSF-filled patch electrode, placed 50 µm away from the soma in the apical direction. The maximum amplitude of the evoked EPSC was smaller in *Ophn*-$1^{-/y}$ neurons than in *Ophn*-$1^{+/y}$ neurons (512.8 ± 69.8 pA, n=9 and 696.5 ± 33.8 pA, n=7; p=0.02; fig 4.4B,C). No difference was observed in the half maximal strength (p=0.2) of the stimulus response curve (fig 4.4C).

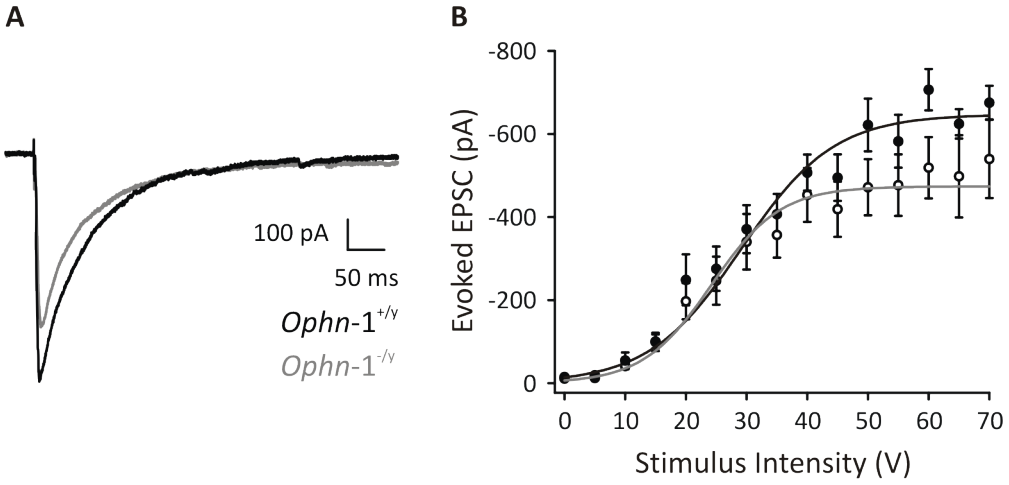

C

	Ophn-1$^{+/y}$	*Ophn*-1$^{-/y}$	p value
Max (pA)	-696.5 ± 33.8	-512.8 ± 69.8	0.02
V_{50} (pA)	31.4 ± 2.6	26.9 ± 1.6	0.2

Figure 4.4 – Reduced evoked EPSCs in *Ophn*-1$^{-/y}$ neurons.

(A) The maximum evoked EPSC amplitude was smaller in *Ophn*-1$^{-/y}$ than in *Ophn*-1$^{+/y}$ layer V pyramidal neurons. **(B)** Input-output relationship of evoked EPSCs fitted with a sigmoidal curve showed smaller maximal in *Ophn*-1$^{-/y}$ (*open circles*, 9 cells from 5 mice) than *Ophn*-1$^{+/y}$ neurons (*filled circles*, 7 cells from 6 mice). **(C)** Mean fit parameters for current-voltage relationship. Mann-Whitney U test with Bonferonni correction α=0.025.

The reduced amplitude of the maximum evoked EPSC may be due to fewer synapses, reduced number of release site or reduced probability of release. To elucidate the mechanism underlying the alterations in excitatory transmission, the latter hypotheses were investigated using a paired pulse protocol which is a measurement of presynaptic release and a high frequency protocol to study vesicle dynamics.

4.5.1 Paired pulse stimulation of evoked EPSCs

Oligophrenin-1 is present in the presynaptic terminal where its immunolabelling overlaps with synaptophysin (Govek *et al.*, 2004). The presence of oligophrenin-1 in the presynaptic terminal implicates a presynaptic function (Powell *et al*., 2012). Studies have reported paired pulse to be depressed in *Ophn*-$1^{-/y}$ neurons (Khelfaoui *et al*., 2007; Saintot, 2010; Powell *et al*., 2012). Pairs of stimuli were delivered at intervals between 10-1500 ms in *Ophn*-$1^{+/y}$ and *Ophn*-$1^{-/y}$ neurons. Paired pulse depression was observed at all intervals from both *Ophn*-$1^{+/y}$ and *Ophn*-$1^{-/y}$ neurons (fig 4.5B). No significant difference was observed in the degree of depression at all inter-pulse intervals (p=0.1).

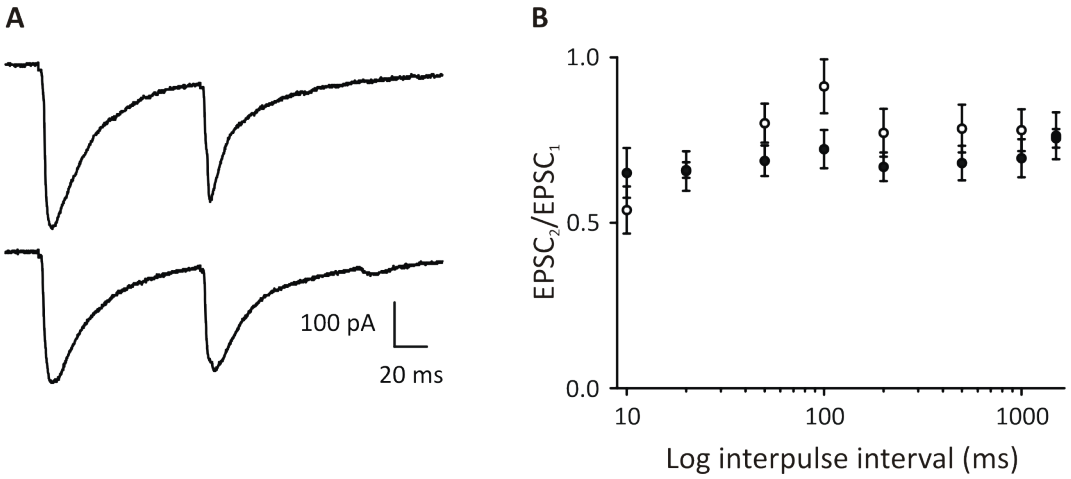

Figure 4.5 – Paired pulse ratio was unchanged in *Ophn*-$1^{-/y}$ layer V pyramidal neurons.

(A) Representative traces of evoked EPSCs trigged by two stimuli delivered at 100 ms inter-pulse interval in *Ophn*-$1^{+/y}$ *(top panel)* and *Ophn*-$1^{-/y}$ *(bottom panel)* layer V pyramidal neurons. **(B)** Paired pulse ratio did not differ between *Ophn*-$1^{+/y}$ (*filled circles*, 10 cells from 7 mice) and *Ophn*-$1^{-/y}$ neurons (*open circles*, 10 cells from 5 mice). Kruskal-Wallis test (p>0.05).

4.5.2 Frequency following of evoked EPSCs

Oligophrenin-1 has been associated with the regulation of vesicle availability at excitatory synapses (Nakano-Kobayashi *et al*., 2009). Therefore, the ability of *Ophn*-$1^{+/y}$ and *Ophn*-$1^{-/y}$ synapses to sustain high frequency firing in layer V pyramidal neurons was examined using a repetitive stimulation protocol. A train of 10 stimuli were delivered at frequencies between 10 and 100 Hz and the amplitude of the evoked EPSCs were measured (fig 4.6A). Responses were normalised to the maximal amplitude of the first response to determine if facilitation or depression had occurred during the train of stimuli. Depression was observed in *Ophn*-$1^{+/y}$ and *Ophn*-$1^{-/y}$ neurons at all pulses and frequencies; the degree of depression did not differ between genotypes ($p=0.7$; fig 4.6B,C).

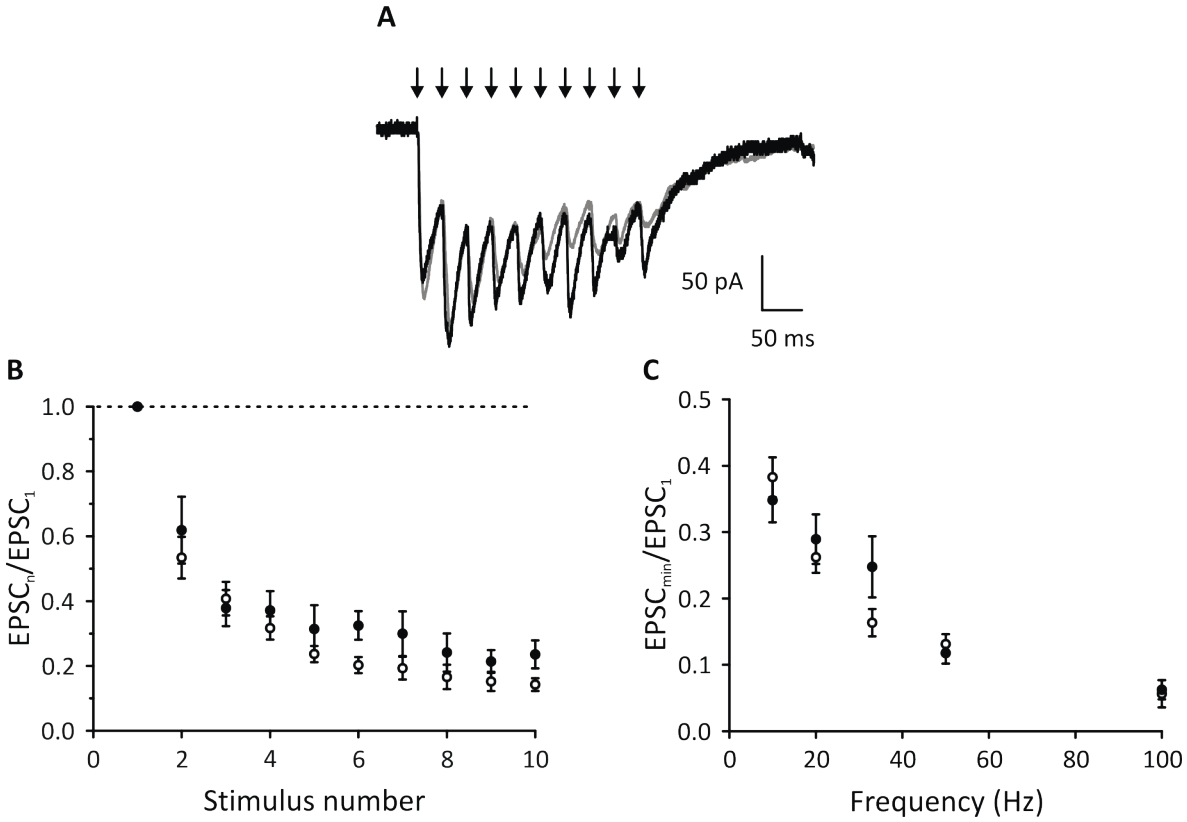

Figure 4.6 – High frequency stimulation was unaltered in *Ophn*-1$^{-/y}$ layer V pyramidal neurons.

(A) Representative traces of evoked EPSCs triggered by 10 stimuli at 33 Hz in *Ophn*-1$^{+/y}$ *(black trace)* and *Ophn*-1$^{-/y}$ *(grey trace)* layer V pyramidal neurons. **(B)** Evoked EPSC amplitude plotted against stimulus number for 33 Hz in *Ophn*-1$^{+/y}$ (*filled circles*, 8 cells from 5 mice) and *Ophn*-1$^{-/y}$ neurons (*open circles*, 10 cells from 5 mice). The evoked EPSC amplitudes were normalised to the first response. **(C)** Minimal EPSC amplitude (mean of the last 4 stimuli) plotted against stimulus frequency. Kruskal-Wallis test ($p>0.05$).

The normal responses following paired pulse stimulation and high frequency stimulation in *Ophn*-$1^{-/y}$ neurons did not suggest an excitatory presynaptic deficit in layer V pyramidal neurons. As synaptic integration is related to neuronal morphology, the reduction in excitatory transmission may be due to altered arborisation; thus, the neuroanatomy of layer V pyramidal neurons was examined.

4.6 Neuroanatomy of layer V pyramidal neurons

Alterations in dendritic arborisation and dendritic spine morphology have extensively been studied as the aetiology of mental retardation (Newey *et al*., 2005). Powell *et al* (2012) found changes in both dendritic tree and spine morphology in dentate gyrus granule neurons. Furthermore, the observation of cortical thinning could be due to less extensive dendritic arbor in cortical neurons. Alexa 488 filled layer V pyramidal neurons from the excitatory transmission study were immunostained for dendritic morphometry. Sholl analysis revealed no significant difference in the total number of intersections between *Ophn*-$1^{+/y}$ and *Ophn*-$1^{-/y}$ layer V pyramidal neurons (98 ± 15, n=12 and 125 ± 16, n=11; respectively; p=0.22; fig 4.7B,C).

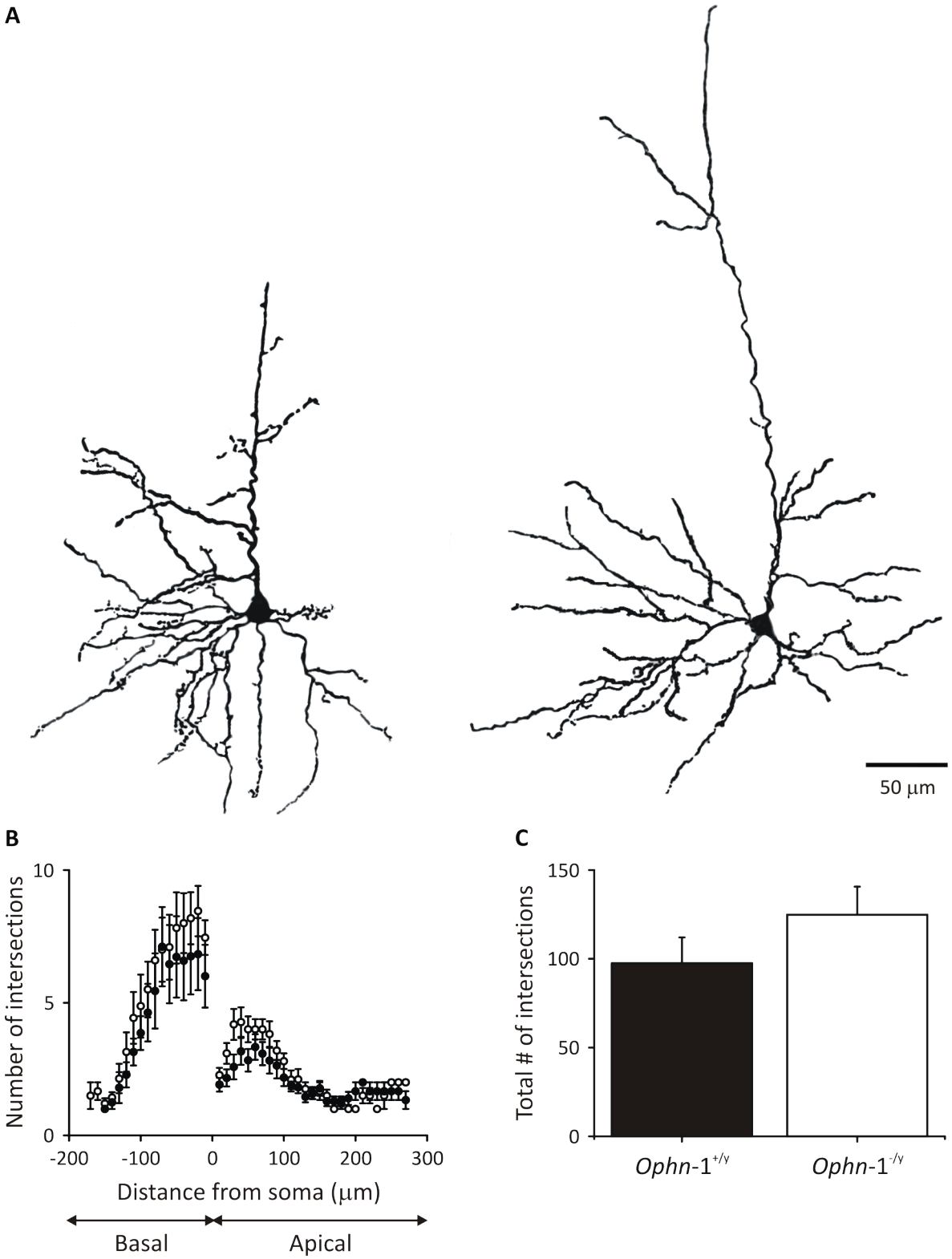
A
50 μm
B
Number of intersections
10
5
0
-200
-100
0
100
200
300
Distance from soma (μm)
Basal
Apical
C
Total # of intersections
150
100
50
0
Ophn-1+/y
Ophn-1-/y

Figure 4.7 – Dendritic arborisation was unchanged in *Ophn*-1$^{-/y}$ layer V pyramidal neurons.

(A) Representative layer V pyramidal neurons filled with Alexa 488, immunostained with anti-rabbit Alexa Fluor 488, followed by biotinylated secondary antibody and processed with DAB in *Ophn*-1$^{+/y}$ *(left panel)* and *Ophn*-1$^{-/y}$ neuron *(right panel)*. Dendritic tree enhancement performed for display purposes. **(B)** Sholl analysis showed no alterations in dendritic arborisation between *Ophn*-1$^{+/y}$ (*filled circle*, 12 cells from 6 mice) and *Ophn*-1$^{-/y}$ neurons (*open circles*, 11 cells from 5 mice). **(C)** The total number of intersections was unaltered in *Ophn*-1$^{-/y}$ neurons. Student's t-test ($p>0.05$).

4.7 Dendritic spines

Alterations in dendritic spine morphology have been associated with loss of function of oligophrenin-1 (Govek *et al*., 2004; Khelfaoui *et al*., 2007; Nadif Kasri *et al*., 2009; Powell *et al*., 2012). Spine density was examined from layer V pyramidal neurons filled with Alexa 488 that were immunostained. No difference was observed in spine density along basal dendrites (*Ophn*-1$^{+/y}$ 0.9 ± 0.1 µm^{-1}, n=7 and *Ophn*-1$^{-/y}$ 0.8 ± 0.1 µm^{-1}, n=10; p=0.4; fig 4.8). On apical dendrites, the overall spine density was less in *Ophn*-1$^{-/y}$ neurons than *Ophn*-1$^{+/y}$ neurons (0.9 ± 0.1 µm^{-1}, n=10 and 1.3 ± 0.1 µm^{-1}, n=7; respectively; p=0.003; fig 4.8).

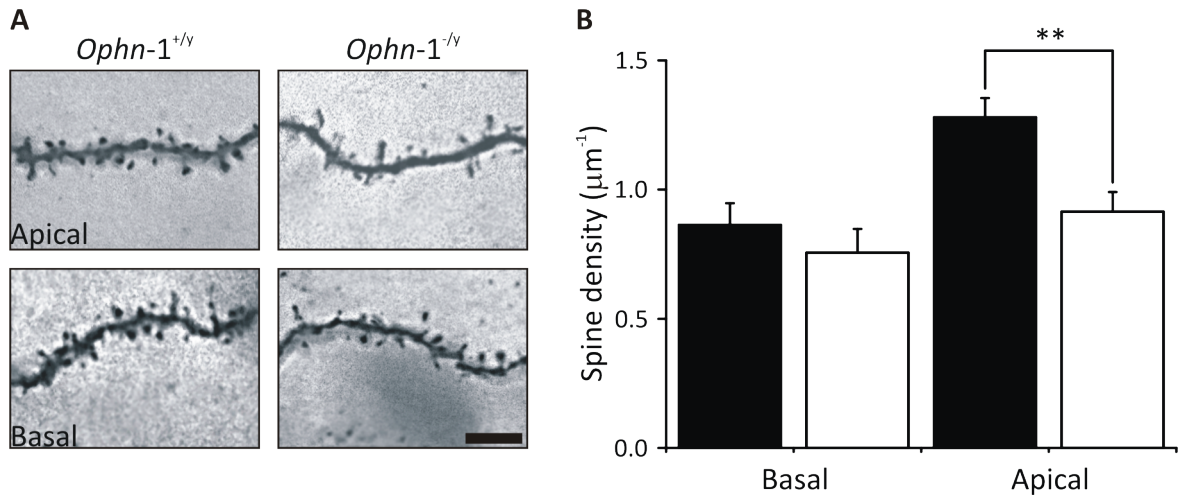

Figure 4.8 – Dendritic spine density was altered in *Ophn*-1$^{-/y}$ layer V pyramidal neurons.

(A) Dendritic spines in *Ophn*-1$^{+/y}$ and *Ophn*-1$^{-/y}$ neurons on apical dendrite *(upper panels)* and basal dendrite *(lower panels)*. Scale bar, 5 µm. **(B)** Densities of dendritic spines were reduced on apical dendrites, without alterations on basal dendrites (*Ophn*-1$^{+/y}$ 7 cells from 5 mice and *Ophn*-1$^{-/y}$ 10 cells from 6 mice). Student's t-test with Bonferonni correction (α=0.025; **=p<0.005).

Alterations in excitatory neurotransmission as a result of altered oligophrenin-1 expression in hippocampal neurons have been widely reported (Powell *et al.*, 2012; Nadif Kasri *et al.*, 2011; Nadif Kasri *et al.*, 2009); some of these changes are replicated in layer V neocortical neurons (altered dendritic spines and reduced synaptic transmission). In contrast to the emerging picture of altered excitatory neurotransmission, the role of oligophrenin-1 in inhibitory synapses is less well understood. Therefore, inhibitory neurotransmission was studied to provide a complete picture of the role of oligophrenin-1 in synaptic transmission.

4.8 Spontaneous IPSCs

Previous work contradicts as to whether inhibitory neurotransmission is altered. Powell *et al*. (2012) reported a reduction in IPSC frequency in dentate gyrus granule neurons from acute hippocampal slices from the *Ophn1* mouse model whereas Nadif Kasri *et al*. (2009) reported IPSCs are unaffected by siRNA knockdown of oligophrenin-1 in CA1 pyramidal neurons. Inhibitory transmission was examined to determine if knockout of *Ophn1* plays a role at inhibitory synapses in layer V pyramidal neurons. Cells were voltage clamped at -80 mV using an internal solution containing an equimolar chloride concentration which shifted the reversal potential of chloride ions from -80 mV to 0 mV, thus allowing IPSCs to be recorded as inward deflections at -80 mV which reversed polarity at 0 mV (data not shown). To confirm isolation of IPSCs, NBQX (20 µM) and D-APV (25 µM) were added to the bath solution. Figure 4.9A shows representative traces of spontaneous IPSCs in layer V neurons which were abolished after bath application of bicuculline (10 µM), confirming a $GABA_A$-ergic origin. No significant difference was observed in the frequency of IPSCs between *Ophn*-$1^{+/y}$ and *Ophn*-$1^{-/y}$ neurons (5.5 ± 0.4 Hz, n=49 and 6.3 ± 0.8 Hz, n=32; respectively; p=0.6; fig 4.9B), nor was there a significant difference in the amplitude of spontaneous IPSCs between *Ophn*-$1^{+/y}$ and *Ophn*-$1^{-/y}$ neurons (43.2 ± 1.9 pA, n=49 and 38.2 ± 2.5 pA, n=32; p=0.1; fig 4.9C).

4.8.1 Miniature IPSCs

Miniature (or mini) IPSCs are action potential independent IPSCs where individual synaptic currents reflect single quanta of neurotransmitter released from the presynaptic terminal. Miniature IPSCs were isolated by superfusion of tetrodotoxin (TTX, 1 μM), a voltage-gated sodium channel blocker that blocks spontaneous action potential firing. Figure 4.9A shows typical mini IPSCs in layer V pyramidal neurons. The frequency of mini IPSCs is significantly less than spontaneous IPSCs in *Ophn*-$1^{+/y}$ and *Ophn*-$1^{-/y}$ neurons (p=0.003 and p=0.0001; respectively; fig 4.9B) without alterations in the amplitude (fig 4.9C). No significant difference was observed in the frequency of mini IPSC between *Ophn*-$1^{+/y}$ and *Ophn*-$1^{-/y}$ neurons (2.8 ± 0.7 Hz, n=8 and 2.4 ± 0.5 Hz, n=7; respectively; p=0.6; fig 4.9B).

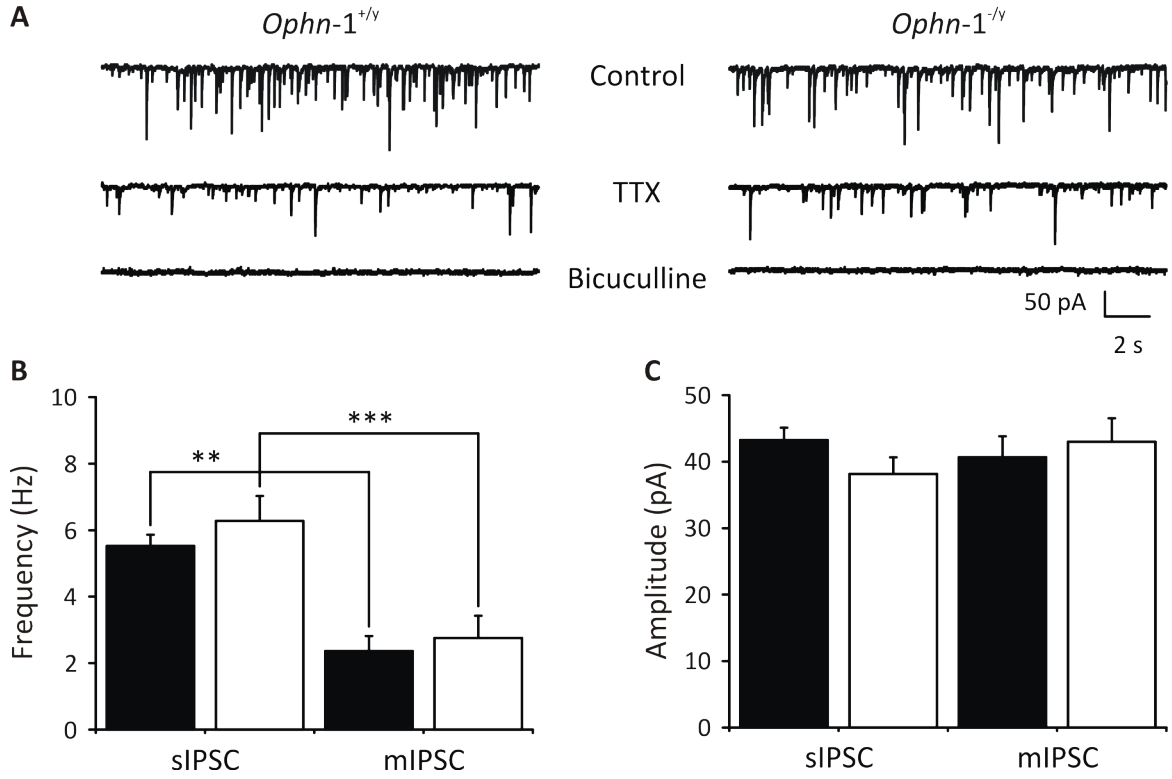

Figure 4.9 – Spontaneous and miniature IPSCs were unaltered in *Ophn*-1$^{-/y}$ neurons.

(A) Representative trace of spontaneous IPSCs *(upper panels)* in *Ophn*-1$^{+/y}$ *(left panels)* and *Ophn*-1$^{-/y}$ *(right panels)* neurons. Superfusion with tetrodotoxin (1 µM) significantly reduced the spontaneous IPSC frequency in both *Ophn*-1$^{+/y}$ and *Ophn*-1$^{-/y}$ neurons *(middle panels, B)*. Miniature IPSCs were abolished in the presence of bicuculline (10 µM; *lower panels*). **(B)** The mean frequency of spontaneous and miniature IPSCs was unaltered in *Ophn*-1$^{-/y}$ neurons. **(C)** The mean amplitude of spontaneous IPSCs were similar to miniature IPSCs and were not different in *Ophn*-1$^{-/y}$ neurons (*Ophn*-1$^{+/y}$ *filled columns,* spontaneous IPSC: 49 cells from 18 mice, mini IPSC 8 cells from 4 mice and *Ophn*-1$^{-/y}$ *open columns*, spontaneous IPSC: 32 cells from 13 mice, mini IPSC: 7 cells from 2 mice). Mann-Whitney U test with Bonferonni correction (α=0.025), **=p<0.005 and ***=p<0.0005. sIPSC, spontaneous IPSC; mIPSC, miniature IPSC.

4.9 Vesicle dynamics in *Ophn1* layer V pyramidal neurons

Oligophrenin-1 has been implicated in the control of synaptic vesicle availability in hippocampal neurons (Khelfaoui *et al*., 2009; Nakano-Kobayashi *et al*., 2009; Powell *et al*., 2012); it could be that if synapses are driven at high frequencies, a difference between genotypes may be observed. To assess whether synaptic vesicle dynamics were altered in layer V neurons, high frequency minimal stimulation (Schneggenburger *et al*., 1999; Powell *et al*., 2012) was used to estimate the size and replenishment rate of the RRP in a single axon/synapse. Single synapse stimulation, using an aCSF-filled patch electrode, was achieved using minimal stimulation to produce an all or nothing IPSC which is interpreted as resulting from activation of a single synapse. Repetitive stimulation of a single synapse (40 stimuli, 20 Hz; fig 4.10A) was used to estimate the size of the RRP and the replenishment rate of vesicles from the reserve pool. By plotting the cumulative IPSC amplitude, two phases can be identified (fig 4.10B). The initial rapid rise reflects vesicle release from the RRP and the subsequent slow rise is the steady state release due to refilling of the RRP from the reserve pool. The RRP size (RRP_{syn}) was determined by back extrapolation of the linear portion between the 20^{th} and 40^{th} stimulus response to time zero. The RRP_{syn} was unaltered between *Ophn*-$1^{+/y}$ and *Ophn*-$1^{-/y}$ neurons (573.8 ± 194.3 pA, n=9 and 407.2 ± 31.3 pA, n=9; respectively; p=0.9; fig 4.10C). The rate of replenishment of the RRP was estimated by measuring the slope of the steady state rise of the cumulative IPSC amplitude between the 20^{th} and 40^{th} stimulus response. The rate of vesicle replenishment was unaltered between *Ophn*-$1^{+/y}$ and *Ophn*-$1^{-/y}$ synapses (12.2 ± 3.2 pA s^{-1} n=9 and 16.0 ± 3.9 pA s^{-1} n=9; respectively; p=0.6; fig 4.10D).

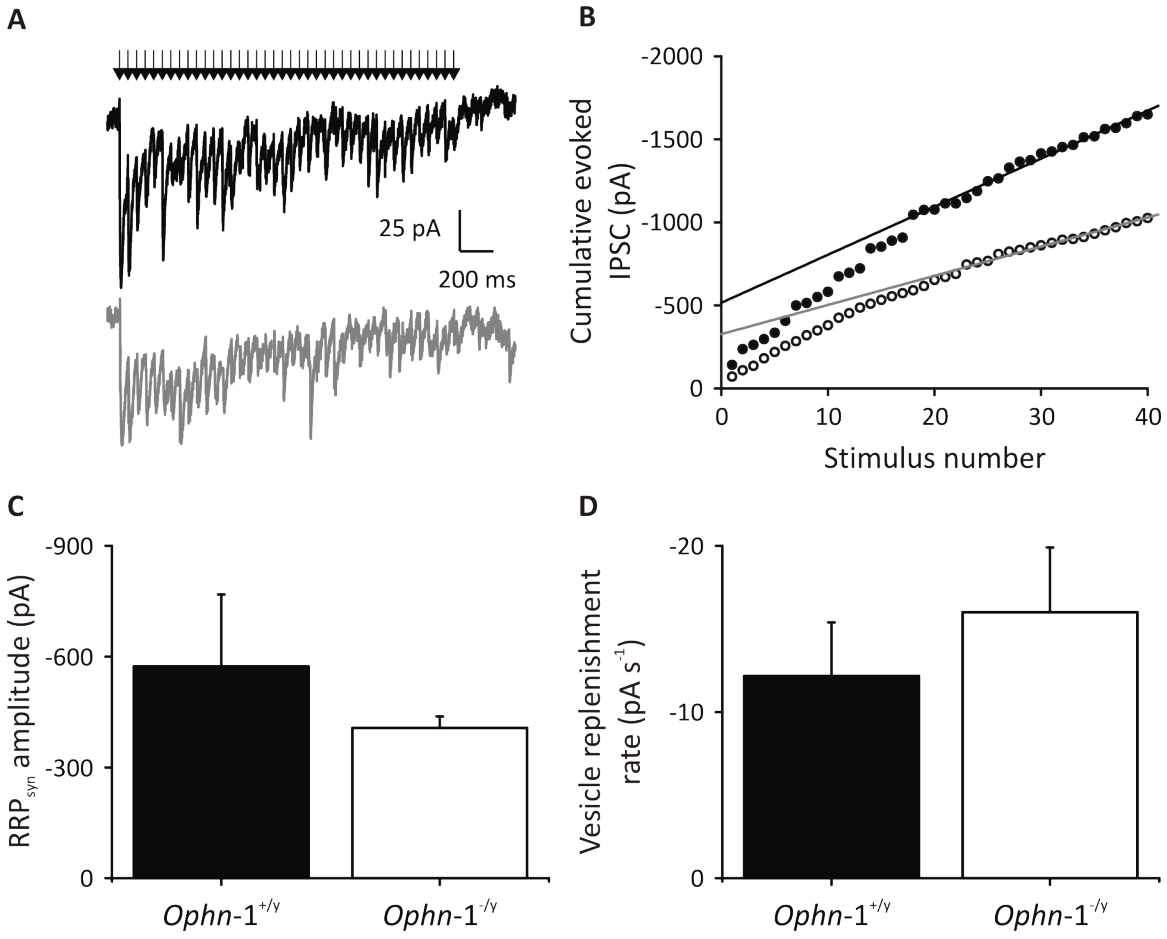

Figure 4.10 – Readily releasable pool size was unaltered in *Ophn*-1$^{-/y}$ neurons.

(A) Averaged train of evoked IPSC, 40 stimuli at 20 Hz, in *Ophn*-1$^{+/y}$ *(black trace)* and *Ophn*-1$^{-/y}$ *(grey trace)* layer V pyramidal neurons. Corresponding cumulative evoked IPSC amplitudes of averaged traces (in **A**) plotted against stimulus number (*Ophn*-1$^{+/y}$, *filled circles* and *Ophn*-1$^{-/y}$, *open circles)*. Data points in the range 20-40 were fitted by linear regression and back extrapolated to time 0 to estimate the size of RRP$_{syn}$. The mean **(B)** RRP$_{syn}$ and **(C)** rate of replenishment was unchanged in *Ophn*-1$^{-/y}$ neurons (*Ophn*-1$^{+/y}$ 9 cells from 5 mice and *Ophn*-1$^{-/y}$ 9 cells from 5 mice). Mann-Whitney U test ($p>0.05$). RRP$_{syn}$, readily releasable pool size.

4.10 IPSCs: layer V pyramidal neurons and dentate gyrus granule cells

Given the lack of difference in inhibitory transmission in layer V pyramidal neurons, perhaps dentate gyrus granule neurons are peculiar. Whole-cell recordings were made from layer V and dentate gyrus granule neurons in the same mice to establish if there is a selective change in the granule neurons. No significant difference was observed in the frequency of IPSCs in both layer V pyramidal neurons and granule neurons between *Ophn*-$1^{+/y}$ and *Ophn*-$1^{-/y}$ neurons ($p=0.6$ and $p=0.7$; respectively; fig 4.11A), nor was there a difference in the amplitude ($p=0.7$ and $p=0.9$; respectively; fig 4.11B).

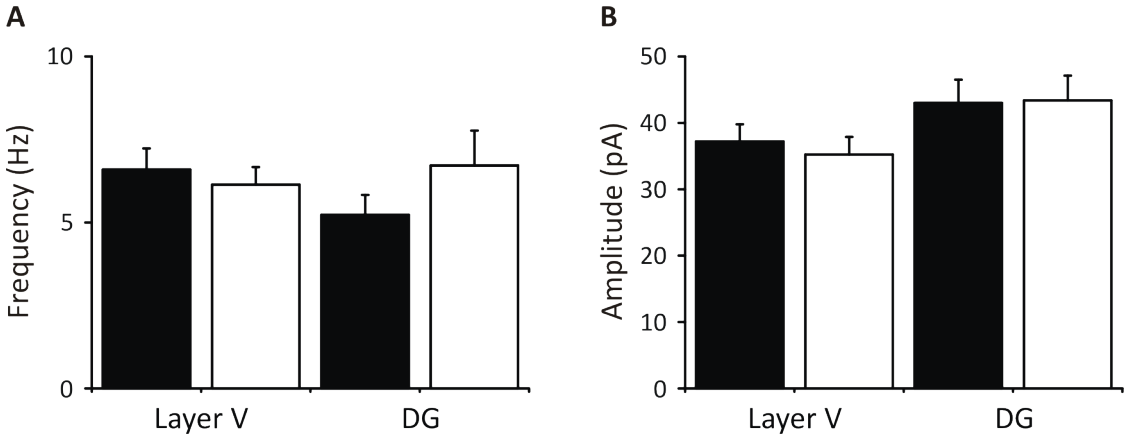

Figure 4.11 – IPSCs were unaltered in layer V pyramidal cells and dentate gyrus granule cells in *Ophn*-1$^{-/y}$ mice.

(A) The mean frequency of spontaneous IPSCs was not different between *Ophn*-1$^{+/y}$ *(filled columns)* and *Ophn*-1$^{-/y}$ neurons *(open columns)* in both layer V pyramidal cells and granule neurons from the same animals. **(B)** The mean amplitude of spontaneous IPSCs was unaltered between *Ophn*-1$^{+/y}$ and *Ophn*-1$^{-/y}$ in layer V pyramidal neurons and granule neurons. *Ophn*-1$^{+/y}$ (layer V: 21 cells from 7 mice; dentate gyrus 13 cells from 7 mice) and *Ophn*-1$^{-/y}$ (layer V: 23 cells from 10 mice; dentate gyrus: 15 cells from 8 mice). Student's t-test ($p>0.05$). DG, dentate gyrus granule neuron.

4.11 Summary

Whole-cell recordings from layer V pyramidal neurons revealed no differences in intrinsic properties or spontaneous EPSCs between *Ophn*-$1^{+/y}$ and *Ophn*-$1^{-/y}$. However putative EPSPs and evoked EPSCs were reduced in *Ophn*-$1^{-/y}$ neurons, without alterations in response to paired and repetitive stimuli. Dendritic tree morphology was unaffected in *Ophn*-$1^{-/y}$ neurons, however region specific reductions in spine density were observed. Spontaneous inhibitory transmission was unaltered in layer V pyramidal neurons; neither the readily releasable pool size, nor the rate of vesicle replenishment was affected in inhibitory synapses. Spontaneous IPSCs were unchanged in both layer V pyramidal neurons and dentate gyrus granule neurons from the same animals. These results suggest deficits in excitatory synaptic transmission in the neocortex that differ from hippocampal deficits and are unlikely due to altered vesicle dynamics. The absence of phenotype in inhibitory transmission in the neocortex could highlight the importance of excitatory deficits which is typically characterised by altered dendritic spine morphology in MR. However the inconsistent inhibitory phenotype in hippocampal neurons with previous studies (Powell *et al.*, 2012; Saintot, 2010) suggest alterations in the *Ophn1* model.

Chapter 5: Investigation of Hippocampal Physiology and Gross Brain Morphology in *Ophn*-1$^{-/y}$ Mice

5.1 Aims

Several studies have identified deficits in inhibitory transmission in hippocampal neurons. Powell and colleagues (2012) reported reduced inhibitory transmission in dentate gyrus granules neurons due to smaller RRP and slower vesicle recycling. Similar results were identified in CA3 pyramidal cells which were associated with impaired kainate-induced gamma oscillations (Saintot, 2010). As the effects of loss of oligophrenin-1 function on synaptic physiology in neocortical and hippocampal neurons were not consistent with previous studies, this raised the question whether other deficits associated with the *Ophn1* model were still present and whether this was still an appropriate model to study the pathophysiology of *Ophn1* MR. The aims of this study were to investigate whether other previously reported hippocampal deficits (e.g. reduced kainate-induced gamma oscillations; Saintot, 2010) and gross morphological changes (e.g. ventricular dilatation; Khelfaoui *et al*., 2007) were still present. Gamma oscillations and synaptic physiology were studied in the CA3 region using extracellular field potentials and the anatomical phenotype of *Ophn*-1$^{-/y}$ mice has been examined using histological techniques. Detailed measurements were made from 6 week old and 3 month old *Ophn1* mice to quantify the volume of lateral and third cerebral ventricles and the degree of neocortical thinning.

5.2 Development of neuronal oscillations

In vitro gamma oscillations were evoked in CA3 by application of kainate, a glutamatergic receptor agonist which tonically activates kainate receptors containing GluR5 and GluR6 subunits (Fisahn, 2005). Slices were placed in the interface recording chamber and neuronal oscillations were recorded by placing an extracellular electrode in the pyramidal cell layer of the CA3c region of the hippocampus. Baseline activity was recorded for 5 minutes; the majority of slices generate irregular activity with little power in the gamma range (fig 5.1B *upper panel*, C *dotted line*). However a subset of slices showed spontaneous gamma oscillations in the absence of kainate (see fig 5.6). Application of kainate (100 nM), induced oscillations within the gamma frequency range (20-80 Hz) which become more regular and synchronous with time (fig 5.1A,B *lower panel*) resulting in the power of these oscillations increasing with time (fig. 5.1A,C).

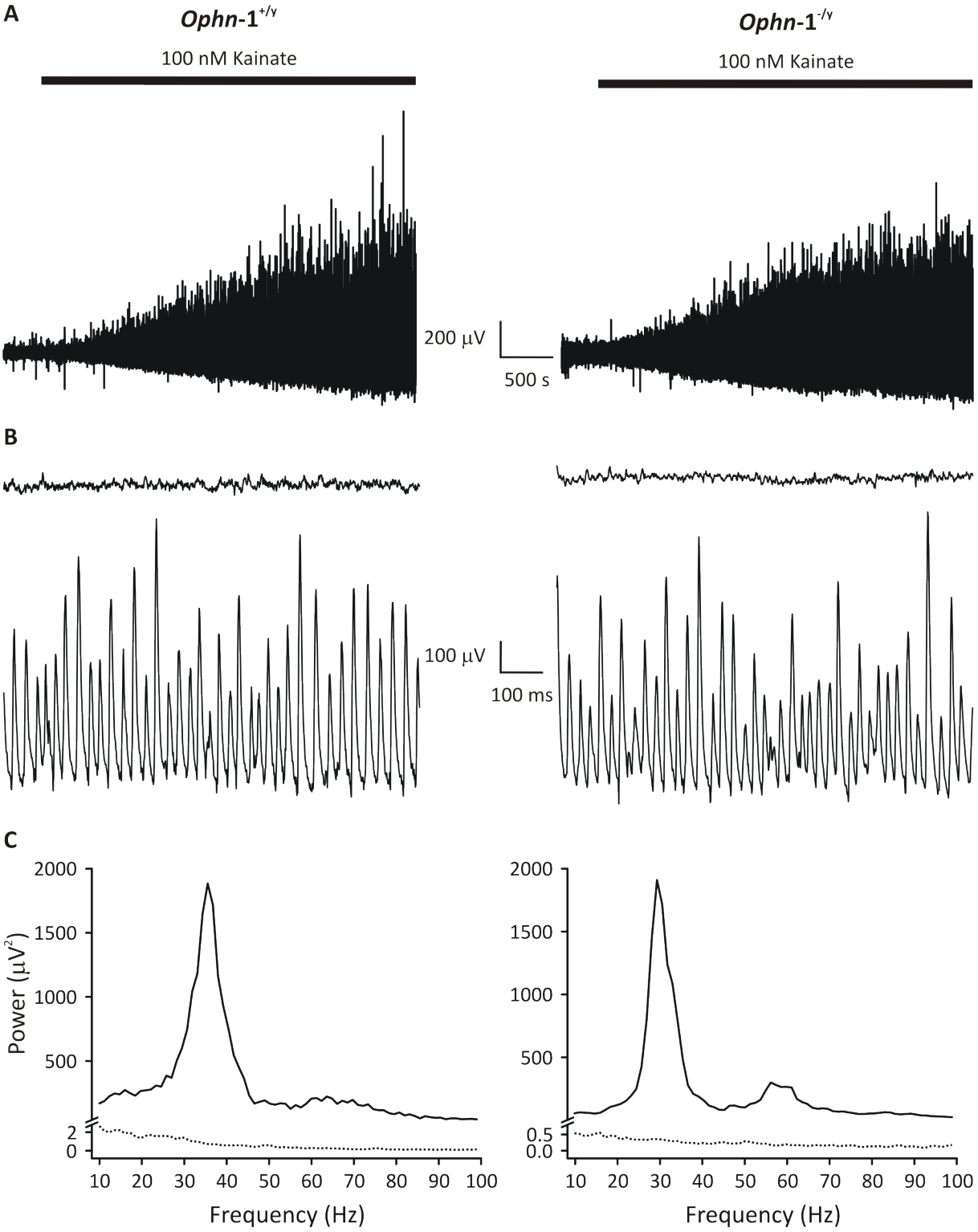
A
Ophn-1+/y
100 nM Kainate
Ophn-1-/y
100 nM Kainate
200 µV
500 s
B
100 µV
100 ms
C
Power (µV2)
2000
1500
1000
500
2
0
0.5
0.0
10 20 30 40 50 60 70 80 90 100
Frequency (Hz)

Figure 5.1 – Development of kainate-induced gamma oscillations.

(A) Application of 100 nM kainate evokes neuronal oscillations in the gamma frequency range in the stratum pyramidale in CA3c in both *Ophn*-$1^{+/y}$ and *Ophn*-$1^{-/y}$ slices. **(B)** Expanded time frame at 0 min (*upper panel*) and 60 min (*lower panel*) following kainate application, demonstrating neuronal synchrony. **(C)** Power spectra at 0 min (*dotted line*) and 60 min (*solid line*).

To confirm that kainate-induced gamma oscillations were driven by inhibitory transmission (Fisahn, 2005), $GABA_A$ antagonist bicuculline (10 μM) was applied. Gamma oscillations were eliminated by application of bicuculline (fig 5.2) in both genotypes.

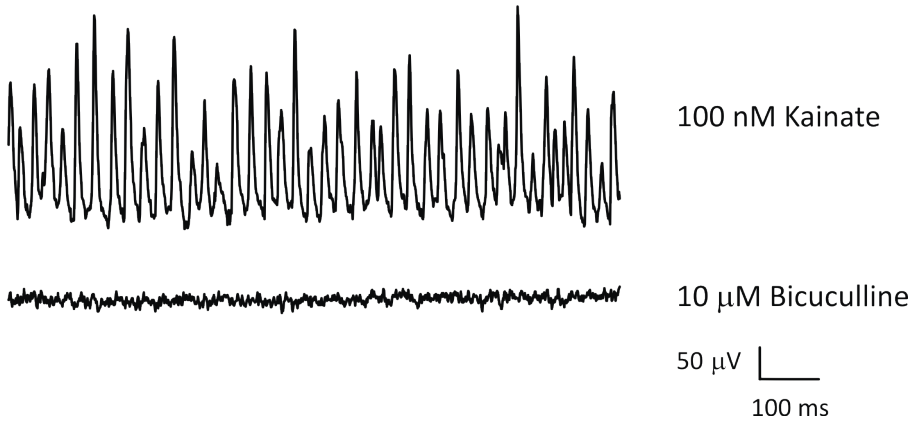

Figure 5.2 – Abolition of gamma oscillations with bicuculline (10 μM).

Representative trace of gamma oscillations evoked by 100 nM kainate *(upper trace)* at 60 min in stratum pyramidale in CA3c in *Ophn*-$1^{+/y}$ slice which were blocked following application of $GABA_A$ receptor antagonist bicuculline *(*10 μM, *lower panel)*.

The power of kainate-induced gamma oscillations gradually increased throughout the 60 minute period after application of kainate (fig 5.3C). The summated power of gamma oscillations in *Ophn*-$1^{+/y}$ slices increased to 21749 ± 3847 μV^2 (n=32) which is considerably larger than at baseline, 88 ± 24 μV^2 (n=32). Peak power also increased with time following kainate application (fig 5.2A). The peak frequency increased from 27 ± 2 Hz (n=32) in the absence of kainate to 35 ± 1 Hz (n=32) after 10 minutes in the presence of kainate, before stabilising at approximately 32 Hz (fig 5.3B). Similar increases in these variables were also observed in *Ophn*-$1^{-/y}$ slices. No significant difference was observed in peak power between *Ophn*-$1^{+/y}$ and *Ophn*-$1^{-/y}$ slices (p=0.5; fig 5.3A), neither the summated power of gamma oscillations (p=0.8; fig 5.3C), nor the peak frequency (p=0.9; fig 5.3B) was altered in *Ophn*-$1^{-/y}$ slices.

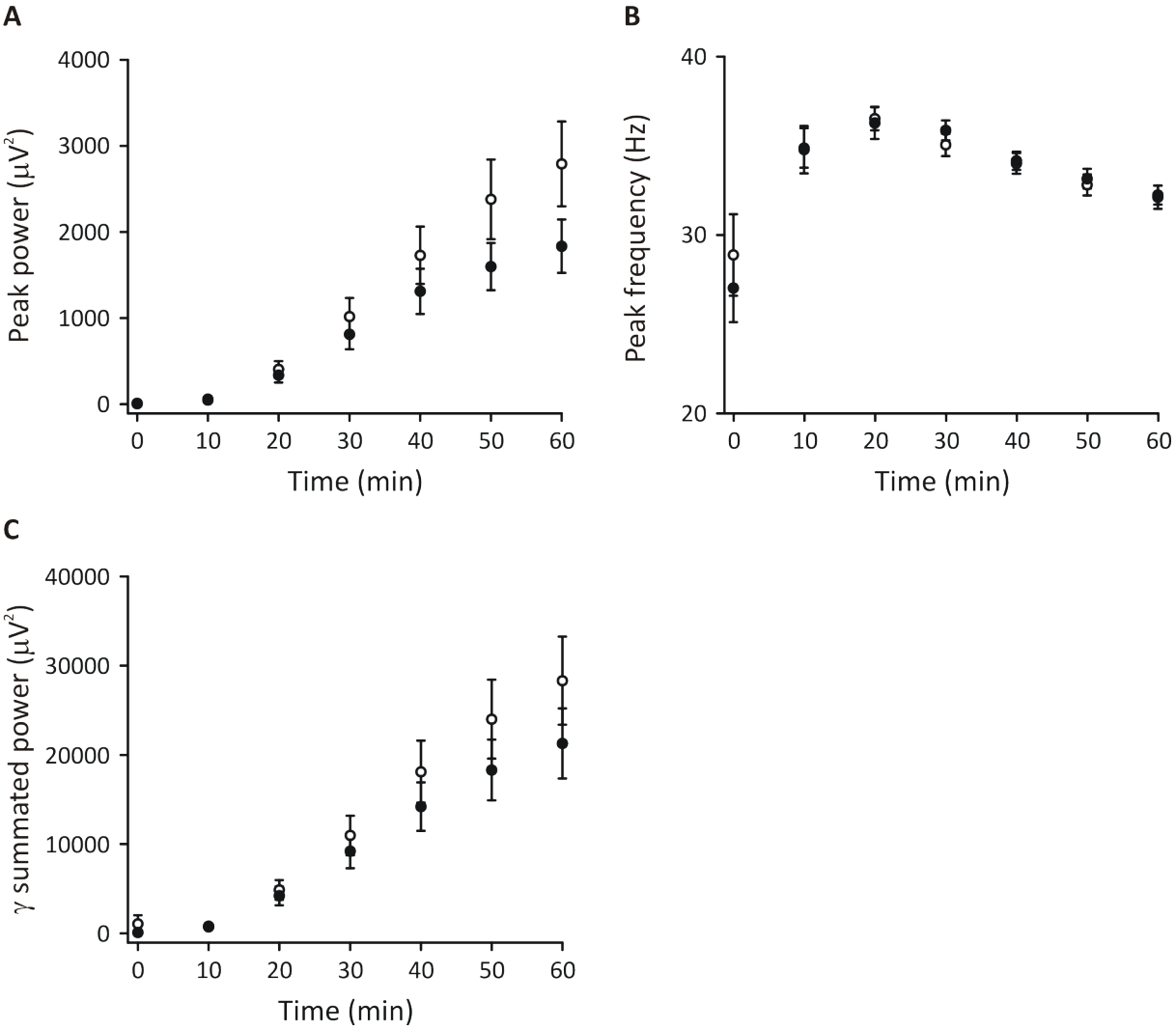

Figure 5.3 – *Ophn*-1$^{-/y}$ slices showed no difference in gamma oscillations.

No difference was observed in the **(A)** peak power, **(B)** peak frequency or **(C)** summated power of gamma oscillations between *Ophn*-1$^{+/y}$ *(filled circles,* 32 slices from 10 mice) and *Ophn*-1$^{-/y}$ *(open circles*, 28 slices from 9 mice) slices in the stratum pyramidale, CA3c. ANOVA ($p>0.05$).

Current source density analysis has shown that gamma oscillations change polarity close to the stratum pyramidale (Pietersen *et al*., 2009); therefore variability in electrode position may be amplified by this transition. To remove this potential confound, gamma oscillations were also examined in the synaptic layer, the stratum radiatum, as the polarity and amplitude of the gamma oscillations are minimally affected by variability in electrode placement (Pietersen *et al*., 2009). The summated power of gamma oscillations in the stratum radiatum increased from 55 ± 15 μV^2 at 0 min to 5510 ± 1022 μV^2 at 60 min (n=24) in *Ophn*-$1^{+/y}$ slices and from 38 ± 6 μV^2 to 6398 ± 935 μV^2 in *Ophn*-$1^{-/y}$ slices (n=31; fig 5.5C). No difference was observed in summated power between *Ophn*-$1^{+/y}$ and *Ophn*-$1^{-/y}$ slices (p=0.5; fig 5.5C) neither the peak power of gamma oscillations (p=0.4; fig 5.5A), nor the peak frequency (p=0.9; fig 5.5B) were altered in *Ophn*-$1^{-/y}$ slices.

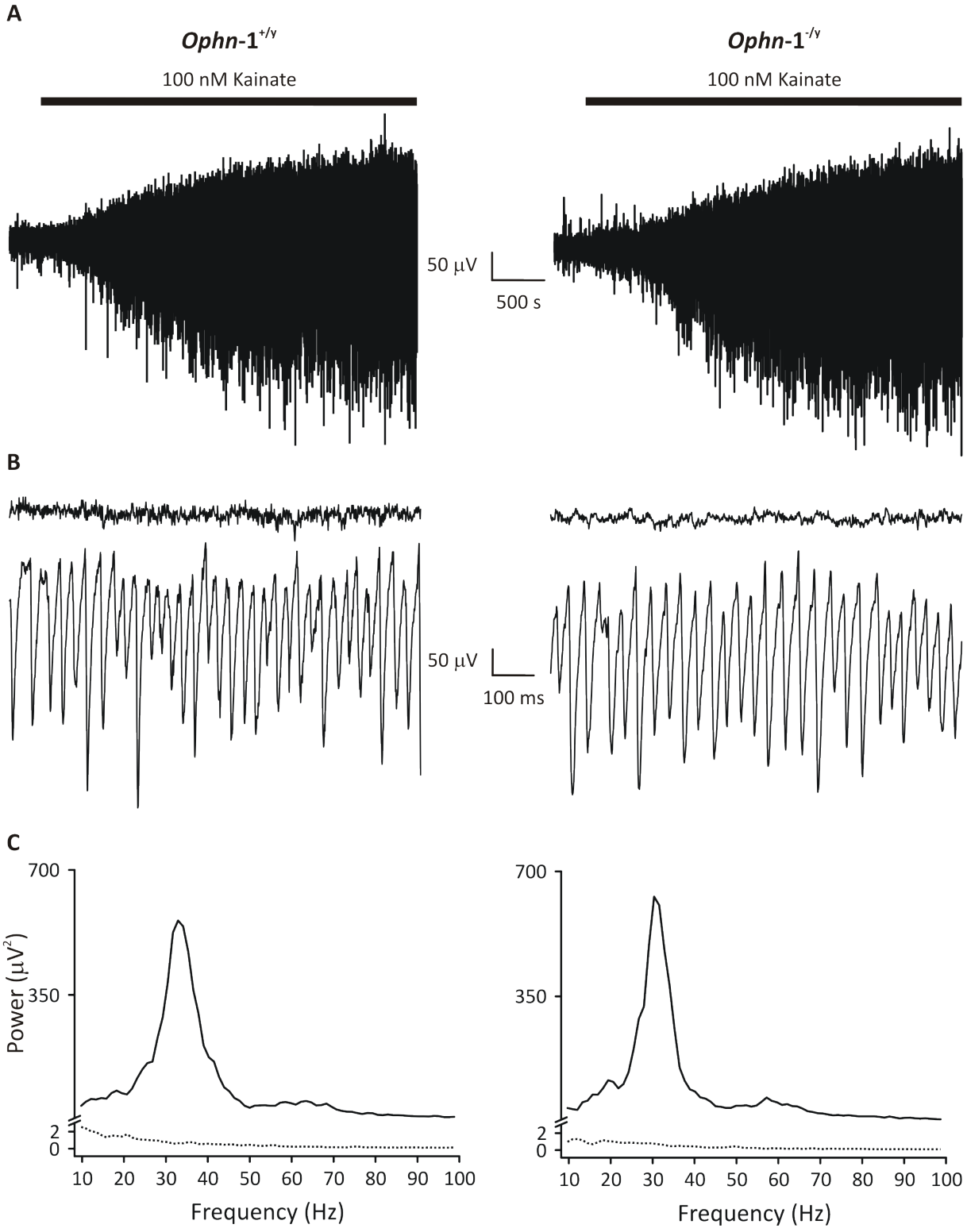
A
Ophn-1+/y
100 nM Kainate
50 μV
500 s
Ophn-1-/y
100 nM Kainate
B
50 μV
100 ms
C
700
350
2
0
Power (μV2)
10 20 30 40 50 60 70 80 90 100
Frequency (Hz)
700
350
2
0
10 20 30 40 50 60 70 80 90 100
Frequency (Hz)

Figure 5.4 – Development of kainate-induced gamma oscillations in CA3 stratum radiatum.

(A) Application of 100 nM kainate evokes neuronal oscillations in the gamma frequency range in the stratum radiatum in CA3c in both *Ophn*-$1^{+/y}$ and *Ophn*-$1^{-/y}$. **(B)** Expanded time frame at 0 min (*upper panel*) and 60 min *(lower panel)* after application of kainate, demonstrating neuronal synchrony with a negative signal. **(C)** Power spectra at 0 min *(dotted line)* and 60 min *(solid line)*.

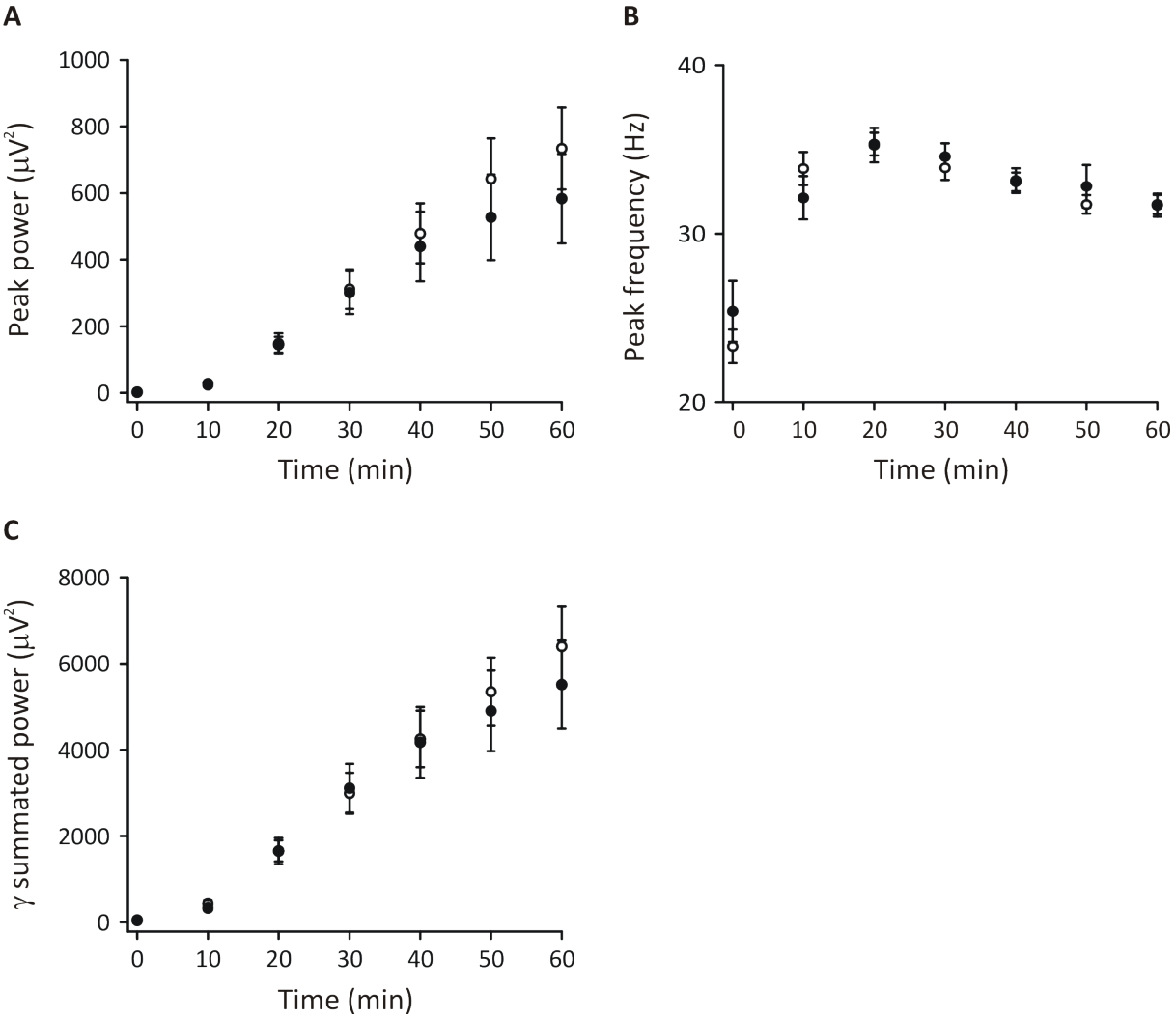

Figure 5.5 – *Ophn*-1$^{-/y}$ slices showed no difference in gamma oscillation in CA3 stratum radiatum.

No difference in **(A)** peak power, **(B)**, peak frequency or **(C)** summated power was observed between *Ophn*-1$^{+/y}$ *(filled circles,* 24 slices from 8 mice) and *Ophn*-1$^{-/y}$ *(open circles,* 31 slices from 9 mice) slices. ANOVA ($p>0.05$).

5.3 Spontaneous gamma oscillations

Various mechanisms may be used to induce gamma oscillations *in vitro* such as activation of muscarinic acetylcholine receptors, metabotropic glutamate receptors and kainate receptors. Recent reports have suggested that gamma oscillations can be recorded in the absence of external stimuli (termed spontaneous gamma; Pietersen *et al.*, 2009), and that these are reduced in *Ophn*-$1^{-/y}$ slices (Andrew Powell, personal communication). These are thought to be more akin to *in vivo* oscillations as they depend on both inhibitory and excitatory transmission. Prior to application of kainate, a subset of slices showed spontaneous gamma oscillations. The incidence of these oscillations was significantly less in *Ophn*-$1^{-/y}$ slices than *Ophn*-$1^{+/y}$ slices; spontaneous oscillations were recorded in 10 out of 23 *Ophn*-$1^{-/y}$ slices from 13 mice (44%) and 12 out of 15 *Ophn*-$1^{+/y}$ slices from 12 mice (80%) (p=0.04; Fishers exact test). Figure 5.6 illustrates representative traces of spontaneous gamma oscillations in *Ophn*-$1^{+/y}$ and *Ophn*-$1^{-/y}$ slices. These oscillations have a smaller amplitude than kainate-induced gamma oscillations. The summated power of gamma oscillations increased from 9 ± 3 μV^2 at 0 minute to 207 ± 97 μV^2 at 60 minutes (n=6) in *Ophn*-$1^{+/y}$ slices (fig 5.7B) and from 13 ± 1 μV^2 at 0 minute to 265 ± 92 μV^2 at 60 minutes (n=7) in *Ophn*-$1^{-/y}$ slices. No significant difference was observed in summated power between *Ophn*-$1^{+/y}$ and *Ophn*-$1^{-/y}$ slices (p=0.7; fig 5.7B), neither the peak power (14 ± 6 μV^2, n=6 and 14 ± 5 μV^2, n=7; respectively; p=0.9; fig 5.7A), nor the peak frequency (31 ± 1 Hz, n=6 and 32 ± 1 Hz, n=7; respectively; p=0.5; fig 5.7C) was different in *Ophn*-$1^{-/y}$ slices.

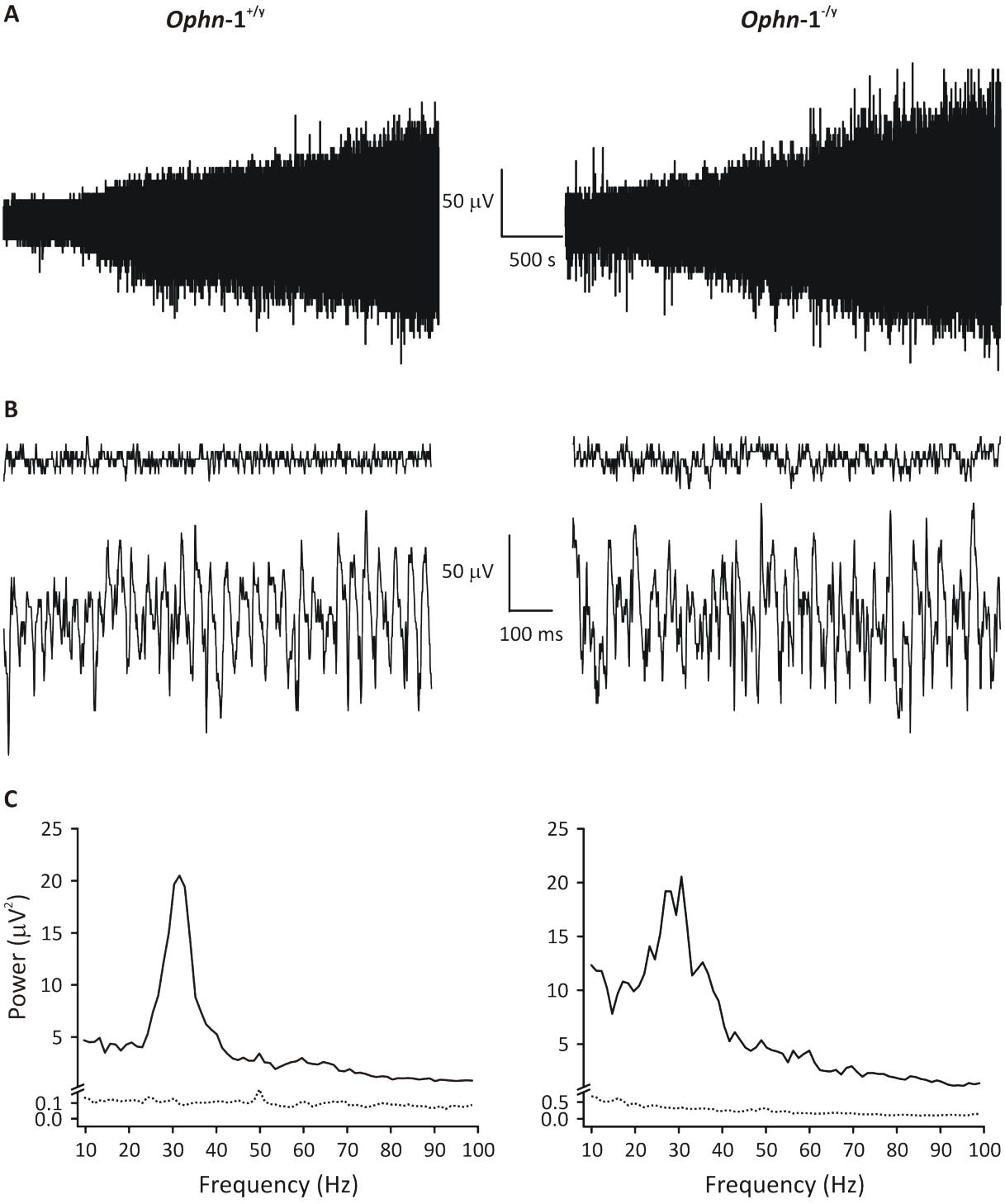
A
Ophn-1+/y
Ophn-1-/y
50 μV
500 s
B
50 μV
100 ms
C
Power (μV2)
25
20
15
10
5
0.1
0.0
0.5
0.0
10 20 30 40 50 60 70 80 90 100
Frequency (Hz)

Figure 5.6 – Development of spontaneous gamma oscillations.

(A) Spontaneous neuronal oscillations in the gamma frequency range recorded prior to kainate application in CA3 stratum pyramidale in *Ophn*-$1^{+/y}$ and *Ophn*-$1^{-/y}$ slice. **(B)** Expanded time frame at 0 min *(upper panel)* and 60 min *(lower panel)*. **(C)** Power spectra at 0 min *(dotted line)* and 60 min *(solid line)*.

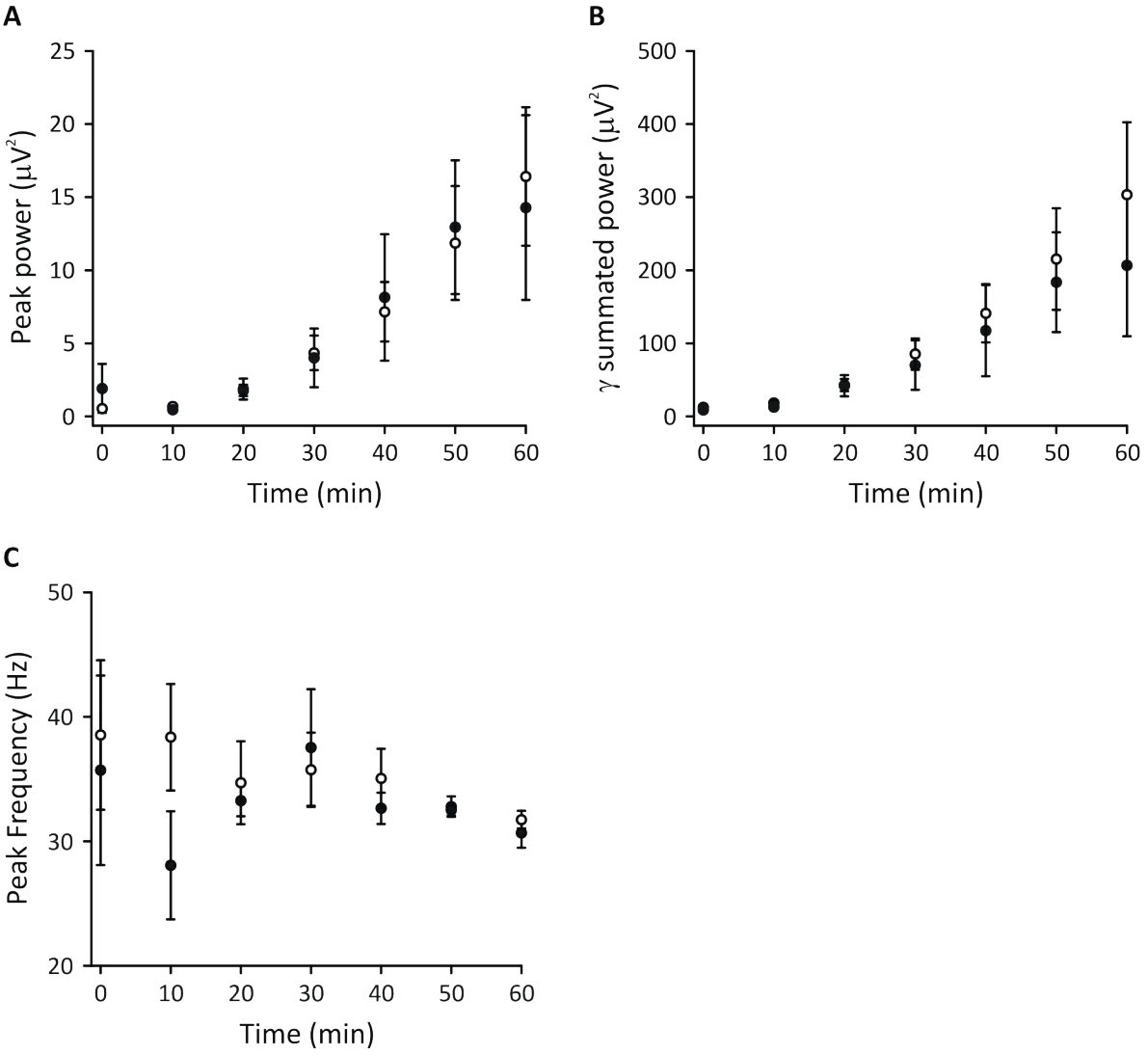

Figure 5.7 – Power and frequency of spontaneous gamma oscillations were unaltered in *Ophn*-1$^{-/y}$ slices.

Spontaneous gamma oscillations recorded prior to kainate application from stratum pyramidale in CA3c. No difference was observed in **(A)** peak power, **(B)** summated power or **(C)** peak frequency between *Ophn*-1$^{+/y}$ *(filled circles,* 6 slices from 5 mice) and *Ophn*-1$^{-/y}$ *(open circles,* 7 slices from 5 mice) slices. ANOVA ($p>0.05$).

The lack of difference in the power of either kainate-induced or spontaneous gamma oscillations in the CA3 region was surprising given previous observations from this laboratory. It is known that the behavioural phenotype is dependent on the background strain of the mice (Pierre Billuart, personal communication); it was important to confirm the presence of other phenotypes associated with this mouse model. Thus, the synaptic strength and rapid vesicle dynamics at the dentate gyrus:CA3 synapse was investigated using single, paired and repetitive stimuli.

5.4 Evoked field potentials in CA3

Powell *et al*. (2012), Saintot (2010) and Khelfaoui *et al*. (2007) found that *Ophn*-$1^{-/y}$ mice showed reduced potentiation in response to paired pulse and high frequency stimulation protocols. To examine if this synaptic malfunction was present, extracellular field potentials were recorded from the stratum pyramidale and stratum radiatum of CA3 region and stimulus response curves were generated. The mossy fibre pathway originating from the hilus was stimulated to evoke population spikes and PSPs recorded from the stratum pyramidale and stratum radiatum, respectively. Figure 5.8A shows representative traces for population spikes recorded from *Ophn*-$1^{+/y}$ and *Ophn*-$1^{-/y}$ slices. The amplitude of the population spike increased as the intensity of the stimulus was increased for both genotypes and reaches a plateau for stimuli above 45 V (fig 5.8B). The amplitude of the population spike at the maximum response, 50 V, was not different between *Ophn*-$1^{+/y}$ and *Ophn*-$1^{-/y}$ slices (-2.1 ± 0.3 mV, n=12 and -2.3 ± 0.5 mV, n=5, respectively, fig 5.8B). Analysis of the whole dataset did not reveal any significant difference in the amplitude of the population

spike between *Ophn*-$1^{+/y}$ and *Ophn*-$1^{-/y}$ slices (p=0.1). Figure 5.8C shows representative traces of PSPs recorded from *Ophn*-$1^{+/y}$ and *Ophn*-$1^{-/y}$ slices and figure 5.8D depicts the input-output relationship of the PSP slope; the slope of the PSP was correlated to stimulus intensity. Stimulus response curves were fitted with a Boltzmann function; the maximal response was unaltered between *Ophn*-$1^{+/y}$ and *Ophn*-$1^{-/y}$ slices (-1227 ± 244 mV/ms and -1171 ± 246 mV/ms; respectively; p=0.9) and the half maximal stimulus intensity, V_{50}, was unaltered (*Ophn*-$1^{+/y}$ 17.2 ± 2.2 V, n=12; *Ophn*-$1^{-/y}$ 26.9 ± 4.4 V, n=5, p=0.04; fig 5.8E). Analysis of the whole dataset for PSP slope revealed a significant difference between genotypes (p=0.01), suggesting a reduction in synaptic strength between dentate gyrus granule cells and CA3 pyramidal cells in *Ophn*-$1^{-/y}$ slices. V_{50} (20.8 ± 0.6 V, range 15-27 V, n=31) was determined for each slice and used for subsequent paired pulse and high frequency stimulation protocols.

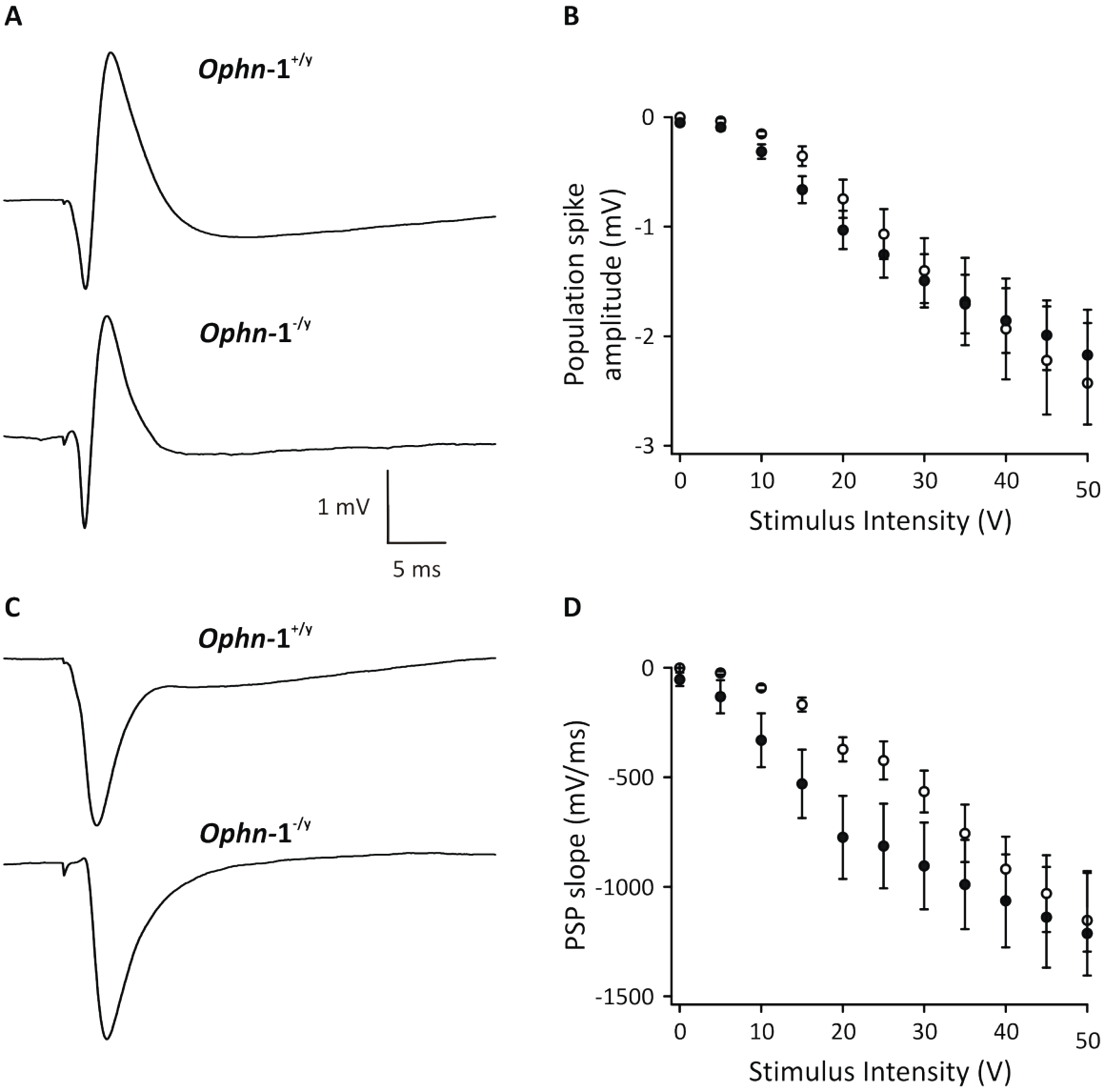

E

	Ophn-1$^{+/y}$	*Ophn*-1$^{-/y}$	p value
Max (mV/ms)	-1227.2 ± 243.9	-1170.8 ± 246.0	0.9
V_{50} (mV/ms)	17.2 ± 2.2	26.9 ± 4.4	0.04

Figure 5.8 – *Ophn*-1$^{-/y}$ slices showed reduced PSP slopes.

(A) Representative population spikes recorded from stratum pyramidale in CA3 in *Ophn*-1$^{+/y}$ and *Ophn*-1$^{-/y}$ slices. **(B)** Stimulus response curve of population spikes recorded in *Ophn*-1$^{+/y}$ *(filled* circles, 12 slices from 4 mice) and *Ophn*-1$^{-/y}$ *(open circles,* 6 slices from 3 mice) slices. No difference in population spike amplitude between genotypes. **(C)** Representative PSPs recorded from stratum radiatum in CA3 in *Ophn*-1$^{+/y}$ and *Ophn*-1$^{-/y}$ slices. **(D)** PSP slopes were smaller in *Ophn*-1$^{-/y}$ slices (5 slices from 3 mice) than *Ophn*-1$^{+/y}$ slices (12 slices from 4 mice) ANOVA, p=0.01. **(E)** Mean fit parameters of Boltzmann function for PSP slope-voltage relationship. Student's t-test with Bonferroni correction α=0.025.

The presence of oligophrenin-1 in the presynaptic terminal implicates a role in presynaptic function (Powell *et al*., 2012, Govek *et al*., 2004, Khelfaoui *et al*., 2007). Previous studies have reported paired pulse to be depressed in *Ophn*-$1^{-/y}$ neurons (Powell *et al*., 2012, Khelfaoui *et al*., 2007, Saintot, 2010). Paired pulse facilitation (PPF) is a phenomenon that depends on presynaptic mechanisms of neurotransmitter release. This is an increase in amplitude of the second EPSP with paired stimuli and thus is considered as a form of short term synaptic plasticity. To investigate if the presynaptic deficits previously identified were still present, paired pulse stimulation protocol was used. Paired stimuli, separated by a defined interval (10-1500 ms) were applied to *Ophn*-$1^{+/y}$ and *Ophn*-$1^{-/y}$ slices. The paired pulse ratio (PPR) was calculated from the ratio of the second response (PSP_2 slope) divided by the first response (PSP_1 slope). Figure 5.9A shows a typical response to an inter-pulse interval of 50 ms for *Ophn*-$1^{+/y}$ and *Ophn*-$1^{-/y}$ slice. No difference in the slope of the PSP was observed. Following an inter-pulse interval of 20 ms, paired pulse facilitation was observed in both *Ophn*-$1^{+/y}$ and *Ophn*-$1^{-/y}$ slices (1.3 ± 0.1, n=11 and 1.3 ± 0.1, n=5, respectively, fig 5.9B). Greater potentiation of response was observed at 50 ms for both *Ophn*-$1^{+/y}$ and *Ophn*-$1^{-/y}$ slices (1.5 ± 0.2, n=11 and 1.2 ± 0.1, n=5, respectively). For inter-pulse intervals greater than 50 ms, there was a decline in facilitation. Paired pulse depression was observed at an inter-pulse interval of 200 ms for *Ophn*-$1^{+/y}$ and *Ophn*-$1^{-/y}$ slices (0.9 ± 0.1, n=11 and 0.7 ± 0.1, n=5, respectively). The PPR plateaus at 1500 ms in *Ophn*-$1^{+/y}$ (1.0 ± 0.1, n=11) and *Ophn*-$1^{-/y}$ (1.0 ± 0.1, n=5) slices. No difference between *Ophn*-$1^{+/y}$ and *Ophn*-$1^{-/y}$ slices at all inter-pulse intervals (p=0.2). These results do not agree with previous results from the dentate gyrus (Powell *et al*., 2012), CA1 (Khelfaoui *et al*., 2007) and CA3 (Saintot, 2010).

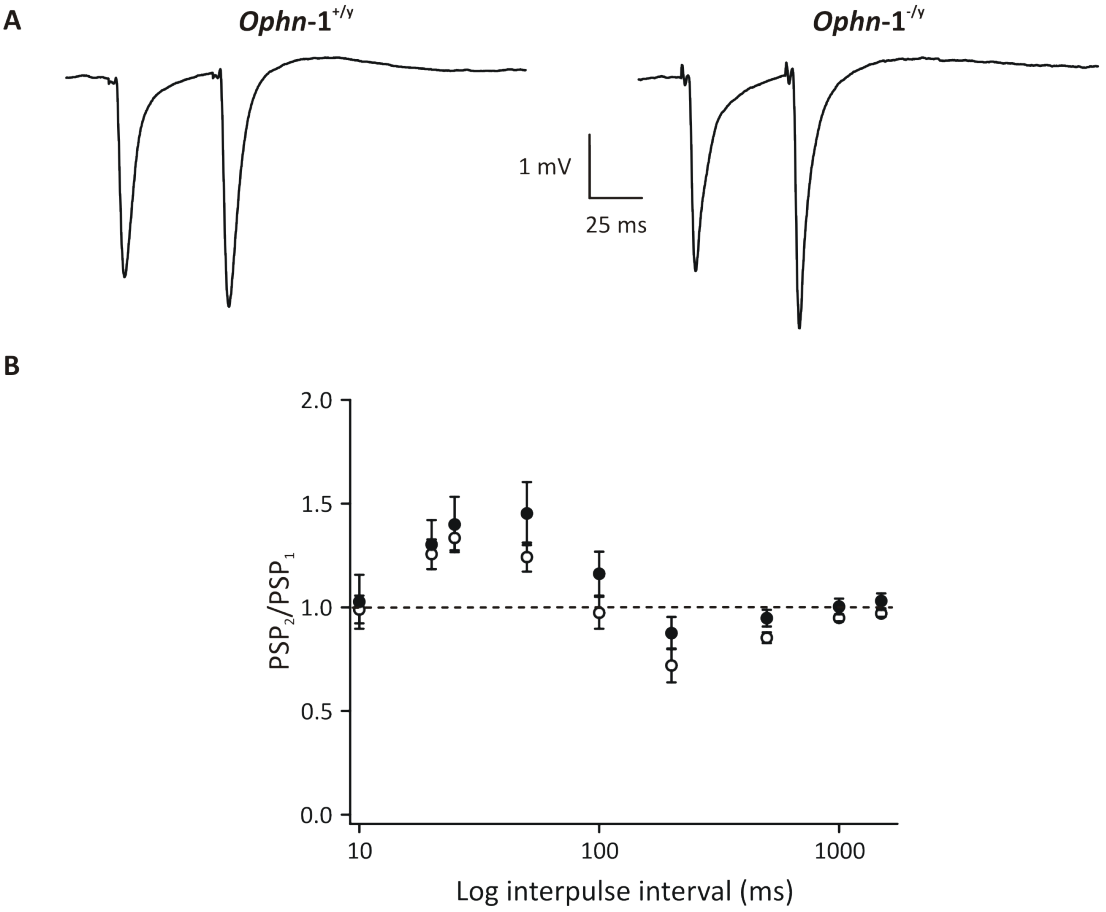

Figure 5.9 – *Ophn*-1$^{-/y}$ slices showed no difference in PSP response to paired stimuli.

(A) Representative trace of PSP recorded from stratum radiatum CA3, with a 50 ms inter-pulse interval in *Ophn*-1$^{+/y}$ *(left panel)* and *Ophn*-1$^{-/y}$ *(right panel)* evoked by stimulation of mossy fibres pathway. **(B)** PSP paired pulse ratio for *Ophn*-1$^{+/y}$ *(filled circles,* 11 slices from 4 mice) and *Ophn*-1$^{-/y}$ *(open circles,* 5 slices from 3 mice) slices did not differ. ANOVA ($p>0.05$).

Having not observed a difference in paired pulse facilitation or depression between *Ophn*-1$^{+/y}$ and *Ophn*-1$^{-/y}$ slices, the ability of both genotypes to follow high frequency stimulation at frequencies which underlie cognitive function (30-100 Hz) was investigated.

This protocol assessed the availability of synaptic vesicles in the presynaptic terminals and their ability to sustain repetitive stimulation. Previous research has shown IPSC facilitation was not present in *Ophn*-$1^{-/y}$ neurons at 33 Hz, and facilitation was weakened at 50 Hz and 100 Hz (Powell *et al*., 2012). High frequency repetitive stimuli were evoked by a train of 40 stimuli at 20 Hz, 33 Hz, 50 Hz and 100 Hz. The PSP slopes were measured for the 1^{st}-10^{th}, 20^{th}, 30^{th} and 40^{th} response and were normalised to the first response.

Figure 5.10A shows a representative trace of PSPs recorded at 33 Hz for *Ophn*-$1^{+/y}$ and *Ophn*-$1^{-/y}$ slice. Both genotypes initially show potentiation in response which gradually disappear with successive stimuli and *Ophn*-$1^{-/y}$ slices show less potentiation than *Ophn*-$1^{+/y}$ slices in the first 10 stimuli (fig 5.10B). Figure 5.10C-F illustrate the PSP ratio of *Ophn*-$1^{+/y}$ and *Ophn*-$1^{-/y}$ slices to repetitive stimulation. At 20 Hz, the PSP ratio following the first stimuli (PSP ratio 1) increased for both *Ophn*-$1^{+/y}$ and *Ophn*-$1^{-/y}$ slices (1.2 ± 0.05, n=12 and 1.3 ± 0.04, n=5; respectively; fig 5.10C). For subsequent stimuli, there was a gradual decline in PSP ratio. *Ophn*-$1^{-/y}$ slices showed a depressed response from the 5^{th} pulse onwards, however *Ophn*-$1^{+/y}$ slices did not show a depressed PSP ratio. Potentiation was significantly smaller in *Ophn*-$1^{-/y}$ slices than *Ophn*-$1^{+/y}$ slices at 20 Hz (p=0.0002). At 33 Hz, similar responses were seen to 20 Hz. Initially an increase in PSP ratio was observed for *Ophn*-$1^{+/y}$ and *Ophn*-$1^{-/y}$ slices (1.2 ± 0.05, n=12 and 1.2 ± 0.02, n=6; respectively; fig 5.10D). For subsequent stimuli, a decline in PSP ratio was observed in *Ophn*-$1^{-/y}$ slices however PSP ratio increased up to the 4^{th} stimuli in *Ophn*-$1^{+/y}$ slices, thereafter a decline in response was also seen. Potentiation was also significantly reduced in *Ophn*-$1^{-/y}$ slices compared to *Ophn*-$1^{+/y}$ slices at 33 Hz (p=0.001) and similar results were seen at 50 Hz; potentiation was significantly reduced

(p=0.04; fig 5.10E). At 100 Hz, after the first stimuli, the PSP ratios were depressed for both *Ophn*-$1^{+/y}$ and *Ophn*-$1^{-/y}$ slices (0.7 ± 0.07, n=12 and 0.7 ± 0.04, n=6; respectively; fig 5.10F). Potentiation did not occur in either genotype at 100 Hz and no significant difference was observed (p=0.2).

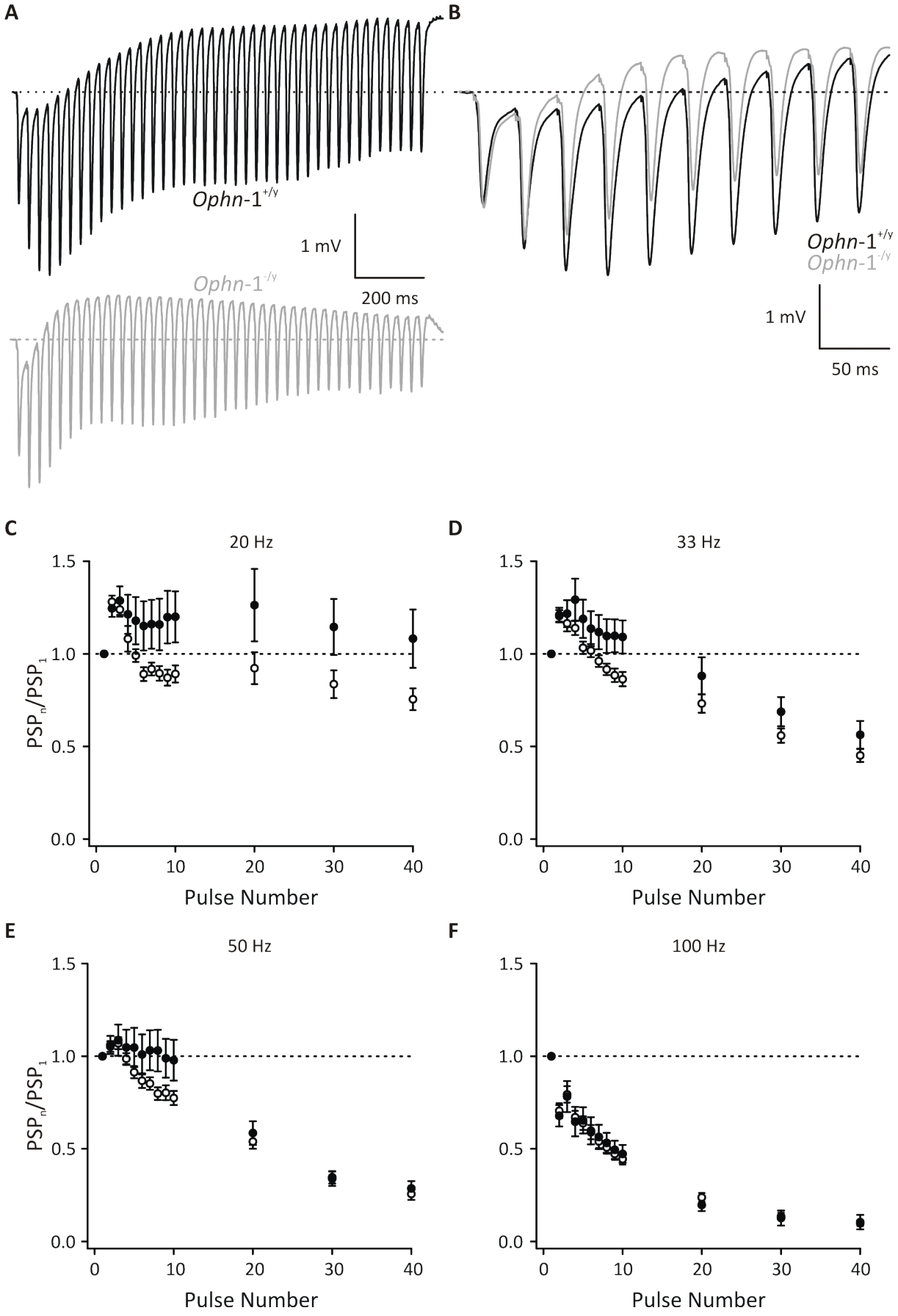
A
Ophn-1+/y
1 mV
200 ms
Ophn-1-/y
B
Ophn-1+/y
Ophn-1-/y
1 mV
50 ms
C
20 Hz
PSPn/PSP1
Pulse Number
D
33 Hz
Pulse Number
E
50 Hz
PSPn/PSP1
Pulse Number
F
100 Hz
Pulse Number

Figure 5.10 – *Ophn*-1$^{-/y}$ slices showed altered responses to repetitive stimulation at high frequencies.

(A) Representative traces of PSPs recorded from CA3, evoked by stimulation of the mossy fibres pathway in *Ophn*-1$^{+/y}$ *(upper panel)* and *Ophn*-1$^{-/y}$ *(lower panel)* slices, 40 stimuli at 33 Hz. **(B)** Expanded time frame of stimuli 1-10 and responses are superimposed in *Ophn*-1$^{+/y}$ *(black trace)* and *Ophn*-1$^{-/y}$ slices *(grey trace)*. **(C)** PSP normalised to the first response, giving PSP ratios for 40 stimuli at 20 Hz, **(D)** 33 Hz, **(E)** 50 Hz and **(F)** 100 Hz (*Ophn*-1$^{+/y}$ 12 slices from 4 mice and *Ophn*-1$^{-/y}$ 5 slices from 3 mice). ANOVA ($p<0.05$).

The lack of difference in the power of kainate-induced or spontaneous gamma oscillations but the presence of reduced frequency dependent facilitation suggests the absence of some previously identified phenotype whilst the presence of others. A defining feature of the *Ophn1* mouse model that recapitulates the human condition is the ventricular enlargement. A systematic analysis of the gross brain anatomy was studied to determine whether ventricles were still abnormal.

5.5 Gross brain anatomy of *Ophn1* mice

Enlarged lateral ventricles and in some cases hydrocephaly has been identified in numerous patients with *OPHN1* mutations (Zanni *et al*., 2005, Bergmann *et al*., 2003, Tentler *et al*., 1999). In the *Ophn1* mouse model of MR, Khelfaoui *et al* (2007) reported enlarged lateral and third ventricles in *Ophn*-1$^{-/y}$ mice. In the present study, brain anatomy was investigated to determine whether this phenotype was still present in *Ophn*-1$^{-/y}$ mice. To determine

whether there were alterations in the ventricular system of 3 month old animals, the volume of the lateral and third ventricles were estimated. Ventricular enlargement was apparent in *Ophn*-$1^{-/y}$ mice at 3 months (fig 5.11). The volume of the lateral ventricles was significantly larger in *Ophn*-$1^{-/y}$ mice than *Ophn*-$1^{+/y}$ mice (7.7 ± 2.5 mm^3, n=6 and 3.4 ± 0.7 mm^3, n=8; respectively; p=0.02; fig 5.13A). No difference was observed in the third ventricle volumes between *Ophn*-$1^{+/y}$ and *Ophn*-$1^{-/y}$ mice (p=0.9; fig 5.13B).

Next, the cerebroventricular volume was measured in young 6 week old males, the age at which electrophysiological experiments were conducted, to determine whether morphological changes observed in older animals were also present in younger animals. Ventricular expansion was evident in *Ophn*-$1^{-/y}$ mice, associated with cortical thinning (fig 5.12). The hippocampus appears to be displaced; the most anterior part of hippocampus appears at a more caudal plane (fig 5.12, *bregma -0.58 to -2.54*). The volume of the lateral ventricles was significantly larger in *Ophn*-$1^{-/y}$ mice than *Ophn*-$1^{+/y}$ mice (26.3 ± 10.5 mm^3, n=6 and 3.8 ± 0.4 mm^3, n=6; respectively; p=0.002; fig 5.13A). No difference was observed in the third ventricle volumes between *Ophn*-$1^{+/y}$ and *Ophn*-$1^{-/y}$ mice (p=0.5; fig 5.13B).

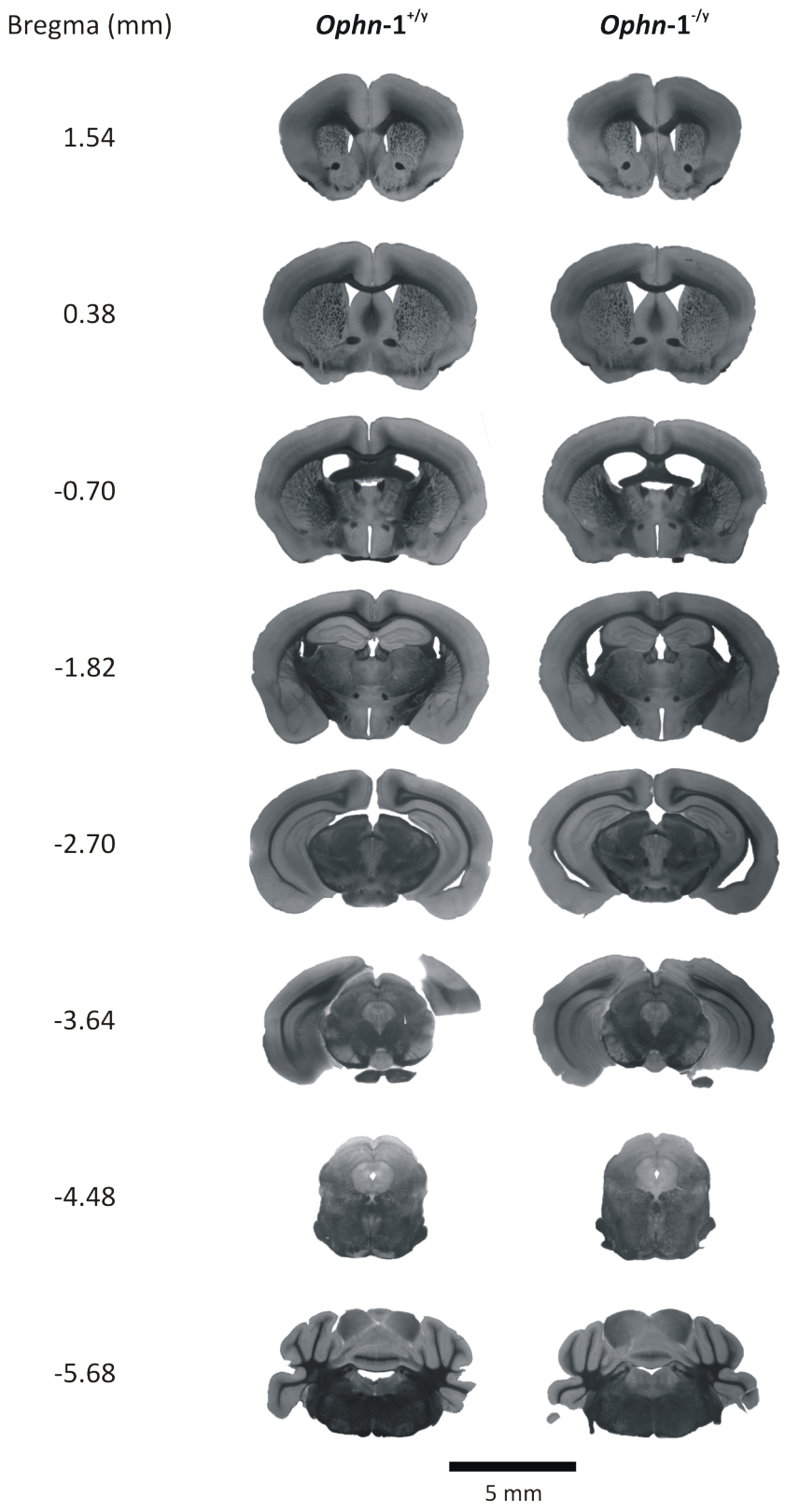
Bregma (mm)
Ophn-1$^{+/y}$
Ophn-1$^{-/y}$
1.54
0.38
-0.70
-1.82
-2.70
-3.64
-4.48
-5.68
5 mm

Figure 5.11 – *Ophn*-1$^{-/y}$ mice develop ventricular enlargement at 3 months.

Serial 100 µm rostral to caudal coronal sections from brains at 3 months in *Ophn*-1$^{+/y}$ *(left panels)* and *Ophn*-1$^{-/y}$ *(right panels)* mice. Each pair of sections represents approximately the same coronal plane, as estimated from the bregma level. Scale bar, 5 mm.

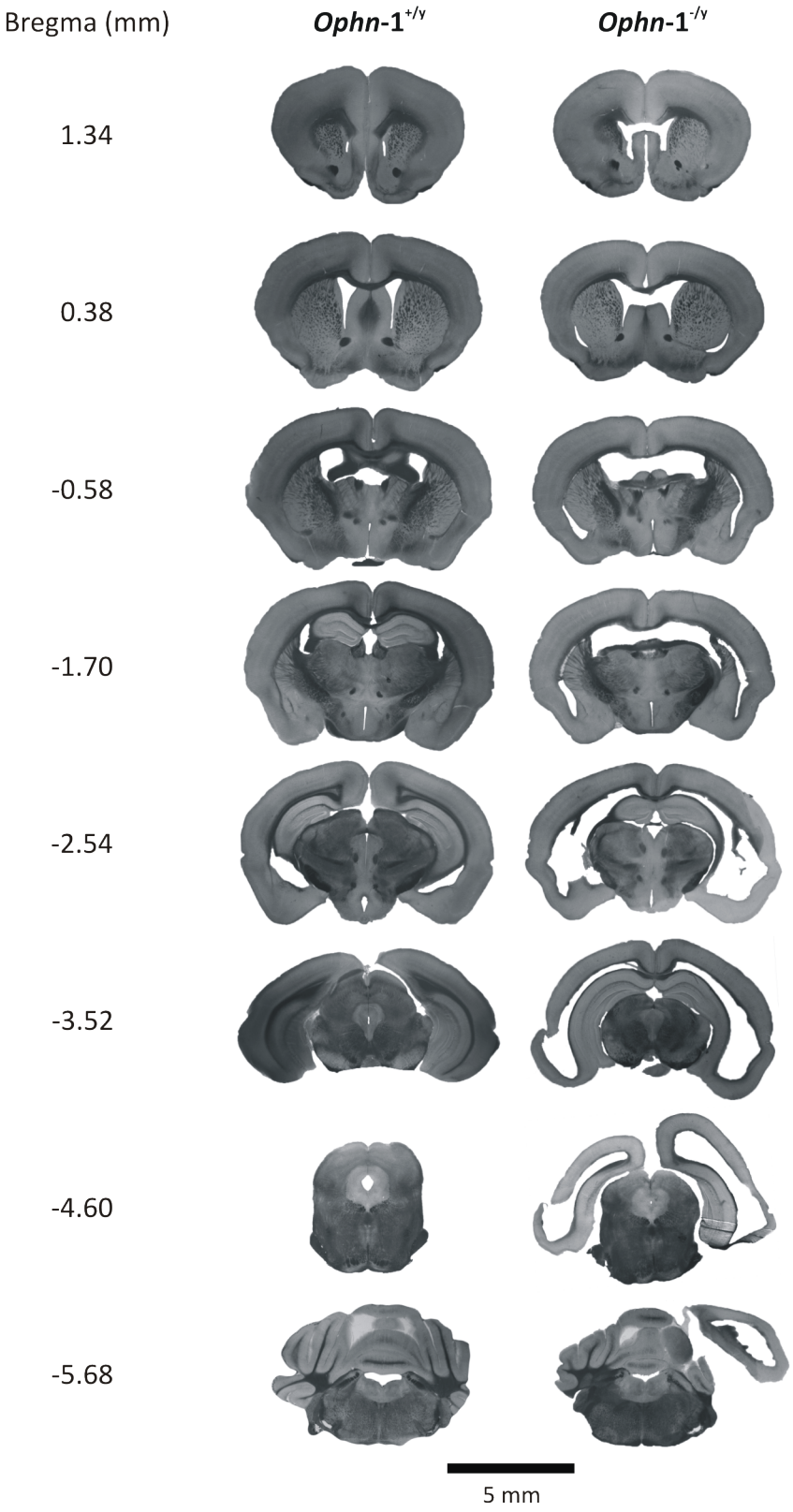
Bregma (mm)
Ophn-1$^{+/y}$
Ophn-1$^{-/y}$
1.34
0.38
-0.58
-1.70
-2.54
-3.52
-4.60
-5.68
5 mm

Figure 5.12 – *Ophn*-1$^{-/y}$ mice develop enlarged ventricles at 6 weeks.

Serial 100 µm rostral to caudal coronal sections from brains at 6 weeks in *Ophn*-1$^{+/y}$ *(left panels)* and *Ophn*-1$^{-/y}$ *(right panels)* mice. Each pair of sections represents approximately the same coronal plane, as estimated from the bregma level. Scale bar, 5 mm.

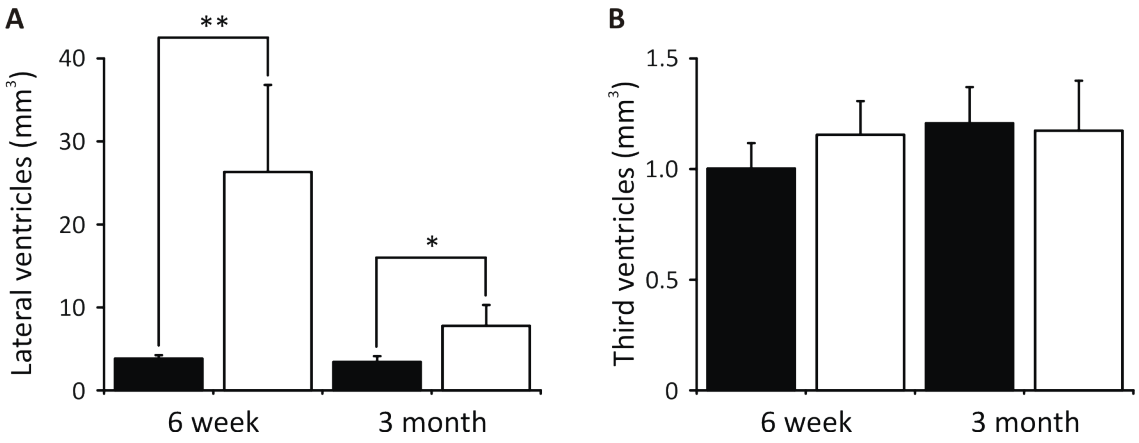

Figure 5.13 – Lateral ventricular enlargement was present in *Ophn*-1$^{-/y}$ mice at 6 weeks and 3 months.

(A) Histogram illustrating mean ventricular volumes for 6 week old mice and 3 month old mice in lateral ventricles and **(B)** third ventricles (6 week: *Ophn*-1$^{+/y}$ *filled columns*, n=6 and *Ophn*-1$^{-/y}$ *open columns,* n=6; 3 month: *Ophn*-1$^{+/y}$ n=8 and *Ophn*-1$^{-/y}$ n=6). Mann-Whitney U test with Bonferroni correction α=0.025, *=p<0.025 and **=p<0.005.

Ventricular dilatation is characteristic of hydrocephalus which usually is accompanied by stretching of adjacent tissue (McAllister, 2012). To determine whether the ventricular expansion was associated with alterations in cortical tissue, the thickness of the neocortex was investigated.

5.6 Cortical thickness

Previous publications have reported thinning of the cerebral cortex in *Ophn*-$1^{-/y}$ mice, however this was not quantified or statistically tested (Khelfaoui *et al*., 2007). The present study shows apparent cortical thinning in *Ophn*-$1^{-/y}$ mice (fig 5.12). The thickness of the motor, somatosensory and auditory cortices were examined in 6 week and 3 month old animals. At 6 weeks, cortical thickness was significantly reduced in the motor cortex of *Ophn*-$1^{-/y}$ mice than *Ophn*-$1^{+/y}$ mice (0.9 ± 0.05 mm, n=6 and 1.1 ± 0.03 mm, n=6; respectively; p=0.01; fig 5.14A). No significant difference was observed in the somatosensory (p=0.1) or auditory cortex (p=0.1). At 3 months, the motor cortex was thinner in *Ophn*-$1^{-/y}$ mice than *Ophn*-$1^{+/y}$ mice (0.9 ± 0.03 mm, n=6 and 1.0 ± 0.02 mm, n=8; respectively; p=0.016; fig 5.14B); neither the somatosensory (p=0.7), nor the auditory (p=0.6) cortices were affected (fig 5.14B). Analysis of the whole dataset with both age groups of mice and all brain regions revealed genotype of mouse had a significant effect on cortical thickness over all brain regions (p=0.002, ANOVA).

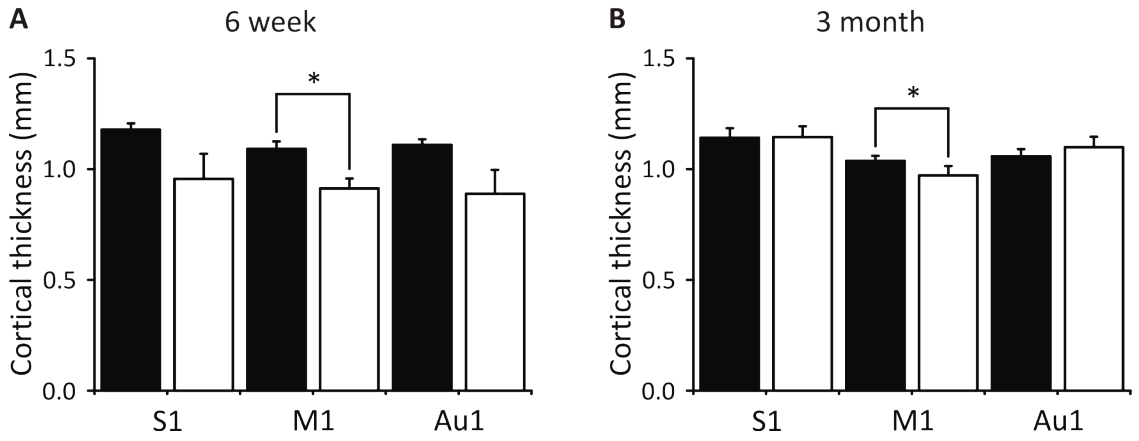

Figure 5.14 – Cortical thickness was reduced in *Ophn*-1$^{-/y}$ mice.

(A) *Ophn*-1$^{-/y}$ show reduced cortical thickness in motor cortex (M1) with no changes in somatosensory (S1) or auditory (Au1) cortex in 6 week old mice (*Ophn*-1$^{+/y}$ *filled columns*, n=6 and *Ophn*-1$^{-/y}$ *open columns,* n=6). **(B)** Reduced cortical thickness in the motor cortex at 3 months in *Ophn*-1$^{-/y}$ mice, without alterations in the somatosensory and auditory cortices (*Ophn*-1$^{+/y}$ n=8 and *Ophn*-1$^{-/y}$ n=6) mice. Student's t-test with Bonferroni correction α=0.017, *=p<0.017.

To determine whether the ventricular expansion caused compression of the surrounding tissue, the total tissue area was measured. Sections containing motor, somatosensory and auditory cortices from approximately the same coronal plane were analysed. Brain tissue area did not differ between *Ophn*-1$^{+/y}$ and *Ophn*-1$^{-/y}$ mice at 6 weeks old, nor 3 months old (Prashan Kangesu, personal communication).

5.7 Summary

The power of kainate-induced gamma oscillations and spontaneous gamma oscillations was not different in *Ophn*-$1^{-/y}$ slices in the CA3 region of the hippocampus, however the incidence of spontaneous gamma oscillations was less. Synaptic strength was reduced between dentate gyrus granule cells and CA3 pyramidal cells. Paired pulse ratio was unchanged suggesting normal presynaptic short term plasticity, although a reduction in potentiation for frequency dependent facilitation at 20, 33 and 50 Hz was observed in *Ophn*-$1^{-/y}$ slices, which could be due to altered vesicle dynamics among other possibilities. These results highlight the absence of previously reported inhibitory deficits whilst the excitatory deficits were preserved, albeit weaker than previously identified. Lateral ventricular enlargement was present in 6 week old and 3 month old *Ophn*-$1^{-/y}$ mice, suggesting the gross morphological phenotype was still present. Ventricular dilatation was associated with a reduction in cortical thickness in the primary motor cortex in both age groups that could be due to stretching as a result of ventricular enlargement or due to neuropil loss. Further investigations are required to elucidate the cause of the neocortical thinning and hydrocephalus.

Chapter 6: Discussion

6.1 Overview

The functional phenotype associated with loss of oligophrenin-1 expression has been explored in neocortical and hippocampal neurons. Extracellular field potentials and whole-cell patch clamp techniques combined with (immuno)histological techniques have been used to investigate neocortical and hippocampal physiology in *Ophn1* mice. This study confirmed the physiological heterogeneity in layer V and the need for accurate identification of neuronal subtypes. The impact of two intracellular tracers, neurobiotin and Alexa 488, on intrinsic properties and synaptic currents were investigated. Neurobiotin prolonged the action potential duration in a concentration dependent manner, but lower concentrations compromised neuronal labelling. Alexa 488 did not alter the electrophysiological properties of neurons, however dendritic staining was less extensive than neurobiotin, although this is unlikely to affect genotype comparisons. The lack of effect of Alexa 488 on electrophysiological recordings enabled it to be used to study synaptic current and dendritic arborisation.

Intrinsic properties were unaltered in *Ophn*-$1^{-/y}$ neurons suggesting normal ion channel physiology. Reduced excitatory transmission was not due to altered vesicle dynamics or dendritic arborisation, but was associated with region-specific alterations in dendritic spine density. In contrast, spontaneous and repetitive inhibitory transmission was normal in

neocortical and hippocampal neurons, the latter finding was inconsistent with previous studies (Powell *et al.*, 2012; Saintot, 2010).

The inconsistent finding raised the question of whether other phenotypes associated with the *Ophn1* model were still present. Kainate-induced gamma oscillations were unaltered in *Ophn*-$1^{-/y}$ slices, however the incidence of spontaneous oscillations was reduced and associated with reduced synaptic strength at the dentate gyrus:CA3 synapse. Short-term plasticity was unaffected although frequency dependent facilitation was attenuated in *Ophn*-$1^{-/y}$ slice. These data highlight the absence of inhibitory phenotype whilst excitatory deficits were still intact. Histological techniques were used to study the gross brain morphology of *Ophn1* mice. Lateral but not third ventricles were expanded and were associated with a reduction in cortical thickness. This study shows the loss of several phenotypes previously reported, whilst others such as altered brain morphology are still preserved.

6.2 Heterogeneity of layer V neurons

The study has confirmed the physiological heterogeneity of layer V neurons and the requirement for morphological characteristics to accurately identify specific neurons. Two broad categories of cells have been recognised here: pyramidal neurons and non pyramidal neurons. Previous reports have categorised these two classes of layer V neurons into further subgroups, fast spiking and low threshold spiking non pyramidal cells (Kawaguchi, 1993) and regular spiking and intrinsically bursting pyramidal cells (McCormick *et al*., 1985). Some

reports have identified that these cell subtypes are physiologically distinct (Kawaguchi, 1993), however as a population of pyramidal and non pyramidal cells, these are not physiologically discrete. Within layer V, a heterogeneous population of pyramidal cells exist, which can be further categorised into distinct populations depending on their projection target (Molnar and Cheung, 2006). The dendritic morphology of these cells vary depending on their projection targets and have distinct physiological properties (Hattox and Nelson, 2007). The present study has characterised the electrophysiological properties of pyramidal cells and has shown that these properties are not distinct from non pyramidal cells and thus is not sufficient to use as a criterion for identification.

6.3 Intrinsic properties of layer V neurons

Many studies have characterised the intrinsic properties of layer V pyramidal cells and results from this study are in agreement with previous reports. Input resistance of pyramidal neurons in this study were similar to those reported for regular spiking pyramidal cells (Schubert *et al*., 2001) and the amplitude of the fast AHP did not differ (Kawaguchi, 1993; Hattox and Nelson, 2007). The action potential half width was 1.5 ms which is slightly longer than previous values ranging between 0.9-1.4 ms (Kawaguchi, 1993; Hattox and Nelson, 2007). These small discrepancies could be due to differences in how half width was measured; this was not precisely defined in either report. In instances where action potential threshold values have been reported, the values from the present study are in agreement (Schubert *et al*., 2006). Despite that these data are in agreement with previous findings, these are not sufficient to classify neuronal types.

6.4 Impact of intracellular tracers on electrophysiology

The purpose of an intracellular tracer in this study was to combine electrophysiology of *Ophn1* neurons with morphological analysis of recorded cells. The ideal tracer must fully label neurons without compromising the physiological properties of the recording. This study evaluated the impact of two substances, neurobiotin and Alexa 488, on electrophysiological recordings and the quality of histological staining.

Impact of neurobiotin on intrinsic properties of layer V pyramidal neurons

During whole-cell recordings from layer V neurons, the intracellular tracer neurobiotin increased action potential duration, without affecting other intrinsic properties such as input resistance, AHPs and firing frequency. The lack of difference in firing frequency in neurobiotin filled cells was unexpected given the prolongation of action potential. The effect of neurobiotin appeared to be concentration-dependent as it increased with the duration of the recording; therefore firing frequency may be altered during prolonged recordings.

Mechanism of action of neurobiotin

The target of neurobiotin is unknown, however the impact on action potential duration mimics the effect of tetraethylammonium (TEA)(Kang *et al*., 2000). Thus, the proposed mechanism of action of neurobiotin is thought to be similar to the action of TEA, by blocking potassium channels activated by depolarisation or calcium activated potassium channels (Schlosser *et al*., 1998). TEA blocks a number of potassium channels; these include voltage gated potassium channels and BK Ca^{2+}-activated K^{+} channels (Hille, 2001). Kang *et al* (2000)

demonstrate activation of three distinct potassium channels in response to action potential activity in layer V pyramidal neurons. Delayed rectifiers K^+ channels (K_{dr}) are unlikely to be involved in repolarisation of single action potentials, but rather regulate the shape during repetitive firing. A-type (I_A) channels are involved in repolarisation but are TEA-insensitive. Fast voltage gated potassium channels (K_f) have brief openings and mainly underlie repolarisation. Additionally, they are TEA-sensitive and are not involved in regulating interspike intervals which can account for why firing frequency was not affected by neurobiotin in the present study. Xi and Xu (1996) reported that neurobiotin increased depolarising and repolarising time, suggesting a possible action on sodium channels in addition to potassium channels.

Fast spiking cells were identified based on their shorter spikes and faster firing frequency. Unlike pyramidal neurons, preliminary observations suggested that neurobiotin did not affect the half width of fast spiking cells. This could be due to differential expression of a particular potassium channel that underlies repolarisation that is expressed in abundance in pyramidal neurons but not fast spiking cells. Fast spiking kinetics are thought to be due to Kv3.1 and Kv3.2 delayed rectifier potassium channels which are highly expressed in fast spiking cells and weakly expressed in pyramidal neurons (Weiser *et al*., 1994; Martina *et al*., 1998). However these channels are sensitive to TEA, but more importantly are not considered to underlie repolarisation (Kang *et al*., 2000). On the other hand, blocking BK Ca^{2+}-activated K^+ channels with dendrotoxin I and K or iberiotoxin has no effect on the spike width, shape or firing frequency of fast spiking cells (Erisir *et al*., 1999). Whereas blocking BK channels in pyramidal neurons results in spike broadening (Sun *et al*., 2003). However there

is mixed evidence on contribution of BK channels to repolarisation. Some studies show BK channels are involved in repolarisation of neocortical pyramidal cells (Sun *et al*., 2003) whereas other studies report BK channels do not contribute to action potential repolarisation or fast AHP under normal conditions (Kang *et al*., 2000). Differences in findings could be due to the diversity of neocortical pyramidal cells. Together these results could further support the mechanism of action of neurobiotin on calcium activated potassium channels. Due to insufficient data from fast spiking cells, no solid conclusions can be drawn. Further experiments using a combination of single channel and whole-cell recordings would be required to identify the potassium channels responsible. Inclusion of TEA, 4-amino pyridine (a selective potassium channel blocker) or iberiotoxin could be used to see if the effect of neurobiotin is additive to the potassium channel inhibitors.

Lower concentration of neurobiotin compromises electrophysiology and morphology

Previous studies have reported neurobiotin (3-6%) increases the duration of action potential, with the effect appearing to be concentration dependent (Xi and Xu, 1996). At present, it is unclear whether lower concentrations can minimise the effect on action potential half width whilst still permitting satisfactory morphological characterisation. The present study showed that lower concentrations of neurobiotin proved inadequate for combined electrophysiology and morphology on both accounts. The lowest concentration of neurobiotin (0.05%) did not increase the action potential half width after 10 minutes of establishment of whole-cell configuration. However the duration of the action potential was increased at 30 minutes; additionally, neuronal staining was compromised with only the

primary apical dendrite being consistently resolvable. Furthermore, dendritic spines could not be resolved compared to more conventional concentrations used for histology.

Alexa 488 does not impact electrophysiology, but compromises morphological studies

Unlike all concentrations of neurobiotin that were tested, Alexa 488 did not significantly alter the intrinsic properties of layer V neurons. In comparison to neurobiotin (0.5%), Alexa 488 stained the dendritic arbor less extensively, but did effectively allow dendritic spines to be resolved and potentially enable characterisation of different types of spines. One explanation for the tracer-dependent differences in arborisation could be due to the heterogeneity of layer V pyramidal neurons. It has been documented that regular spiking layer V neurons have a less extensive arbor compared to intrinsically bursting neurons (Chagnac-Amitai *et al*., 1990; Schubert *et al*., 2001). Furthermore, the length of the apical dendritic tree is different among layer V neurons with different projection targets in mice. Pyramidal cell that have callosal projections have less arborisation than those that project to corticothalamic regions (Hattox and Nelson, 2007). However it is unlikely that the majority of Alexa 488 filled neurons were pyramidal neurons with less extensive arborisation.

A more likely explanation is the differences in the process of delivery of the tracer into the cell and their respective molecular size. Neurobiotin is a small molecule (Molecular mass is 358) and is a non-polar compound that is actively pushed into the cell via iontophoresis. Alexa 488 is considerably larger, (Molecular weight is 570) and enters the cell via passive diffusion. The distribution of Alexa 488 into the cell can be evaluated by measuring its diffusion coefficient. The average length of the primary apical dendrite of a layer V

pyramidal neuron is approximately 800 µm. The diffusion coefficient of Alexa 488 is 380 $\mu m^2/s$; assuming a single, linear apical dendrite, it would take approximately 14 minutes to cross a distance of 800 µm. As the duration of recordings varied between 20-40 minutes depending on the type of electrophysiological experiment, it is unlikely that the less extensive arborisation using Alexa 488 results from inadequate filling. The more likely explanation is that at the extremities of the dendritic arborisation, there is a markedly reduced Alexa 488 concentration such that there is insufficient epitope to be recognised by the anti-Alexa 488 antibody. This suggests that Alexa 488 may not be a suitable substitute for studying neuronal morphology combined with electrophysiological recordings. An additional potential limitation of Alexa 488 staining methodology is the increased number of processing steps required compared to neurobiotin. Each reaction step will result in a small loss of signal (as no reaction is 100% accurate), which will result in a reduction in signal at each step. Many steps could also result in strong background staining as the overall incubation time for all steps is greater which will increase non-specific staining. The development of a method which permits accurate morphological analysis using Alexa-based dyes will be advantageous as a major compromise when using fluorescent dyes in brain slices is the low signal:noise ratio, which prevents detailed morphological analysis without the use of two-photon confocal microscopy. Additionally, fluorescent samples are extremely susceptible to degradation during long-term storage; a problem that is minimised when using the method outlined here.

Potential modification of the protocol to improve neuronal staining may be to increase the concentration of Alexa 488 in the recording solution. This may, however, increase

background staining as a result of the positive pressure applied prior to establishing the whole-cell recording. An increase in background staining may obscure morphological changes, particularly in the perisomatic region. A further modification would be to delay fixation of slices following electrophysiological recordings; this would allow further diffusion of Alexa 488 to occur resulting in improved neuronal labelling.

Intracellular tracers and postsynaptic currents

The kinetics and amplitude of excitatory and inhibitory postsynaptic currents were unaltered by neurobiotin (0.5%) and Alexa 488. The lack of difference with neurobiotin was not unexpected as the proposed mechanism of action is blockade of potassium channels and the patch pipette contained caesium which blocks all potassium channels.

Alternative methods to study electrophysiology and morphology

Another approach for studying electrophysiology combined with morphology is to use Lucifer yellow. Although it has been reported that Lucifer yellow also prolongs action potential duration (Tasker *et al.*, 1991). Alternatively, biocytin, a variant of neurobiotin, is commonly used and gives similar results for intracellular staining (Kita and Armstrong, 1991). The molecular structure of biocytin is similar to neurobiotin, however bioctyin has a slightly longer carbon chain and does not have an ammonium group. Structurally, neither neurobiotin nor biocytin are similar to TEA. Tseng *et al*. (1991) found no effect on action potential half width with 1% biocytin filled intracellular electrodes in corticospinal layer V pyramidal neurons. Intracellular recordings from 2% biocytin filled neurons were

comparable to control recordings in hypothalamic neurons (Tasker *et al*., 1991). An advantage of the use of biocytin over Alexa 488 is the reduced number of histochemical steps involved. However, it is unclear whether biocytin has similar effects to neurobiotin on whole-cell recordings. Previous studies examining the effect of neurobiotin on electrophysiological recordings have found that the type of electrophysiological recording determines if the tracer alters intrinsic properties. Whole-cell recordings using 1% neurobiotin had a substantial impact on action potential duration by 10 minutes (Schlosser *et al*., 1998) but during *in vitro* intracellular recordings with 2%, the action potential was unaffected during 1 hr long recordings (Schlosser *et al*., 1998), or *in vivo* with 3%, an effect is only seen after 30 minutes of recording or when depolarising current injections were greater than 1 nA (Xi and Xu, 1996). An alternative approach to study electrophysiology and morphology is to use yellow fluorescent protein (YFP)-expressing mice such as Thy1-YFP, which positively stains layer V pyramidal neurons (Feng *et al.*, 2000). This will enable electrophysiology and morphology to be analysed without either being compromised.

Intracellular tracer conclusions

Taken together, these results demonstrate the heterogeneity of layer V pyramidal neuron physiology and highlight the need for morphology to confirm cell type. Neurobiotin prolonged action potential duration in a concentration dependent manner, which proved to be inadequate for whole-cell current clamp recordings as a lower concentration compromised both electrophysiology and morphology. Alexa 488 immunostaining was sufficient to identify between pyramidal and non pyramidal cells but insufficient for whole neuron morphological analysis. For example, to identify between callosal projecting and

corticothalamic projecting pyramidal cells, Alexa 488 would not be suitable in the time window to compare morphology. Despite the inadequate fill, it is unlikely this will contribute to genotype comparison of dendritic arbor.

6.5 Intrinsic properties of *Ophn1* neocortical neurons

Alterations in passive or active intrinsic properties could give an indication of abnormal cell physiology (e.g. malfunctioning ion channels). The present study used current clamp recordings to assess the intrinsic properties in layer V pyramidal neurons. *Ophn*-$1^{-/y}$ neurons showed no difference in membrane resistance, firing frequency, action potential half width and afterhyperpolarisations. These data suggest the expression and functionality of ion channels were unaltered by loss of oligophrenin-1 in the recorded population of pyramidal cells. This observation is supported by the lack of difference in dendritic morphology, as dendritic structure is related to firing properties (Mainen and Sejnowski, 1996). Additionally, it correlates with previous studies that reported no change in intrinsic properties in dentate gyrus granule neurons (Powell *et al*., 2012) and CA1 & CA3 pyramidal neurons (Saintot, 2010).

6.6 Altered excitatory transmission in *Ophn*-$1^{-/y}$ layer V pyramidal neurons

Putative EPSPs were reduced in Ophn-$1^{-/y}$ layer V pyramidal neurons

Spontaneous events were reduced in *Ophn*-$1^{-/y}$ neurons. These were likely to be EPSPs as they were recorded at a membrane potential close to the reversal potential of IPSCs and

resulted in depolarisations. To accurately measure whether excitatory transmission was altered in *Ophn*-1$^{-/y}$ layer V pyramidal neurons, spontaneous excitatory postsynaptic currents were analysed.

Spontaneous EPSCs were unaffected in Ophn-1$^{-/y}$ layer V pyramidal neurons

Neither frequency nor amplitude of spontaneous EPSCs were significantly different between genotypes, this suggests the functionality of the presynaptic terminal and postsynaptic glutamate receptors was normal in *Ophn*-1$^{-/y}$ neurons. A reduced spontaneous EPSC frequency would fit with previous studies (Nadif Kasri *et al*., 2009; Saintot, 2010; Powell *et al*., 2012). A power calculation revealed the statistical comparison had a power of 0.22, indicating the results are underpowered. Given that a value of around 0.8 is ideal to prevent false negative statistical results, it would require approximately 110 cells (to detect a 0.05 level of change) to be confident of the statistical result.

Perhaps the lack of difference between genotypes is due to the heterogeneity of layer V pyramidal neurons. There is a lot of variation in the wild type data which is evident from the standard deviation value, and this could suggest that EPSCs are recorded from two populations of cell (i.e. regular spiking and intrinsically bursting pyramidal cells). Excitatory input onto regular spiking and intrinsically bursting cells is different from layers II/III, IV and VI (Schubert *et al*., 2001), however the dendritic complexity is also different between these two types of pyramidal neurons (Chagnac-Amitai *et al*., 1990) and such differences were not reflected in dendritic morphometry analysis.

It is evident that more experiments are required to clarify whether alterations in spontaneous excitatory transmission are present. Distinction between intrinsically bursting and regular spiking pyramidal neurons is necessary before making genotype comparisons, to ensure any differences are due to loss of oligophrenin-1 and not heterogeneity of layer V neurons.

Reduced evoked EPSCs in Ophn-1$^{-/y}$ layer V pyramidal neurons

The maximum amplitude of the evoked EPSC was significantly reduced in *Ophn*-1$^{-/y}$ layer V pyramidal neurons, suggesting that loss of function of oligophrenin-1 results in a reduction in synaptic strength at the glutamatergic synapses. The origin of the reduction could be from various areas as layer V neurons receive synaptic input from many regions, including: layers II-VI, other cortical areas and subcortical structures (e.g. the thalamus). The reduction could be due to a number of reasons; one possibility is that the number of neurons were reduced. Khelfaoui *et al*. (2007) have reported hippocampal neuronal density is unaffected, however given that cortical thickness is altered in *Ophn*-1$^{-/y}$ mice, a reduction in the number of neurons could be possible. Another explanation for the reduced evoked excitatory transmission is that the number of excitatory synapses were reduced. Dendritic spines are the major site of excitatory transmission (Hotulainen and Hoogenraad, 2010) and these were reduced in *Ophn*-1$^{-/y}$ neurons. However spines are not necessarily reliable markers of excitatory synapses (Harris, 1999) as it is possible that a proportion of the synapses are directly located on the dendritic shaft; quantification of excitatory synapse density would resolve this. Alterations in the number or kinetics of glutamate receptors could affect the evoked EPSC maximum amplitude, but this is unlikely as the amplitude of the spontaneous

EPSC was unaffected. An alternative reason for the reduced evoked EPSC would be altered vesicle dynamics. To further explore the nature of the reduced excitatory transmission, synapses were tested using paired and repetitive stimuli to examine the rapid vesicle dynamics in *Ophn*-$1^{-/y}$ synapses.

Vesicle dynamics are unchanged in excitatory neocortical synapses

The presence of oligophrenin-1 in the presynaptic terminal suggests a presynaptic function (Govek *et al*., 2004), where it is thought to function as a regulator of synaptic vesicle dynamics (Khelfaoui *et al*., 2009; Saintot, 2010; Powell *et al*., 2012). Excitatory synapses were tested with paired stimuli (10-1500 ms). Paired pulse depression was observed at all intervals, where the second evoked EPSC was reduced; no difference in the degree of depression was observed between genotypes. These findings suggest no alterations in the excitatory presynaptic function, suggesting that calcium/vesicle dynamics were unaltered in *Ophn*-$1^{-/y}$ neurons. This result is in accordance with paired pulse stimulation from evoked EPSCs recorded in CA1 neurons (Nadif Kasri *et al*., 2009; Nakano-Kobayashi *et al*., 2009; Saintot, 2010), but not CA3 (Saintot, 2010), nor dentate gyrus granule neurons (Powell *et al*., 2012).

To further assess the functionality and vesicle availability of *Ophn*-$1^{-/y}$ excitatory layer V synapses, synapses were repetitively driven at various frequencies (10 stimuli at 10-100 Hz). Depression of the evoked EPSCs were observed at all pulses and all frequencies for both *Ophn*-$1^{+/y}$ and *Ophn*-$1^{-/y}$ neurons, demonstrating both genotypes are unable to sustain high frequency stimulation in layer V pyramidal neurons. The results suggest the rapid vesicle

dynamics were unaltered in *Ophn*-1$^{-/y}$ neurons. These results are in agreement with CA1 neurons but not CA3 (Saintot, 2010) from the *Ophn1* mouse model, nor presynaptic knockdown of *Ophn1* in CA1 (Nakano-Kobayashi *et al*., 2009).

Dendritic morphology of layer V neurons is unaltered

Alterations in dendritic arborisation have been reported in many studies on MR (reviewed in Newey *et al*., 2005). Rho GTPases are involved in the regulation of dendritic complexity; activation of RhoA inhibits growth of dendritic arbor (Tashiro *et al*., 2000), therefore it could be that dendritic complexity is reduced in *Ophn*-1$^{-/y}$ layer V neurons and that this could contribute to the reduction in cortical thickness. Reductions in dendritic arbor and cortical volume are seen in other forms of MR such as Rett syndrome (Belichenko *et al*., 2008; Stuss *et al*., 2012). Furthermore, dendritic arborisation is reduced in dentate gyrus granules neurons in *Ophn*-1$^{-/y}$ neurons and these neurons have reduced excitatory input (Powell *et al*., 2012). The present study used Alexa 488 to examine the dendritic arborisation of *Ophn*-1$^{+/y}$ and *Ophn*-1$^{-/y}$ layer V pyramidal neurons.

Sholl analysis revealed no difference in the complexity of the dendritic tree between *Ophn*-1$^{+/y}$ and *Ophn*-1$^{-/y}$ layer V pyramidal neurons. The caveat to this statement is that although the arborisation of proximal dendrites were unaltered in *Ophn*-1$^{-/y}$ neurons, the inadequate fill means that the morphology of distal dendrites remains unknown and this might affect the detection of changes that could contribute to cortical thickness. Despite the more incomplete fills with Alexa 488 than with neurobiotin, it is unlikely this will affect the comparison between genotypes as Alexa 488 entry is by passive diffusion. Given that

whole-cell patch clamp recordings are spatially restricted to the perisomatic region and proximal dendrites as a result of space clamp, morphology and electrophysiology can be correlated. Findings of unaltered arborisation were similar to a previous study that showed the global structure of neurons was unchanged in CA1 pyramidal neurons (Khelfaoui *et al*., 2007) but not dentate gyrus granule neurons (Powell *et al*., 2012).

Region specific alterations in dendritic spines

Mental retardation has consistently been associated with alterations in dendritic spine morphology in this model (Khelfaoui *et al*., 2007; Powell *et al*., 2012) and more generally across causes of MR (Kaufmann and Moser, 2000; Newey *et al*., 2005). The present study revealed that spine density was unaltered on basal dendrites, whereas apical dendrites showed significant spine loss. Khelfaoui *et al* (2007) found similar region specific alteration in spine density; the number of spines were unaltered in basal dendrites, but reduced on apical dendrites in CA1 pyramidal *Ophn*-$1^{-/y}$ neurons. The degree of spine loss (~30%) in layer V pyramidal neurons was similar to CA1 pyramidal neurons (Khelfaoui *et al*., 2007). The reduction in spine density in CA1 pyramidal neurons and dentate gyrus granule neurons is primarily due to loss of mature mushroom spines, without alterations in filopodia density.

The present study supports previous reports that show oligophrenin-1 regulates spine dynamics (Khelfaoui *et al*., 2007; Powell *et al*., 2012) possibly by retraction of spines via RhoA activity (Govek *et al*., 2004). The data also highlights region specific changes in spine density which may be due to differential control (e.g. RhoA and Rac1 or other RhoGAPs/GEFs) or differential input between basal and apical dendrites (Petreanu *et al*.,

2009). Although spines are not synonymous with input, as previously mentioned some synapses may also be located directly on the dendritic shaft or some spines may have silent synapses (Harris, 1999).

Excitatory transmission conclusions

The mechanism underlying the reduction in excitatory transmission remains to be elucidated. Further experiments are required to determine why the maximum evoked EPSC and apical (but not basal) dendritic spine density were reduced without significant alterations in spontaneous neurotransmission, paired stimuli and repetitive stimuli. These results were surprising as all neurons previously investigated show reductions in excitatory transmission which was attributed to altered vesicle dynamics or AMPA receptor turnover (Khelfaoui *et al*., 2009; Nadif Kasri *et al*., 2009; Saintot, 2010; Powell *et al*., 2012). Given that dendritic spine density is reduced on the apical dendrites in *Ophn*-1$^{-/y}$ neurons, it may be worth exploring excitatory input on apical dendrites distal to the soma using dual somatic-dendritic patch clamp recordings. The reduction in excitatory transmission may be due to: altered presynaptic release probability of synaptic vesicles or amount of neurotransmitter (glutamate), fewer neurons or fewer synapses. However, the finding of reduced evoked EPSC is inconsistent with all other excitatory measures. Given the strong evidence supporting the absence of several phenotypes, the evoked EPSC result could be a false positive and therefore should be interpreted with caution.

6.7 Inhibitory transmission was unaltered in *Ophn*-1$^{-/y}$ layer V neurons

The frequency and amplitude of spontaneous inhibitory transmission were unaltered in *Ophn*-1$^{-/y}$ layer V pyramidal neurons. These results suggest that spontaneous activity is normal and that loss of function of oligophrenin-1 in layer V pyramidal neurons does not impact the presynaptic release of GABA or the functionality of postsynaptic GABA receptors. The observation that spontaneous IPSCs were unaffected in *Ophn*-1$^{-/y}$ neurons was surprising although previous studies examined synaptic transmission in the hippocampus. Different outcomes have been reported for inhibitory transmission in *Ophn*-1$^{-/y}$ neurons, where no differences were observed in the frequency of events in CA1 neurons (Nadif Kasri *et al*., 2009; Saintot, 2010) but were reduced in dentate gyrus granule neurons (Powell *et al*., 2012) and CA3 pyramidal neurons (Saintot, 2010).

To address whether oligophrenin-1 loss of function alters vesicle availability in layer V pyramidal neurons, the RRP size was characterised in *Ophn*-1$^{-/y}$ terminals.

Readily releasable pool was unaltered in Ophn-1$^{-/y}$ synapses

Vesicle dynamics were assessed using a high frequency minimal stimulation protocol at a single synapse/axon (Schneggenburger *et al*., 1999; Powell *et al*., 2012). A minimal stimulus, delivered to a synapse on an apical dendrite, evoked an all or nothing IPSC. High frequency stimulation causes depression of the evoked IPSC amplitudes and enables estimation of the number of vesicles in the RRP. No alterations were observed in the number of synaptic vesicles within the RRP or the replenishment rate in *Ophn*-1$^{-/y}$ synapses, suggesting that

oligophrenin-1 function is not necessary for the normal vesicle recycling, endocytosis and vesicle availability in layer V inhibitory synapses. This contradicts findings from hippocampal neurons, where the RRP size and rate of replenishment are reduced in *Ophn*-1$^{-/y}$ dentate gyrus granule neurons (Powell *et al*., 2012) and CA3 neurons (Saintot, 2010). These data suggest that oligophrenin-1 does not play a key role in the regulation of synaptic vesicle dynamics at inhibitory synapses in neocortical neurons. Together, spontaneous IPSC and repetitive stimuli data suggest that oligophrenin-1 may play a major role at inhibitory synapses in some neurons (e.g. some hippocampal neurons) more than others (e.g. neocortical neurons).

6.8 Inhibitory hippocampal physiology is unaltered in *Ophn*-1$^{-/y}$ neurons

Inhibitory transmission was unaltered in Ophn-1$^{-/y}$ dentate gyrus granule neurons

Given the lack of difference in inhibitory transmission in layer V pyramidal neurons, perhaps hippocampal neurons are peculiar. A comparison study of spontaneous inhibitory transmission from layer V pyramidal neurons and dentate gyrus granule neurons from the same mice revealed no difference between genotypes in either cell type. The absent phenotype in granule neurons was unexpected as this is not in agreement with previous findings (Powell *et al*., 2012). Although it is not unusual for discrepancies in physiological data across laboratories, being unable to replicate findings from the same laboratory gave cause for concern. The discrepancy with earlier work is unlikely due to experimental preparations and protocols as these were carried out identically to Powell *et al* (2012). Perhaps the most plausible hypothesis for the loss of the hippocampal synaptic phenotype

over 4 years is genetic drift (see section 6.11). The lack of inhibitory deficit coincided with weakened/loss of other phenotypes including weakened excitatory phenotype, unaltered gamma oscillations and unaltered behaviour). It was important to revisit whether other hippocampal and anatomical phenotypes associated with this mouse model still exist.

Ophn-1$^{-/y}$ slices showed no alterations in kainate-induced gamma oscillations

Altered kainate-induced gamma oscillations have previously been shown in *Ophn*-1$^{-/y}$ slices in CA3 region of the hippocampus (Saintot, 2010). Given the observation that the synaptic phenotype appears altered/weaker, gamma oscillations were studied to examine if this phenotype was still present. The lack of difference in gamma oscillations between *Ophn*-1$^{+/y}$ and *Ophn*-1$^{-/y}$ slices was unexpected but not surprising given that inhibitory transmission was normal in *Ophn*-1$^{-/y}$ dentate gyrus granule neurons. Kainate-induced oscillations rely solely on inhibition mediated by $GABA_A$ receptors (Fisahn *et al*, 2004) and the loss of this phenotype is likely to be directly related to the loss of the inhibitory synaptic phenotype. As *in vivo* gamma oscillations in CA3 depend on a balance between synaptic excitation and inhibition (Atallah and Scanziani, 2009), there are advantages of using other models. An alternative model is the use of carbachol, a cholinergic agonist, to induce gamma oscillations that are dependent on both phasic excitation and phasic inhibition (Fisahn *et al*., 1998). A natural and possibly more suitable model for studying gamma oscillations is spontaneous oscillations (Pietersen *et al*., 2009).

The incidence of spontaneous gamma oscillations was less in Ophn-1$^{-/y}$ slices

No difference in power or frequency of spontaneous gamma oscillations was observed between *Ophn*-1$^{+/y}$ and *Ophn*-1$^{-/y}$ slices. This observation was not in agreement with previous studies which illustrate reduced power of spontaneous gamma oscillations in *Ophn*-1$^{-/y}$ slices (Andrew Powell, personal communication). Measuring the power of spontaneous oscillations may introduce bias into the results due to the nature of analysis. The criterion for spontaneous gamma oscillations is summated power in the 25-35 Hz band is greater than that in the 10-20 Hz band (Pietersen *et al*., 2009). By selecting only slices with gamma band higher than beta band, only a subset of *Ophn*-1$^{-/y}$ data is being selected. This is essentially skewing the data by analysing *Ophn*-1$^{-/y}$ slices only when gamma power is strongest. The data selection for spontaneous gamma oscillations excludes slices where gamma is weaker than the noise, which perhaps does reflect weaker power, or it could be because the circuitry required is absent in some slices/mice.

The incidence of spontaneous gamma oscillations was significantly reduced in *Ophn*-1$^{-/y}$ slices and was consistent for multiple slices from the same animal. One explanation for the reduction is that *Ophn*-1$^{-/y}$ slices are unable to generate spontaneous gamma oscillation; reviewing the mechanism underlying spontaneous and kainate-induced oscillations may help explain this statement (see below).

Comparison of spontaneous and kainate-induced oscillations

The underlying mechanism of spontaneous gamma oscillations is not fully understood but they have been shown to depend on both excitatory and inhibitory transmission; it has been

speculated that they are more akin to *in vivo* oscillations (Pietersen *et al*., 2009). Spontaneous and kainate-induced gamma oscillations in CA3 are locally generated and moderate activity of adjacent networks (Pietersen *et al*., 2009). They share basic network mechanisms, however pharmacologically they differ substantially. Spontaneous oscillations are associated with phasic inhibition but are less dependent on perisomatic inhibitory input that enables instantaneous synchronisation (Pietersen *et al*., 2009), suggesting that different sets of interneurons are involved in synchronisation of spontaneous and kainate-induced gamma oscillations. Pyramidal cell firing is proposed to be synchronised by phasic inhibition through mossy fibre associated interneurons and activation by associational fibres for spontaneous oscillations (Pietersen *et al*., 2009) whereas kainate-induced are synchronised by parvalbumin positive fast spiking interneurons (Fuchs *et al*., 2007). Spontaneous oscillations depend on fast AMPA receptor mediated EPSPs, but are unlikely to be involved in oscillation synchronisation but instead, excite interneurons which in turn mediate rhythmic inhibition (Pietersen *et al*., 2009). However for kainate-induced oscillations, GABAergic inhibition is sufficient as interneurons are directly activated (Bartos *et al*., 2007).

Inconsistencies in gamma oscillation data

Spontaneous gamma oscillation data from the CA3 region is inconsistent between genotypes; Saintot (2010) found no difference in power whereas a reduction was observed by other colleagues (present study; Andrew Powell, personal communication). Alterations in kainate-induced gamma oscillations were observed by Saintot (2010), but not in other studies (present study; Alger, 2011). In all instances, preparation and experimental conditions were identical, thus the robustness and the validity of the mouse model can be

questioned. It is possible that subtle changes in the phenotypes have occurred that have weakened the phenotype producing confounding results. These changes could be due to environmental factors (e.g. housing) or biological factors (e.g. genetic drift, see section 6.11)

6.9 Altered evoked field potentials in *Ophn*-1$^{-/y}$ slices

No difference in paired stimuli in Ophn-1$^{-/y}$ slices in CA3

In light of the lack of altered paired pulse phenotype in neocortical neurons, this phenotype was reassessed in CA3. Paired pulse ratio was unaltered in *Ophn*-1$^{-/y}$ slices. This observation was unexpected as previous studies have reported reduced paired pulse facilitation in CA1 and CA3 resulting from altered vesicle recycling (Khelfaoui *et al*., 2007; Saintot, 2010). Differences in experimental preparation and protocol cannot explain the different findings between the present study on CA3 and Saintot (2010) as these were carried out identically. Similar to the absence of other phenotypes (e.g. gamma oscillations), the difference in findings could be due to a weakened phenotype (see section 6.11)

Altered responses to repetitive stimuli in Ophn-1$^{-/y}$ slices in CA3

Our laboratory has previously shown that in *Ophn*-1$^{-/y}$ CA3 and dentate gyrus granule neuron synapses are unable to follow high frequency stimulation due to reduced vesicle availability (Powell *et al*., 2012; Saintot, 2010). Using high frequency stimulation, the present study showed that in CA3, *Ophn*-1$^{-/y}$ slices had significantly altered responses than *Ophn*-1$^{+/y}$ slices at 20 Hz, 33 Hz and 50 Hz. Initially, at these frequencies, both *Ophn*-1$^{+/y}$ and *Ophn*-1$^{-/y}$ slices

show a potentiation in response which gradually disappears with successive stimuli, however at 20 Hz, only *Ophn*-1$^{+/y}$ slices were able to sustain the response during repetitive stimuli. One explanation for this finding is that *Ophn*-1$^{-/y}$ slices have a decreased RRP size and slower vesicle recycling meaning that the time frame between the stimuli is not sufficient to allow the vesicle pool to be refilled. This is in accordance with previous findings which demonstrated impaired vesicle recycling following repetitive stimulation at 20 Hz (Saintot, 2010) or reduced endocytosis of synaptic vesicles (Khelfaoui *et al*., 2009) in *Ophn*-1$^{-/y}$ mice and in siRNA knockdown of *Ophn1* (Nakano-Kobayashi *et al*., 2009). Saintot (2010) also observed smaller RRP in CA3 pyramidal neuron synapses of *Ophn*-1$^{-/y}$ neurons following high frequency stimulation protocols.

Although the high frequency stimulation results agree with the previously proposed deficits in *Ophn*-1$^{-/y}$ slices, based on the current data it is not possible to exclude other explanations of the deficit. Attenuation in postsynaptic responses with successive stimulation could be due to desensitisation of AMPA receptors as oligophrenin-1 regulates the endocytosis of AMPA receptors at the postsynaptic terminal (Khelfaoui *et al*., 2009) and control AMPA receptor stabilisation (Nadif Kasri *et al*., 2009).

CA3 Ophn1 phenotype conclusions

The lack of difference in kainate-induced gamma oscillations suggests inhibitory synapses in CA3 neurons are unaffected by loss of *Ophn1*. The differences in field EPSPs and spontaneous gamma oscillations suggest deficits in excitatory transmission. Excitatory transmission at CA3 synapses has not been fully explored in the present study or previous

studies. Whole-cell recordings from CA3 pyramidal neurons could be used to examine spontaneous and evoked excitatory transmission, combined with paired and repetitive stimuli and measures of neuronal morphology to help elucidate the mechanism underlying the deficits.

6.10 Altered brain morphology in *Ophn*-1$^{-/y}$ mice; association with thinned cortex

Ventricular enlargement and hydrocephaly have been described in human patients with *OPHN1* mutations (Bergmann *et al*., 2003) and in the *Ophn1* mouse model (Khelfaoui *et al*., 2007). Given that the present study failed to replicate most of the physiological phenotypes found previously, brain morphology was examined to determine whether the ventricular dilatation was still present. Observations during slice preparation indicated this phenotype was still present. Quantification of ventricles in perfusion fixed brains showed they were larger in *Ophn*-1$^{-/y}$ mice than *Ophn*-1$^{+/y}$ mice at 6 weeks and 3 months. No significant difference was observed in the degree of ventricular dilatation between these age groups; this is not in accordance with previous findings. Khelfaoui *et al* (2007) reported the incidence of enlarged ventricles are present at the age of 1 month but worsens with time. However in the present study, the degree of ventricular enlargement was not different between 6 week and 3 month old mice. In some cases, ventricular expansion resulted in the development of hydrocephalus. Evan's ratio (ratio of ventricular width to brain width) can be used to describe whether hydrocephalus is present; a value of >0.3 or 0.4 is generally accepted for both humans and rodents (Li *et al*., 2008). Khelfaoui *et al* (2007) claimed the ventricle dilatation was not due to hydrocephalus. There are numerous caveats to these assertions.

Firstly, ventricular dilatation analysis presented by Khelfaoui *et al* is mostly qualitative; they report an increase incidence of ventricular expansion without reporting detailed measurements. Secondly, they discuss that cerebral aqueduct does not appear to be reduced, without quantifying. Inspection of their data may suggest a reduction in the cerebral aqueduct which could be indicative of aqueduct stenosis. Furthermore, in the present study, observations of sections containing the cerebral aqueduct and fourth ventricle indicate the aqueduct is smaller, suggesting obstruction. However, complete measurements of the sylvius aqueduct and fourth ventricle were not taken as part of these were missing due to the nature the how the sections were prepared.

Mechanism underlying ventricular enlargement

Various malfunctions could underlie expansion of the ventricles. Obstruction of the fourth ventricle and/or sylvius aqueduct (aqueductal stenosis), overproduction or failure to absorb CSF, impaired proliferation of the cells lining the ventricles and impairments of cilia have been shown to cause enlargement of the ventricles (Ishihara *et al*., 2010). The presence of oligophrenin-1 in the choroid villi, ependymal and cerebral blood vessels (Khelfaoui *et al*., 2007) raises the hypothesis that oligophrenin-1 is involved in secretion or reabsorption of CSF.

The hypothesis that increased CSF pressure leads to brain compression and pathophysiology is not supported by the following observations. Not all mice show ventricular expansion and Khelfaoui *et al*. (2007) found no correlation between the behavioural phenotype and dilatation of the ventricles. Furthermore, in the kaolin induced hydrocephaly model,

performance in the Morris water maze is unaffected (Del Bigio *et al*., 2003). Additionally, not all human patients with *OPHN1* mutations show ventricular dilatation (Bergmann *et al*., 2003), and such cases do not always show a correlation between ventricular dilatation and degree of cognitive deficit (Pirozzi *et al*., 2011).

Alterations in brain structures in Ophn-1$^{-/y}$ mice

Total brain area was measured to identify whether the ventriculomegaly resulted in overall compression of brain structures. No difference in brain size was observed between genotypes, suggesting compression of brain tissue. Brain areas surrounding the cerebral ventricles were examined to identify affected structures. The subcortical area appeared to be reduced in *Ophn*-1$^{-/y}$ mice however this was not significant (p=0.07). A power calculation revealed the statistical comparison had a power of 0.4, suggesting the results are underpowered. Approximately 30 brains would be required to be confident of the statistical result. Hippocampal volume was unaltered in 6 week old *Ophn*-1$^{-/y}$ mice (Prashan Kangesu, personal communication). This fits with previous reports, stating the structure of the hippocampus and neuronal densities are unaffected in *Ophn*-1$^{-/y}$ mice (Khelfaoui *et al*., 2007). Observations of a displaced hippocampus, combined with unaltered hippocampal volume could suggest a longitudinal increase in brain size.

Reduced cortical thickness in Ophn-1$^{-/y}$ mice

Cortical thickness was measured in the primary motor, primary somatosensory, primary auditory and lateral entorhinal cortices. The choices of these areas were two-fold. The motor

cortex was of interest as one of the behavioural phenotype reported in *Ophn*-1$^{-/y}$ mice is novelty driven hyperactivity (Khelfaoui *et al*., 2007). The overall architecture of this region was analysed to identify whether structural abnormalities were present between genotypes. Somatosensory, auditory and lateral entorhinal cortices were measured because these areas surround the lateral ventricles at different coronal planes from bregma. Cortical thickness was reduced *Ophn*-1$^{-/y}$ mice in the motor cortex in 6 week and 3 month old mice, without alterations in somatosensory, auditory and lateral entorhinal cortices. One caveat to this methodology is that one cannot be certain of which regions in *Ophn*-1$^{-/y}$ slices were analysed, due to the gross malformations of brains in *Ophn*-1$^{-/y}$ animals. Observations that the anterior hippocampus first appears at a more caudal level in *Ophn*-1$^{-/y}$ than in *Ophn*-1$^{+/y}$ animals raise the question whether the cortical regions measured are also displaced. Different cortices are defined by the type of cells located in that region. Examination of cell types could identify if these regions are present in the slices examined in *Ophn*-1$^{-/y}$ mice. For example, Nissl stained sections show that the motor cortex, located in the frontal lobe, has been described as agranular cytoarchitecture due to absence/lack of layer IV neurons (reviewed in Kirkcaldie, 2012). Nevertheless, univariate analysis of cortical thickness with age of mouse and brain region revealed genotype of mouse had a significant effect on cortical thickness and that age and brain region did not. Therefore, over the four brain regions examined, the cortical thickness was reduced.

The reduction in cortical thickness can be explained by changes in dendritic arborisation or cell/neuropil loss. Although dendritic complexity was unaltered in *Ophn*-1$^{-/y}$ layer V pyramidal neurons, dendritic morphology was not examined in layers I-IV and VI and non

pyramidal layer V neurons. However the reduction in cortical thickness was an overall reduction rather than a layer specific cell loss (Prashan Kangesu, personal communication). Another explanation could be due to neuronal loss or neuropil loss. Khelfaoui *et al* (2007) found no difference in neuronal density in CA1 neurons, however it is not surprising given that hippocampal volume appears to be normal (Prashan Kangesu, personal communication). Further studies are required to determine whether reduced cortical thickness is due to loss of cortical neurons and/or glia.

6.11 *Ophn1* mouse model of MR: a suitable model for MR?

To study the pathophysiology of *OPHN1* XLMR, it is important that the *Ophn1* mouse model shows symptoms reminiscent of the human disorder. Humans with *OPHN1* mutations show many pathophysiologies associated with moderate to severe MR, commonly cerebellar hypoplasia and lateral ventricle dilatation (Bergmann *et al*., 2003; Zanni *et al*., 2005). The mouse model generated by Khelfaoui *et al* (2007) recapitulates some of the human phenotypes such as cognitive, behavioural and social deficits in addition to cerebral ventricular dilatation (and hydrocephaly). The model enables investigation of *Ophn1* loss of function in absence of brain samples from patients.

Loss of phenotype: genetic drift and epigenetic factors

It could be that loss of oligophrenin-1 function affects some neurons more so than others, for example, perhaps the peculiarity lies within the hippocampus (e.g. dentate gyrus granule

neurons and CA1 and CA3 pyramidal neurons) and not within cortical neurons (e.g. layer V pyramidal neurons). However examination of spontaneous IPSCs in dentate gyrus granule neurons which revealed no difference in frequency, and loss of gamma oscillation in CA3 suggests the phenotypes are weaker or absent than previously reported.

The loss of some phenotypes could not be explained by the presence of oligophrenin-1 as genotyping confirmed that *Ophn1* was knocked out. Numerous environmental and biological factors can affect the phenotypic variability in mice (Yoshiki and Moriwaki, 2006). One explanation of the expression of some phenotypes and not others could be genetic drift, i.e. changes in gene frequency in the absence of selective pressure (Stevens *et al*., 2007). It is driven by the accumulation of spontaneous mutations which can randomly become fixed in a population and occur slowly and subtly (Taft *et al*., 2006). Spontaneous mutations in other genes could desensitise some phenotypes in *Ophn1* mice. This hypothesis is supported by the loss of behavioural phenotypes in *Ophn1* mice bred to different genetic background strains (see below). *De novo* mutations are common in mice and can become fixed within a colony due to genetic drift over many generations (Stevens *et al*., 2007). More than 10 generations can result in the development of sub-strains. Changes in gene frequency could be introduced from occasional non-sibling breeding with outside stock. Genetic variation could be avoided by periodically back crossing to the parental strain. Additionally, the impact of spontaneous mutations, genetic drift and thus loss of phenotypes can also be avoided by cryopreservation of embryos, which can be used to refresh stock of colonies after 10 generations (http://jaxmice.jax.org/geneticheath/drift.html).

Some of the phenotypes described in the *Ophn1* mouse model were strain dependent. The impairments in spatial navigation assessed with the Morris water maze was observed in *Ophn1* C57BL/6 but not in *Ophn1* mice bred to a different genetic background with F_1 mice (50% C57BL/6JOrl and 50% DVA/2J). C57BL/6 *Ophn*-$1^{-/y}$ mice show no improvement in distance travelled to find the hidden platform during the learning trials and no difference in the distance travelled in each of the quadrant. However no difference in the learning phase or time spent in each quadrant was observed between F_1 *Ophn*-$1^{+/y}$ and F_1 *Ophn*-$1^{-/y}$ mice (Pierre Billuart, personal communication). It is possible that other genetic mutations in the C57BL/6 mice are present that modulate the behavioural phenotype. For example, C57BL/6 may express lower levels of other RhoGAP proteins so the phenotype is enhanced.

The strongest phenotype previously identified in the *Ophn1* mouse model was the impairments in spatial learning, assessed with the Morris water maze (Khelfaoui *et al*., 2007). The behavioural phenotypes have not been conducted in the present study and therefore cannot be certain whether these animals have cognitive deficits. A previous study of behavioural characterisation has identified that *Ophn*-$1^{-/y}$ mice have novelty driven hyperactivity (Khelfaoui *et al*., 2007). Activity levels were measured in the actimeter, Y-maze, open-field and O-maze; *Ophn*-$1^{-/y}$ mice display higher levels of activity than *Ophn*-$1^{+/y}$ mice and the hyperactivity was novelty driven as it decreased with habituation. A recent study in this lab found that *Ophn*-$1^{-/y}$ mice do not show the hyperactivity phenotype when exposed to a novel environment (the actimeter). The lack of phenotype was correlated with a reduction in potentiation following high frequency stimulation in CA3 neurons in *Ophn*-$1^{-/y}$ slices (Buck, 2011; Gill, 2011).

Environmental enrichment

Many studies have shown that cognitive and neural development can be facilitated by environmental enrichment. Housing animals in an enriched environment can result in various structural brain changes such as an increased number of neurons, dendritic arborisation and synapses, particularly in the neocortex and hippocampus (reviewed in van Praag *et al*., 2000). During the three year period this study was conducted, many changes were made to the housing environment of the animals which were beyond my control and were not notified when they occurred. Animals were housed in different cages exposing them to a new environment, new objects were introduced to the cage and the type of food was changed. Previous studies have identified that the physical environment of mice can impact the outcome of an experiment. Housing conditions, types of food and the environment of the home cage can have significant consequences on neurobiology and genetically modified mice can be "rescued" from cognitive deficits as a result of environmental enrichment (Nithianantharajah and Hannan, 2006). Calorically restriction diet in a mouse model of Rett syndrome demonstrated an improvement in exploratory and motor behaviours (Mantis *et al*., 2009). Foetal alcohol syndrome is a common cause of MR. Rats that are exposed to prenatal alcohol show deficits in plasticity that are associated with reductions in NMDA receptors; these changes were improved with enriched environmental conditions (Rema and Ebner, 1999). Environmental enrichment in a mouse model of fragile X syndrome promotes morphological (increase spine density, dendritic length and branching) and behavioural (normal exploration patterns and restores habituation) recovery and increases levels of AMPA GluR1 subunits (Restivo *et al*., 2005).

Viability of Ophn-1$^{-/y}$ neurons

One issue with the *Ophn1* mouse model is the possibility of skew in data obtained. In some animals, electrophysiological recordings were not feasible due to reduced cell viability; this usually occurred in severely affected animals. This could be due to abnormalities in gross brain morphology (e.g. ventricular expansion), which may have impacted the integrity of the brain. In some instances, animals appeared to develop hydrocephalus and were culled beforehand by the animal housing unit. Therefore, data acquisition was not feasible in severely affected animals and electrophysiological data represent animals with a mild-moderate phenotype.

Validity of the Ophn1 mouse model of MR

The *Ophn1* mouse model lacks reproducibility; numerous studies have been conducted which fail to reproduce data or contradict one another such as inconsistencies in hippocampal physiology in CA1 (Khelfaoui *et al*., 2007; Saintot, 2010), CA3 (present study; Gill, 2011; Saintot, 2010; Alger, 2011), dentate gyrus (present study; Powell *et al*., 2012) and novelty driven hyperactivity (Khelfaoui *et al*., 2007; Buck, 2011). Being able to replicate data within and across laboratories strengthens the conclusiveness of the phenotypes and minor variations in environmental factors and methodological differences become trivial.

This study demonstrates the impact of oligophrenin-1 loss of function is minimal on synaptic function. Perhaps long-term knockout of *Ophn1* induces a compensatory mechanism that enhances GTPase activity of RhoA/Rac1/Cdc42 in synapses. Alternatively, oligophrenin-1 may be a major regulator in cerebral ventricles but not neurons.

Phenotype stability

The present study highlights that some excitatory phenotypes were intact, albeit weaker, whereas most inhibitory phenotypes were absent. The stability of excitatory phenotypes could illustrate the importance of deficits in excitatory transmission in MR. MR is traditionally considered a disorder of the postsynaptic compartment, presumably due to characteristic alterations in dendritic spine morphology which are the primary recipients of excitatory input. An alternative view is that rather being a poor model of the human condition, the dependence of certain aspects of the phenotype on the genetic makeup of the individual animal may be a more accurate model. The labile nature of some phenotypes and not others in the *Ophn1* deficiency model could be useful for the human disease. The clinical presentation of individual patients with *OPHN1* mutations is not as a homogenous group of symptoms: for example, individuals from the same family reported by Al-Owain *et al* (2011) showed variable incidence of ventriculomegaly, which was not directly related to intellectual function. Furthermore, the incidence of seizures in individuals with *OPHN1* mutations is highly variable even within the same family (Pirozzi *et al.*, 2011; Al-Owain *et al.*, 2011). The variability in phenotypes between patients is likely due to differences in genetic backgrounds and mutations in the *OPHN1* gene could manifest in different ways based on those background genes. This is supported by the dependency of the *Ophn1* loss of function mutation phenotype on the background strain of the mice (Pierre Billuart, personal communication). Another example is from a recent study examining deleterious ion channels variants known to cause epilepsy that were found more frequently present in healthy individuals than epilepsy cases (Klassen *et al.*, 2011). This study identified mutations in epilepsy genes which increase susceptibility of seizures although many individuals in the

population have mutations in these epilepsy related genes but do not suffer from seizures. This study highlighted that no variant is pathogenic by itself, but only in certain familial context. Depending on the polymorphisms an individual has determines whether disease causing genes will manifest into disease related symptoms. A “disease gene” is only pathogenic in the presence of a presumably smaller number of other variants in the pathway related genes (Klassen *et al.*, 2011). In some conditions, there may be certain molecules whose function may be absolutely critical to disease expression, but this may not be the case for RhoGAP proteins. An excess of RhoGAP proteins are present where they outnumber the GTPases they regulate by two- to three-fold (Tcherkezian and Lamarche-Vane, 2007). Deficiency in one RhoGAP may be easily rescued by other members of this large protein superfamily. Interestingly it is not known whether asymptomatic mutations of *OPHN1* are present in the general population, as has been reported for epilepsy susceptibility genes (Klassen *et al.*, 2011; Ottman *et al.*, 2010. Taken together these reports suggest that similar to symptoms in patients, the presentation of phenotypes is defined by the precise genetic make-up of the individual, suggesting the model may be an accurate representation of the human condition.

6.12 Future experiments

Biochemistry of RhoA, Rac1 and Cdc42

OPHN1 promotes GTPase activity of RhoA, Rac1 and Cdc42 *in vitro* (Billuart *et al*., 1998) and *in vivo* (Fauchereau *et al*., 2003) thus leading to inactivation of these proteins. Loss of *OPHN1* expression results in constitutive activation of its target molecules. It may be that Rho activity is altered from the originally identified phenotype, or perhaps there is a shift leading to differential expression of active substrates. For example, Rho activity may be overactive in the ependymal cells that line the ventricular system, responsible for cerebrospinal fluid secretion, accounting for the ventricular expansion whereas activity could be at normal levels in some neurons. One approach to address whether Rho activity is differentially up-regulated would be to use a *in situ* glutathione-S-transferase (GST) pull down assay. Rho-GST fusion tagged protein corresponding to a Rho binding domain specifically binds to and precipitates the active form Rho-GTP and not Rho-GDP. Primary antibody directed against GST and secondary antibody for detection then can be used to quantify the degree of Rho activity. This can enable comparisons between genotypes and also identify whether there are cell specific changes in Rho activity.

Knockdown vs. knockout

It might be argued that more consistent result are obtained using genetic techniques such as siRNA (Govek *et al*., 2004; Nadif Kasri *et al*., 2009) and this may provide a more useful way of understanding key oligophrenin-1 functions. However siRNA silences genes, reducing mRNA

levels but not completely knocking down. Such turning down of oligophrenin-1 may not resemble the human disorder as well as knockout of the gene as all but one *OPHN1* mental retardation is due loss of function mutations.

6.13 Conclusions

It is evident that more experiments are required to understand the mechanisms of reduced excitatory transmission in neocortical pyramidal neurons. Additional experiments are also required to determine the role of oligophrenin-1 in ventricular expansion and gross brain morphology. Given the labile nature of phenotypes associated with the *Ophn1* mouse model of mental retardation in this lab and others, it does raise the question of using this model to understand the pathophysiology of oligophrenin-1 mutations in mental retardation.

Chapter 7: References

AL-OWAIN, M., KAYA, N., AL-ZAIDAN, H., AL-HASHMI, N., AL-BAKHEET, A., AL-MUHAIZEA, M., CHEDRAWI, A., BASRAN, R. K. & MILUNSKY, A. (2011) Novel intragenic deletion in OPHN1 in a family causing XLMR with cerebellar hypoplasia and distinctive facial appearance. *Clin.Genet.,* **79,** 363-370.

ALGER, M. (2011) Vesicle dynamics in a mouse model of intellectual disability. BMedSc, University of Birmingham.

ALLEN, K. M., GLEESON, J. G., BAGRODIA, S., PARTINGTON, M. W., MACMILLAN, J. C., CERIONE, R. A., MULLEY, J. C. & WALSH, C. A. (1998) Pak3 mutation in nonsyndromic x-linked mental retardation *Nat Genet,* **20,** 25-30.

ATALLAH, B. V. & SCANZIANI, M. (2009) Instantaneous modulation of gamma oscillation frequency by balancing excitation with inhibition *Neuron,* **62,** 566-577.

BABILONI, C., ALBERTINI, G., ONORATI, P., MURATORI, C., BUFFO, P., CONDOLUCI, C., SARA, M., PISTOIA, F., VECCHIO, F. & ROSSINI, P. M. (2010) Cortical sources of EEG rhythms are abnormal in down syndrome. *Clin Neurophysiol,* **121,** 1205-12.

BARTOS, M., VIDA, I. & JONAS, P. (2007) Synaptic mechanisms of synchronized gamma oscillations in inhibitory interneuron networks *Nat.Rev.Neurosci.,* **8,** 45-56.

BECK, H. & YAARI, Y. (2008) Plasticity of intrinsic neuronal properties in cns disorders *Nat Rev Neurosci,* **9,** 357-69.

BEDESCHI, M. F., NOVELLI, A., BERNARDINI, L., PARAZZINI, C., BIANCHI, V., TORRES, B., NATACCI, F., GIUFFRIDA, M. G., FICARAZZI, P., DALLAPICCOLA, B. & LALATTA, F. (2008) Association of syndromic mental retardation with an xq12q13.1 duplication encompassing the oligophrenin 1 gene *Am.J.Med.Genet.A,* **146A,** 1718-1724.

BEIERLEIN, M., GIBSON, J. R. & CONNORS, B. W. (2003) Two dynamically distinct inhibitory networks in layer 4 of the neocortex *J Neurophysiol,* **90,** 2987-3000.

BELICHENKO, N. P., BELICHENKO, P. V., LI, H. H., MOBLEY, W. C. & FRANCKE, U. (2008) Comparative study of brain morphology in MECP2 mutant mouse models of Rett syndrome *J Comp Neurol,* **508,** 184-95.

BERGMANN, C., ZERRES, K., SENDEREK, J., RUDNIK-SCHONEBORN, S., EGGERMANN, T., HAUSLER, M., MULL, M. & RAMAEKERS, V. T. (2003) Oligophrenin 1 (OPHN1) gene mutation causes syndromic x-linked mental retardation with epilepsy, rostral ventricular enlargement and cerebellar hypoplasia *Brain,* **126,** 1537-1544.

BIENVENU, T., DER-SARKISSIAN, H., BILLUART, P., TISSOT, M., DES PORTES, V., BRULS, T., CHABROLLE, J. P., CHAUVEAU, P., CHERRY, M., KAHN, A., COHEN, D., BELDJORD, C., CHELLY, J. & CHERIF, D. (1997) Mapping of the x-breakpoint involved in a balanced x;12 translocation in a female with mild mental retardation *Eur J Hum Genet,* **5,** 105-9.

BILLUART, P., BIENVENU, T., RONCE, N., DES, PORTES. V., VINET, M. C., ZEMNI, R., ROEST, C. H., CARRIE, A., FAUCHEREAU, F., CHERRY, M., BRIAULT, S., HAMEL, B., FRYNS, J. P., BELDJORD, C., KAHN, A., MORAINE, C. & CHELLY, J. (1998) Oligophrenin-1 encodes a rhogap protein involved in x-linked mental retardation *Nature,* **392,** 923-926.

BLISS, T. V. & LOMO, T. (1973) Long-lasting potentiation of synaptic transmission in the dentate area of the anaesthetized rabbit following stimulation of the perforant path *J Physiol,* **232,** 331-56.

BOGGIO, E. M., LONETTI, G., PIZZORUSSO, T. & GIUSTETTO, M. (2010) Synaptic determinants of rett syndrome. *Front Synaptic Neurosci.,* **2,** 28.

BRAGIN, A., JANDO, G., NADASDY, Z., HETKE, J., WISE, K. & BUZSAKI, G. (1995) Gamma (40-100 hz) oscillation in the hippocampus of the behaving rat *J Neurosci,* **15,** 47-60.

BUCK, S. C. (2011) Does inhibition of the rho kinase cascade reverse behavioural and physiological changes seen in ophn-1 deficit mice*?* BMedSc, University of Birmingham.

BUXHOEVEDEN, D. P. & CASANOVA, M. F. (2002) The minicolumn hypothesis in neuroscience *Brain,* **125,** 935-51.

BUZSAKI, G., BUHL, D. L., HARRIS, K. D., CSICSVARI, J., CZEH, B. & MOROZOV, A. (2003) Hippocampal network patterns of activity in the mouse *Neuroscience,* **116,** 201-211.

BUZSAKI, G. & DRAGUHN, A. (2004) Neuronal oscillations in cortical networks *Science,* **304,** 1926-9.

CANTAGREL, V., LOSSI, A. M., BOULANGER, S., DEPETRIS, D., MATTEI, M. G., GECZ, J., SCHWARTZ, C. E., VAN MALDERGEM, L. & VILLARD, L. (2004) Disruption of a new X linked gene highly expressed in brain in a family with two mentally retarded males. *J Med Genet,* **41,** 736-42.

CHAGNAC-AMITAI, Y., LUHMANN, H. J. & PRINCE, D. A. (1990) Burst generating and regular spiking layer 5 pyramidal neurons of rat neocortex have different morphological features *J Comp Neurol,* **296,** 598-613.

CHELLY, J., KHELFAOUI, M., FRANCIS, F., CHERIF, B. & BIENVENU, T. (2006) Genetics and pathophysiology of mental retardation *Eur.J.Hum.Genet.,* **14,** 701-713.

CHIURAZZI, P., SCHWARTZ, C. E., GECZ, J. & NERI, G. (2008) XLMR genes: Update 2007 *Eur.J.Hum.Genet.,* **16,** 422-434.

CHRISTOPHE, E., DOERFLINGER, N., LAVERY, D. J., MOLNAR, Z., CHARPAK, S. & AUDINAT, E. (2005) Two populations of layer v pyramidal cells of the mouse neocortex: Development and sensitivity to anesthetics *J Neurophysiol,* **94,** 3357-67.

CONNORS, B. W. & GUTNICK, M. J. (1990) Intrinsic firing patterns of diverse neocortical neurons *Trends Neurosci,* **13,** 99-104.

CROSSMAN, A. R., NEARY, D. (2005) Neuroanatomy: An illustrated colour text*,* London, Churchill Livingstone.

CSICSVARI, J., JAMIESON, B., WISE, K. D. & BUZSAKI, G. (2003) Mechanisms of gamma oscillations in the hippocampus of the behaving rat *Neuron,* **37,** 311-322.

DEFELIPE, J. & FARINAS, I. (1992) The pyramidal neuron of the cerebral cortex: Morphological and chemical characteristics of the synaptic inputs *Prog Neurobiol,* **39,** 563-607.

DELAUNOY, J., ABIDI, F., ZENIOU, M., JACQUOT, S., MERIENNE, K., PANNETIER, S., SCHMITT, M., SCHWARTZ, C. & HANAUER, A. (2001) Mutations in the x-linked rsk2 gene (rps6ka3) in patients with coffin-lowry syndrome *Hum Mutat,* **17,** 103-16.

DEL BIGIO, M. R., WILSON, M. J. & ENNO, T. (2003) Chronic hydrocephalus in rats and humans: White matter loss and behavior changes *Ann Neurol,* **53,** 337-46.

DES PORTES, V., BODDAERT, N., SACCO, S., BRIAULT, S., MAINCENT, K., BAHI, N., GOMOT, M., RONCE, N., BURSZTYN, J., ADAMSBAUM, C., ZILBOVICIUS, M., CHELLY, J. & MORAINE, C. (2004) Specific clinical and brain mri features in mentally retarded patients with mutations in the oligophrenin-1 gene *Am.J.Med.Genet.A,* **124A,** 364-371.

DOLEN, G., OSTERWEIL, E., RAO, B. S., SMITH, G. B., AUERBACH, B. D., CHATTARJI, S. & BEAR, M. F. (2007) Correction of fragile x syndrome in mice *Neuron,* **56,** 955-62.

DOUGLAS, R. J. & MARTIN, K. A. (2004) Neuronal circuits of the neocortex *Annu Rev Neurosci,* 27**,** 419-51.

ERISIR, A., LAU, D., RUDY, B. & LEONARD, C. S. (1999) Function of specific K^+ channels in sustained high-frequency firing of fast-spiking neocortical interneurons *J Neurophysiol,* **82,** 2476-89.

FAUCHEREAU, F., HERBRAND, U., CHAFEY, P., EBERTH, A., KOULAKOFF, A., VINET, M. C., AHMADIAN, M. R., CHELLY, J. & BILLUART, P. (2003) The rhogap activity of ophn1, a new f-actin-binding protein, is negatively controlled by its amino-terminal domain *Mol.Cell Neurosci.,* **23,** 574-586.

FENG, G., MELLOR, R. H., BERNSTEIN, M., KELLER-PECK, C., NGUYEN, Q. T., WALLACE, M., NERBONNE, J. M., LICHTMAN, J. W. & SANES, J. R. (2000) Imaging neuronal subsets in transgenic mice expressing multiple spectral variants of GFP. *Neuron,* **28,** 41-51.

FIALA, J. C., SPACEK, J. & HARRIS, K. M. (2002) Dendritic spine pathology: Cause or consequence of neurological disorders? *Brain Res Brain Res Rev,* **39,** 29-54.

FISAHN, A. (2005) Kainate receptors and rhythmic activity in neuronal networks: Hippocampal gamma oscillations as a tool *J.Physiol,* **562,** 65-72.

FISAHN, A., CONTRACTOR, A., TRAUB, R. D., BUHL, E. H., HEINEMANN, S. F. & MCBAIN, C. J. (2004) Distinct roles for the kainate receptor subunits Glur5 and Glur6 in kainate-induced hippocampal gamma oscillations *J.Neurosci.,* **24,** 9658-9668.

FISAHN, A., PIKE, F. G., BUHL, E. H. & PAULSEN, O. (1998) Cholinergic induction of network oscillations at 40 hz in the hippocampus in vitro *Nature,* **394,** 186-189.

FRIES, P., NIKOLIC, D. & SINGER, W. (2007) The gamma cycle *Trends Neurosci.,* **30,** 309-316.

FRINTS, S. G., FROYEN, G., MARYNEN, P. & FRYNS, J. P. (2002) X-linked mental retardation: Vanishing boundaries between non-specific (MRX) and syndromic (MRXS) forms *Clin Genet,* **62,** 423-32.

FUCHS, E. C., ZIVKOVIC, A. R., CUNNINGHAM, M. O., MIDDLETON, S., LEBEAU, F. E., BANNERMAN, D. M., ROZOV, A., WHITTINGTON, M. A., TRAUB, R. D., RAWLINS, J. N. & MONYER, H. (2007) Recruitment of parvalbumin-positive interneurons determines hippocampal function and associated behavior *Neuron,* **53,** 591-604.

GILL, K. K., SAINTOT, P., POWELL, A.D. JEFFERYS, J.G. (2011) Altered synaptic transmission in the CA3 region in a mouse model of mental retardation. University of Oxford. *Proc Ph*ysiol *Soc,* **PC53**.

GOVEK, E. E., NEWEY, S. E., AKERMAN, C. J., CROSS, J. R., VAN DER VEKEN, L. & VAN AELST, L. (2004) The X-linked mental retardation protein oligophrenin-1 is required for dendritic spine morphogenesis *Nat.Neurosci.,* **7,** 364-372.

GOVEK, E. E., NEWEY, S. E. & VAN AELST, L. (2005) The role of the Rho GTPpases in neuronal development *Genes Dev.,* **19,** 1-49.

GRAY, C. M. & SINGER, W. (1989) Stimulus-specific neuronal oscillations in orientation columns of cat visual cortex *Proc Natl Acad Sci U S A,* **86,** 1698-702.

GRICE, S. J., SPRATLING, M. W., KARMILOFF-SMITH, A., HALIT, H., CSIBRA, G., DE HAAN, M. & JOHNSON, M. H. 2001. Disordered visual processing and oscillatory brain activity in autism and Williams syndrome. *Neuroreport,* **12,** 2697-700.

GUY, J., GAN, J., SELFRIDGE, J., COBB, S. & BIRD, A. (2007) Reversal of neurological defects in a mouse model of rett syndrome *Science,* **315,** 1143-7.

HARRIS, K. M. (1999) Structure, development, and plasticity of dendritic spines *Curr Opin Neurobiol,* **9,** 343-8.

HATTOX, A. M. & NELSON, S. B. (2007) Layer V neurons in mouse cortex projecting to different targets have distinct physiological properties *J.Neurophysiol.,* **98,** 3330-3340.

HAUSSER, M., SPRUSTON, N. & STUART, G. J. (2000) Diversity and dynamics of dendritic signaling *Science,* **290,** 739-44.

HERRMANN, C. S., MUNK, M. H. & ENGEL, A. K. (2004) Cognitive functions of gamma-band activity: Memory match and utilization *Trends Cogn Sci.,* **8,** 347-355.

HILLE, B. (2001) Ion channels of excitable membranes 3rd Edition*,* Sunderland, Sinauer Associates Inc.

HORTON, J. C. & ADAMS, D. L. (2005) The cortical column: A structure without a function *Philos Trans R Soc Lond B Biol Sci,* **360,** 837-62.

HOTULAINEN, P. & HOOGENRAAD, C. C. (2010) Actin in dendritic spines: Connecting dynamics to function *J.Cell Biol.,* **189,** 619-629.

HUMEAU, Y., GAMBINO, F., CHELLY, J. & VITALE, N. (2009) X-linked mental retardation: Focus on synaptic function and plasticity *J.Neurochem.,* **109,** 1-14.

HUTTENLOCHER, P. R. (1970) Dendritic development and mental defect *Neurology,* **20,** 381.

HUTTENLOCHER, P. R. (1974) Dendritic development in neocortex of children with mental defect and infantile spasms *Neurology,* **24,** 203-210.

INLOW, J. K. & RESTIFO, L. L. (2004) Molecular and comparative genetics of mental retardation *Genetics,* **166,** 835-881.

ISHIHARA, K., AMANO, K., TAKAKI, E., SHIMOHATA, A., SAGO, H., EPSTEIN, C. J. & YAMAKAWA, K. (2010) Enlarged brain ventricles and impaired neurogenesis in the ts1cje and ts2cje mouse models of down syndrome *Cereb Cortex,* **20,** 1131-43.

JENSEN, O. & LISMAN, J. E. (1996) Hippocampal CA3 region predicts memory sequences: Accounting for the phase precession of place cells *Learn.Mem.,* **3,** 279-287.

JIN, P. & WARREN, S. T. (2003) New insights into fragile X syndrome: From molecules to neurobehaviors *Trends Biochem Sci,* **28,** 152-8.

KANG, J., HUGUENARD, J. R. & PRINCE, D. A. (2000) Voltage-gated potassium channels activated during action potentials in layer v neocortical pyramidal neurons *J Neurophysiol,* **83,** 70-80.

KAUFMANN, W. E. & MOSER, H. W. (2000) Dendritic anomalies in disorders associated with mental retardation *Cereb.Cortex,* **10,** 981-991.

KAWAGUCHI, Y. (1993) Groupings of nonpyramidal and pyramidal cells with specific physiological and morphological characteristics in rat frontal cortex *J Neurophysiol,* **69,** 416-31.

KHELFAOUI, M., DENIS, C., VAN GALEN, E., DE BOCK, F., SCHMITT, A., HOUBRON, C., MORICE, E., GIROS, B., RAMAKERS, G., FAGNI, L., CHELLY, J., NOSTEN-BERTRAND, M. & BILLUART, P. (2007) Loss of x-linked mental retardation gene oligophrenin1 in mice impairs spatial memory and leads to ventricular enlargement and dendritic spine immaturity *J.Neurosci.,* **27,** 9439-9450.

KHELFAOUI, M., PAVLOWSKY, A., POWELL, A. D., VALNEGRI, P., CHEONG, K. W., BLANDIN, Y., PASSAFARO, M., JEFFERYS, J. G., CHELLY, J. & BILLUART, P. (2009) Inhibition of rhoa pathway rescues the endocytosis defects in oligophrenin1 mouse model of mental retardation *Hum.Mol.Genet.,* 18**,** 2575-2583.

KIRKCALDIE, M. T. K. 2012. Neocortex. *In:* WATSON, C., PAXINO, G., PUELLES, L. (ed.) The mouse nervous system. 1st ed. London: Academic Press.

KITA, H. & ARMSTRONG, W. (1991) A biotin-containing compound n-(2-aminoethyl)biotinamide for intracellular labeling and neuronal tracing studies: Comparison with biocytin *J.Neurosci.Methods,* **37,** 141-150.

KLASSEN, T., DAVIS, C., GOLDMAN, A., BURGESS, D., CHEN, T., WHEELER, D., MCPHERSON, J., BOURQUIN, T., LEWIS, L., VILLASANA, D., MORGAN, M., MUZNY, D., GIBBS, R. & NOEBELS, J. (2011) Exome sequencing of ion channel genes reveals complex profiles confounding personal risk assessment in epilepsy. *Cell,* **145,** 1036-48.

KOHN, M., STEINBACH, P., HAMEISTER, H. & KEHRER-SAWATZKI, H. (2004) A comparative expression analysis of four MRX genes regulating intracellular signalling via small GTPases *Eur J Hum Genet,* **12,** 29-37.

KUTSCHE, K., YNTEMA, H., BRANDT, A., JANTKE, I., NOTHWANG, H. G., ORTH, U., BOAVIDA, M. G., DAVID, D., CHELLY, J., FRYNS, J. P., MORAINE, C., ROPERS, H. H., HAMEL, B. C., VAN BOKHOVEN, H. & GAL, A. (2000) Mutations in ARHGEF6, encoding a guanine nucleotide exchange factor for Rho GTPases, in patients with X-linked mental retardation *Nat Genet,* **26,** 247-50.

LAUMONNIER, F., BONNET-BRILHAULT, F., GOMOT, M., BLANC, R., DAVID, A., MOIZARD, M. P., RAYNAUD, M., RONCE, N., LEMONNIER, E., CALVAS, P., LAUDIER, B., CHELLY, J., FRYNS, J. P., ROPERS, H. H., HAMEL, B. C., ANDRES, C., BARTHELEMY, C., MORAINE, C. & BRIAULT, S. (2004) X-linked mental retardation and autism are associated with a mutation in the NLGN4 gene, a member of the neuroligin family *Am J Hum Genet,* **74,** 552-7.

LEBEAU, F. E., TOWERS, S. K., TRAUB, R. D., WHITTINGTON, M. A. & BUHL, E. H. (2002) Fast network oscillations induced by potassium transients in the rat hippocampus in vitro *J.Physiol,* **542,** 167-179.

LI, J., MCALLISTER, J. P., 2ND, SHEN, Y., WAGSHUL, M. E., MILLER, J. M., EGNOR, M. R., JOHNSTON, M. G., HAACKE, E. M. & WALKER, M. L. (2008) Communicating hydrocephalus in adult rats with kaolin obstruction of the basal cisterns or the cortical subarachnoid space *Exp Neurol,* **211,** 351-61.

LINSEMAN, D. A. & LOUCKS, F. A. (2008) Diverse roles of Rho family GTPases in neuronal development, survival, and death *Front Biosci.,* **13,** 657-676.

LJUBIMOVA, J. Y., KHAZENZON, N. M., CHEN, Z., NEYMAN, Y. I., TURNER, L., RIEDINGER, M. S. & BLACK, K. L. (2001) Gene expression abnormalities in human glial tumors identified by gene array *Int J Oncol,* **18,** 287-95.

LUHMANN, H. J. & PRINCE, D. A. (1991) Postnatal maturation of the GABAergic system in rat neocortex *J Neurophysiol,* **65,** 247-63.

LUO, L. (2000) Rho GTPases in neuronal morphogenesis. *Nat Rev Neurosci,* **1,** 173-80.

MAEKAWA, M., ISHIZAKI, T., BOKU, S., WATANABE, N., FUJITA, A., IWAMATSU, A., OBINATA, T., OHASHI, K., MIZUNO, K. & NARUMIYA, S. (1999) Signaling from Rho to the actin cytoskeleton through protein kinases ROCK and LIM-kinase *Science,* **285,** 895-898.

MAINEN, Z. F. & SEJNOWSKI, T. J. (1996) Influence of dendritic structure on firing pattern in model neocortical neurons *Nature,* **382,** 363-6.

MANTIS, J. G., FRITZ, C. L., MARSH, J., HEINRICHS, S. C. & SEYFRIED, T. N. (2009) Improvement in motor and exploratory behavior in Rett syndrome mice with restricted ketogenic and standard diets *Epilepsy Behav,* **15,** 133-41.

MARKRAM, H., TOLEDO-RODRIGUEZ, M., WANG, Y., GUPTA, A., SILBERBERG, G. & WU, C. (2004) Interneurons of the neocortical inhibitory system *Nat Rev Neurosci,* **5,** 793-807.

MARTINA, M., SCHULTZ, J. H., EHMKE, H., MONYER, H. & JONAS, P. (1998) Functional and molecular differences between voltage-gated K^+ channels of fast-spiking interneurons and pyramidal neurons of rat hippocampus *J Neurosci,* **18,** 8111-25.

MCALLISTER, J. P. (2012) Pathophysiology of congenital and neonatal hydrocephalus. *Semin Fetal Neonatal Med.,* **17,** 285-94.

MCCORMICK, D. A., CONNORS, B. W., LIGHTHALL, J. W. & PRINCE, D. A. (1985) Comparative electrophysiology of pyramidal and sparsely spiny stellate neurons of the neocortex *J Neurophysiol,* **54,** 782-806.

MOLNAR, Z. & CHEUNG, A. F. (2006) Towards the classification of subpopulations of layer V pyramidal projection neurons *Neurosci Res,* **55,** 105-15.

MOUNTCASTLE, V. B. (1997) The columnar organization of the neocortex *Brain,* **120,** 701-22.

NADIF KASRI, N., NAKANO-KOBAYASHI, A., MALINOW, R., LI, B. & VAN AELST, L. (2009) The Rho-linked mental retardation protein oligophrenin-1 controls synapse maturation and plasticity by stabilizing ampa receptors *Genes Dev.,* **23,** 1289-1302.

NADIF KASRI, N., NAKANO-KOBAYASHI, A. & VAN AELST, L. (2011) Rapid synthesis of the X-linked mental retardation protein Ophn-1 mediates mGluR-dependent LTD through interaction with the endocytic machinery *Neuron,* **72,** 300-15.

NAKANO-KOBAYASHI, A., NADIF KASRI, N., NEWEY, S. E. & VAN AELST, L. (2009) The Rho-linked mental retardation protein Ophn-1 controls synaptic vesicle endocytosis via endophilin a1 *Curr.Biol.,* **19,** 1133-1139.

NEGISHI, M. & KATOH, H. (2002) Rho family GTPases as key regulators for neuronal network formation *J.Biochem.,* **132,** 157-166.

NEWEY, S. E., VELAMOOR, V., GOVEK, E. E. & VAN AELST, L. (2005) Rho GTPases, dendritic structure, and mental retardation *J.Neurobiol.,* **64,** 58-74.

NITHIANANTHARAJAH, J. & HANNAN, A. J. (2006) Enriched environments, experience-dependent plasticity and disorders of the nervous system *Nat Rev Neurosci,* **7,** 697-709.

O'DONNELL, W. T. & WARREN, S. T. (2002) A decade of molecular studies of fragile X syndrome *Annu Rev Neurosci,* **25,** 315-38.

OTTMAN, R., HIROSE, S., JAIN, S., LERCHE, H., LOPES-CENDES, I., NOEBELS, J.L., SERRATOSA, J., ZARA, F. & SCHEFFER, I.E. (2010) Genetic tesing in the epilepsies – report of the ILAE Genetics Commission. *Epilepsia*. **51**, 655-70.

PETER, B. J., KENT, H. M., MILLS, I. G., VALLIS, Y., BUTLER, P. J., EVANS, P. R. & MCMAHON, H. T. (2004) BAR domains as sensors of membrane curvature: The amphiphysin bar structure *Science,* **303,** 495-9.

PETREANU, L., MAO, T., STERNSON, S. M. & SVOBODA, K. (2009) The subcellular organization of neocortical excitatory connections *Nature,* **457,** 1142-5.

PHILIP, N., CHABROL, B., LOSSI, A. M., CARDOSO, C., GUERRINI, R., DOBYNS, W. B., RAYBAUD, C. & VILLARD, L. (2003) Mutations in the oligophrenin-1 gene (Ophn-1) cause X linked congenital cerebellar hypoplasia *J.Med.Genet.,* **40,** 441-446.

PIETERSEN, A. N., PATEL, N., JEFFERYS, J. G. & VREUGDENHIL, M. (2009) Comparison between spontaneous and kainate-induced gamma oscillations in the mouse hippocampus in vitro *Eur.J.Neurosci.,* **29,** 2145-2156.

PINHEIRO, N. A., CABALLERO, O. L., SOARES, F., REIS, L. F. & SIMPSON, A. J. (2001) Significant overexpression of oligophrenin-1 in colorectal tumors detected by CDNA microarray analysis *Cancer Lett,* **172,** 67-73.

PIROZZI, F., DI RAIMO, F. R., ZANNI, G., BERTINI, E., BILLUART, P., TARTAGLIONE, T., TABOLACCI, E., BRANCACCIO, A., NERI, G. & CHIURAZZI, P. (2011) Insertion of 16 amino acids in the BAR domain of the oligophrenin 1 protein causes mental retardation and cerebellar hypoplasia in an Italian family *Hum.Mutat.,* **32,** E2294-E2307.

POWELL, A. D., GILL, K. K., SAINTOT, P. P., JIRUSKA, P., CHELLY, J., BILLUART, P. & JEFFERYS, J. G. (2012) Rapid reversal of impaired inhibitory and excitatory transmission but not spine dysgenesis in a mouse model of mental retardation *J Physiol,* **590,** 763-76.

PURPURA, D. P. (1974) Dendritic spine "dysgenesis" and mental retardation *Science,* **186,** 1126-1128.

RAMAKERS, G. J. (2002) Rho proteins, mental retardation and the cellular basis of cognition *Trends Neurosci.,* **25,** 191-199.

REMA, V. & EBNER, F. F. (1999) Effect of enriched environment rearing on impairments in cortical excitability and plasticity after prenatal alcohol exposure *J Neurosci,* **19,** 10993-1006.

RESTIVO, L., FERRARI, F., PASSINO, E., SGOBIO, C., BOCK, J., OOSTRA, B. A., BAGNI, C. & AMMASSARI-TEULE, M. (2005) Enriched environment promotes behavioral and morphological recovery in a mouse model for the fragile X syndrome *Proc Natl Acad Sci U S A,* **102,** 11557-62.

ROPERS, H. H. & HAMEL, B. C. (2005) X-linked mental retardation *Nat.Rev.Genet.,* **6,** 46-57.

RUBIO-GARRIDO, P., PEREZ-DE-MANZO, F., PORRERO, C., GALAZO, M. J. & CLASCA, F. (2009) Thalamic input to distal apical dendrites in neocortical layer 1 is massive and highly convergent *Cereb Cortex,* **19,** 2380-95.

SAINTOT, P. P. (2010) Electrophysiological characterisation of a mouse deficient for oligophrenin 1: A mouse model of intellectual disability. Ph.D. Thesis, University of Birmingham.

SCHLOSSER, B., TEN, B. G. & SUTOR, B. (1998) The intracellular tracer neurobiotin alters electrophysiological properties of rat neostriatal neurons *Neurosci.Lett.,* **249,** 13-16.

SCHNEGGENBURGER, R., MEYER, A. C. & NEHER, E. (1999) Released fraction and total size of a pool of immediately available transmitter quanta at a calyx synapse *Neuron,* **23,** 399-409.

SCHUBERT, D., KOTTER, R., LUHMANN, H. J. & STAIGER, J. F. (2006) Morphology, electrophysiology and functional input connectivity of pyramidal neurons characterizes a genuine layer Va in the primary somatosensory cortex *Cereb Cortex,* **16,** 223-36.

SCHUBERT, D., STAIGER, J. F., CHO, N., KOTTER, R., ZILLES, K. & LUHMANN, H. J. (2001) Layer-specific intracolumnar and transcolumnar functional connectivity of layer V pyramidal cells in rat barrel cortex *J Neurosci,* **21,** 3580-92.

SHEPHERD, G. M. (2004) The synaptic organization of the brain*,* Oxford, Oxford University Press.

SHOLL, D. A. (1953) Dendritic organization in the neurons of the visual and motor cortices of the cat *J.Anat.,* **87,** 387-406.

SHOLL, D. A. (1956) The measurable parameters of the cerebral cortex and their significance in its organization *Prog.Neurobiol.*, **2,** 324-333.

SKUSE, D. H. (2005) X-linked genes and mental functioning *Hum Mol Genet,* **14,** R27-32.

STEVENS, J. C., BANKS, G. T., FESTING, M. F. & FISHER, E. M. (2007) Quiet mutations in inbred strains of mice *Trends Mol Med,* **13,** 512-9.

STUSS, D. P., BOYD, J. D., LEVIN, D. B. & DELANEY, K. R. (2012) MECP2 mutation results in compartment-specific reductions in dendritic branching and spine density in layer 5 motor cortical neurons of YFP-h mice *PLoS One,* **7,** e31896.

SUN, X., GU, X. Q. & HADDAD, G. G. (2003) Calcium influx via L- and N-type calcium channels activates a transient large-conductance Ca^{2+}-activated K^{+} current in mouse neocortical pyramidal neurons *J Neurosci,* **23,** 3639-48.

SWANSON, L. W. (2003) Brain architecture: Understanding the basic plan*,* Oxford, Oxford University Press.

TAFT, R. A., DAVISSON, M. & WILES, M. V. (2006) Know thy mouse *Trends Genet,* **22,** 649-53.

TAMAMAKI, N. & TOMIOKA, R. (2010) Long-range gabaergic connections distributed throughout the neocortex and their possible function *Front Neurosci,* **4,** 202.

TASHIRO, A., MINDEN, A. & YUSTE, R. (2000) Regulation of dendritic spine morphology by the Rho family of small GTPases: Antagonistic roles of Rac and Rho *Cereb Cortex,* **10,** 927-38.

TASKER, J. G., HOFFMAN, N. W. & DUDEK, F. E. (1991) Comparison of three intracellular markers for combined electrophysiological, morphological and immunohistochemical analyses *J.Neurosci.Methods,* **38,** 129-143.

TCHERKEZIAN, J. & LAMARCHE-VANE, N. (2007) Current knowledge of the large RhoGAP family of proteins. *Biol Cell,* **99,** 67-86.

TENTLER, D., GUSTAVSSON, P., LEISTI, J., SCHUELER, M., CHELLY, J., TIMONEN, E., ANNEREN, G., WILLARD, H. F. & DAHL, N. (1999) Deletion including the oligophrenin-1 gene associated with enlarged cerebral ventricles, cerebellar hypoplasia, seizures and ataxia *Eur.J.Hum.Genet.,* **7,** 541-548.

THE JACKSON LAB http://jaxmice.jax.org/genetichealth/drift.html. Accessed 15/05/3013-

THOMSON, A. M. (2010) Neocortical layer 6, a review *Front Neuroanat,* **4,** 13.

THOMPSON, S. M., MASUKAWA, L. M. & PRINCE, D. A. (1985) Temperature dependence of intrinsic membrane properties and synaptic potentials in hippocampal CA1 neurons in vitro *J Neurosci,* **5,** 817-24.

TRAUB, R. D., BIBBIG, A., LEBEAU, F. E., BUHL, E. H. & WHITTINGTON, M. A. (2004) Cellular mechanisms of neuronal population oscillations in the hippocampus in vitro *Annu.Rev.Neurosci.,* **27,** 247-278.

TRAUB, R. D., WHITTINGTON, M. A., BUHL, E. H., JEFFERYS, J. G. & FAULKNER, H. J. (1999) On the mechanism of the gamma --> beta frequency shift in neuronal oscillations induced in rat hippocampal slices by tetanic stimulation *J.Neurosci.,* **19,** 1088-1105.

TRAUB, R. D., WHITTINGTON, M. A., COLLING, S. B., BUZSAKI, G. & JEFFERYS, J. G. (1996) Analysis of gamma rhythms in the rat hippocampus in vitro and in vivo *J.Physiol,* **493,** 471-484.

TSENG, G. F., PARADA, I. & PRINCE, D.A. (1991). Double-labelling with rhodamine beads and biocytin: a technique for studying corticospinal and other projection neurons in vitro. *J.Neurosci.Methods* **37**, 121-131.

VAILLEND, C., POIRIER, R. & LAROCHE, S. (2008) Genes, plasticity and mental retardation. *Behav Brain Res,* **192,** 88-105.

VAN PRAAG, H., KEMPERMANN, G. & GAGE, F. H. (2000) Neural consequences of environmental enrichment *Nat Rev Neurosci,* **1,** 191-8.

WEISER, M., VEGA-SAENZ DE MIERA, E., KENTROS, C., MORENO, H., FRANZEN, L., HILLMAN, D., BAKER, H. & RUDY, B. (1994) Differential expression of shaw-related k+ channels in the rat central nervous system *J Neurosci,* 14**,** 949-72.

WHITTINGTON, M. A., TRAUB, R. D. & JEFFERYS, J. G. (1995) Synchronized oscillations in interneuron networks driven by metabotropic glutamate receptor activation *Nature,* **373,** 612-615.

WIJETUNGE, L. S., CHATTARJI, S., WYLLIE, D. J. & KIND, P. C. (2013) Fragile X syndrome: from targets to treatments. *Neuropharmacology,* **68,** 83-96.

WITTWER, B., KIRCHEISEN, R., LEUTELT, J., ORTH, U. & GAL, A. (1996) New X-linked mental retardation syndrome with the gene mapped tentatively in Xp22.3. *Am J Med Genet,* **64,** 42-9.

XI, X. Z. & XU, Z. C. (1996) The effect of neurobiotin on membrane properties and morphology of intracellularly labeled neurons *J.Neurosci.Methods,* **65,** 27-32.

XIAO, J., NEYLON, C. B., HUNNE, B. & FURNESS, J. B. (2003) Oligophrenin-1, a Rrho GTPase-activating protein (RhoGAP) involved in X-linked mental retardation, is expressed in the enteric nervous system *Anat.Rec.A Discov.Mol.Cell Evol.Biol.,* **273,** 671-676.

XIAO, J., NEYLON, C. B., NICHOLSON, G. A. & FURNESS, J. B. (2004) Evidence that a major site of expression of the Rho-GTPase activating protein, Oligophrenin-1, is peripheral myelin *Neuroscience,* **124,** 781-787.

YOSHIKI, A. & MORIWAKI, K. (2006) Mouse phenome research: Implications of genetic background *ILAR J,* **47,** 94-102.

YUSTE, R. & BONHOEFFER, T. (2001) Morphological changes in dendritic spines associated with long-term synaptic plasticity *Annu Rev Neurosci,* **24,** 1071-89.

ZANNI, G., SAILLOUR, Y., NAGARA, M., BILLUART, P., CASTELNAU, L., MORAINE, C., FAIVRE, L., BERTINI, E., DURR, A., GUICHET, A., RODRIGUEZ, D., DES, P. V., BELDJORD, C. & CHELLY, J. (2005) Oligophrenin 1 mutations frequently cause X-linked mental retardation with cerebellar hypoplasia. *Neurology,* **65,** 1364-1369.

Appendix I: Altered synaptic transmission in the CA3 region in a mouse model of mental retardation

Gill KK, Saintot PP, Powell AD & Jefferys JGR. Altered synaptic transmission in the CA3 region in a mouse model of mental retardation (2011). University of Oxford, *Proc Physiol Soc* 23, PC53.

Mental retardation (MR) affects 2-3% of the population, those due to X-linked mutations are a common cause of moderate to severe MR (Ramakers, 2002). *OPHN*-1 (*Ophn*-1 in mice) is one of the genes implicated in X-linked mental retardation (XLMR), encoding oligophrenin-1, a RhoGAP protein. Loss of function mutations affect Rho GTPase-dependent signalling pathways and alter actin cytoskeleton dynamics which are important in vesicle dynamics and dendritic spine structure, the site of neurotransmission (Khelfaoui et al., 2007). Recent research has suggested oligophrenin-1 regulates endocytosis of synaptic vesicles (Khelfaoui et al., 2009). At present, no drug treatment is available for MR and treatment is primarily through educational therapy. The mechanisms underlying the cognitive decline in MR are poorly understood and better knowledge may enable better pharmacological intervention. *Ophn*-1 mice (male 15-30g, 3-10 weeks old) were anaesthetised by intraperitoneal injection of medetomidine (1mg/kg) and ketamine (76mg/kg). Values are expressed as mean ± S.E.M, analysed by ANOVA, Mann-Whitney U or Student's t-test. To investigate the role of oligophrenin-1 in synaptic function, extracellular postsynaptic field potentials (PSPs) were recorded from the stratum radiatum in the CA3c region of the hippocampus and evoked by stimulating the hilus. The amplitude of the PSP increased with larger stimulus intensities; *Ophn*-$1^{-/y}$ responses were smaller than in *Ophn*-$1^{+/y}$ slices (p=0.011, n=5 and n=12, respectively). To investigate the role of oligophrenin-1 in secretory vesicle availability at frequencies relevant to cognition, synaptic responses to repetitive stimuli (40 stimuli at 33 Hz) were examined. *Ophn*-$1^{-/y}$ slices showed less potentiation than *Ophn*-$1^{+/y}$ slices (p=0.001, n=5 and n=12, respectively). To further elucidate the synaptic changes associated with oligophrenin-1 loss of function, whole cell patch-clamp recordings were used to examine synaptic activity of CA3c pyramidal neurons. The frequency of spontaneous EPSCs and IPSCs (excitatory postsynaptic potentials and inhibitory postsynaptic potentials) was lower in *Ophn*-$1^{-/y}$ than *Ophn*-$1^{+/y}$ neurons (sEPSCs: 1.67±0.37 Hz, n=9; 6.91±1.50 Hz n=8, p=0.003; sIPSCs: 8.78±0.81 Hz, n=7; 12.63±0.76 n=7, p=0.009, respectively). The ability of synapses to follow high frequency stimulation (33 Hz) was examined. IPSCs were built up with successive stimuli, reaching a steady level within 10 stimuli in *Ophn*-$1^{+/y}$ neurons; IPSC facilitation was much weaker in *Ophn*-$1^{-/y}$ than *Ophn*-$1^{+/y}$ neurons. (p=0.001, n=9 and n=17, respectively).

This study demonstrates a synaptic malfunction which may be due to altered vesicle dynamics at the presynaptic terminal as a result of reduced readily releasable pool size or impaired endocytosis, although alterations in AMPA receptor dynamics or long term depression may also contribute (Khelfaoui et al., 2009).

Appendix II: Altered electrophysiological properties of neurobiotin labelled neocortical layer V neurons

Gill KK, Jefferys JGR & Powell AD. Impact of neurobiotin labelling on electrophysiological recordings of neocortical layer V pyramidal neurons. Program No. 304.17 Neuroscience 2011 Abstracts. Washington D.C. Society for Neuroscience, 2011. Online.

The intracellular tracer neurobiotin is widely used for morphological analysis of neurons following electrophysiological characterisation. Previous studies have reported that neurobiotin prolongs action potential (AP) duration in whole cell patch clamp recordings but detailed analysis of whether postsynaptic currents (PSCs) are similarly affected, is lacking. Furthermore, previous research has suggested that the effect of neurobiotin is concentration dependent, but it has not been examined whether lower concentrations minimise its impact on electrophysiological recordings, whilst maintaining the ability to examine neuronal morphology. We initially studied the effect of neurobiotin on AP half widths using whole cell recordings from layer V neocortical neurons *in vitro* of C57/B6 male mice and examined the concentration dependence. Neurobiotin (0.5%) resulted in a 1.6-fold elongation of AP duration than in unlabelled neurons (2.04 ± 0.19 ms, n = 8 and 1.29 ± 0.11 ms, n = 20, respectively, p = 0.001) without affecting intrinsic properties such as AP firing frequency or fast afterhyperpolaration (fAHP). In contrast, a lower concentration of neurobiotin (0.05%) did not significantly alter AP half width (1.58 ± 0.21 ms, n = 7, p >0. 05), fAHP nor AP firing frequency, although morphological analysis was still possible. We examined the effect of different concentrations of neurobiotin on spontaneous IPSCs (sIPSCs) and miniature IPSCs (mIPSCs). In contrast to action potential duration, neurobiotin did not affect the amplitude (0.5%: 49.8 ± 4.8 pA, n = 8 and 0%: 50.6 ± 2.6 pA, n = 35, p>0.05) or interevent interval (0.5%: 274.2 ± 72.8 ms and 285.9 ± 25.3 ms) of sIPSC. Similarly, neurobiotin did not affect mIPSC amplitude (0.5%: 38.2 ± 3.2 pA, n = 7 and 0%: 40.5 ± 1.9 pA, n = 25, p>0.05) or interevent interval (0.5%: 507.4 ± 127.2 ms, n = 7 and 0%: 515.6 ± 53.9 ms, n = 25, p>0.05). This study demonstrates that reducing the concentration of neurobiotin to as low as 0.05% enables morphological analysis of neurons without compromising electrophysiological characterisation.

Appendix III: Altered brain morphology in a mouse model of mental retardation

Gill KK, Kangesu P, Jefferys JGR & Powell AD. Altered brain morphology in a mouse model of mental retardation. Accepted for IUPS, 2013.

Mental retardation (MR) affects 2-3% of the population; those due to X-linked mutations are a common cause of moderate to severe MR. *OPHN1* (*Ophn*-1 in mice) is one of the genes implicated in X-linked mental retardation (XLMR), encoding oligophrenin-1, a RhoGAP protein. Loss of function mutations affect Rho GTPase-dependent signalling pathways and alter actin cytoskeleton dynamics which are important for many neuronal functions, including morphogenesis and neuroepithelial development. Structural abnormalities, namely, abnormal cerebral ventricles typically associated with hydrocephalus, have been shown in brains of MR patients with *OPHN1* mutations and *Ophn*-1 null mice. A systematic study has been conducted to explore alterations in brain anatomy in *Ophn*-1 mice.

Ophn-1 mice (male 15-30g, 6 week old (n=6 for both genotypes) and 3 month old (*Ophn*-$1^{+/y}$ n=8 and *Ophn*-$1^{-/y}$ n=6)) were anaesthetised by i.p. injection of medetomidine (1mg/kg) and ketamine (76mg/kg). Values are expressed as mean ± S.E.M, analysed by ANOVA or Student's t-test. To investigate the impact of loss of oligophrenin-1 on cerebral ventricles, ventricular volumes were analysed. Lateral ventricles were larger in *Ophn*-$1^{-/y}$ mice than *Ophn*-$1^{+/y}$ mice at 6 weeks of age (26.2±10.5 mm^3 and 3.81±0.44 mm^3; respectively; p=0.002) and 3 months of age (7.78±2.54 mm^3 and 3.42±6.99 mm^3; respectively; p=0.02). Lateral ventricle dilatation was associated with a reduction in motor cortex thickness (6 weeks: *Ophn*-$1^{-/y}$ 0.91±0.05 mm and *Ophn*-$1^{+/y}$ 1.09±0.03 mm; p=0.01 and 3 months: *Ophn*-$1^{-/y}$ 0.94±0.03 and *Ophn*-$1^{+/y}$ 1.04±0.02 mm; p=0.016) without alteration in somatosensory, auditory and ectorhinal cortices. Hippocampal volume was similar in *Ophn*-$1^{+/y}$ and *Ophn*-$1^{-/y}$ mice (7.38±1.40 mm^3 and 9.29±0.7 mm^3; respectively; p=0.23), neither the thalamus area (15.78±0.91 mm^2 and 13.46±0.69 mm; respectively; p=0.07) nor total brain area (51.8±1.6 mm^2 and 46.9±3.05 mm^2 respectively; p=0.18) were affected.

This study demonstrates brain malformation in *Ophn*-$1^{-/y}$ mice, primarily expansion of the lateral ventricles, which may be due to loss of oligophrenin-1 expression in ependymal cells, chorial villi or endothelium. Thus, this could result in impairments in cilia function, ependymal proliferation, abnormal production/absorption of cerebral spinal fluid or obstruction of cerebral aqueduct and/or fourth ventricle. How the ventriculomegaly and reduction in cortical thickness contribute to the cognitive deficits remains to be explored.

Appendix IV: Rapid reversal of impaired inhibitory and excitatory transmission but not spine dysgenesis in a mouse model of mental retardation

Powell AD, Gill KK, Saintot PP, Jiruska P, Chelly J, Billuart P & Jefferys JGR. Rapid reversal of impaired inhibitory and excitatory transmission but not spine dysgenesis in a mouse model of mental retardation (2012). *J Physiol.* 590, 763-775.